For Reference

NOT TO BE TAKEN FROM THIS ROOM

THE UNIVERSITY OF ALBERTA

PHONON EFFECTS ON ELECTRON TUNNELLING

INTO SUPERCONDUCTORS

by

J. S. Rogers

A THESIS

SUBMITTED TO THE FACULTY OF GRADUATE STUDIES

IN PARTIAL FULFILLMENT OF THE REQUIREMENTS FOR THE DEGREE

OF DOCTOR OF PHILOSOPHY

DEPARTMENT OF PHYSICS

EDMONTON, ALBERTA

AUGUST, 1964

THE UNIVERSITY OF ALBERTA

PHONON EFFECTS ON ELECTRON TUNNELLING

INTO SUPERCONDUCTORS

by

J. S. Rogers

A THESIS

SUBMITTED TO THE FACULTY OF GRADUATE STUDIES

IN PARTIAL FULFILLMENT OF THE REQUIREMENTS FOR THE DEGREE

OF DOCTOR OF PHILOSOPHY

DEPARTMENT OF PHYSICS

EDMONTON, ALBERTA

AUGUST, 1964

UNIVERSITY OF ALBERTA

FACULTY OF GRADUATE STUDIES

The undersigned certify that they have read, and
recommend to the Faculty of Graduate Studies for acceptance,
a thesis entitled PHONON EFFECTS ON ELECTRON TUNNELLING INTO
SUPERCONDUCTORS, submitted by J. S. Rogers, in a partial
fulfillment of the requirements for the degree of Doctor
of Philosophy.

ACKNOWLEDGEMENTS

I wish to express my gratitude to Dr. Woods, my research supervisor, both for his cheerful encouragement and guidance during the course of this research, and for the complete freedom given me with regard to new ideas.

Special thanks are also due to Dr. J. G. Adler for suggesting this area of research to me and for many valuable discussions pertaining to both the research and the cryostat.

I wish to thank Mr. D. W. Penner for preparing an excellent aluminum specimen for our mutual use.

Acknowledgements are also due to the technical staff of the physics department for dealing with my various problems in a co-operative manner.

I am most grateful to my wife for the constant encouragement which she has given me, and also for typing this thesis.

Finally, it is a pleasure to acknowledge the alternating financial support of the Physics Department and the National Research Council during the course of this work.

ABSTRACT

Since 1960 there has been considerable
interest in experiments involving electron tunnelling
into superconductors. This new technique, which is
simple in principle, provides a direct method of
observing the modification of the electronic density
of states that take place in a metal when it becomes
superconducting. A forbidden gap forms about the
Fermi energy in the density of states of the superconductor
and much smaller variations in the density of states
occur at energies above the Fermi energy by an amount
equal to the predominant phonon energies of the metal.

Investigations of this energy region have been
made for the metals lead, tin, indium, aluminum, and
mercury. The results found for lead and tin are in
agreement with published results, and the results found
for indium and aluminum are new. Phonon effects should
be observable in mercury, but specimens are difficult to
prepare and the results obtained with the one specimen
tested were uninterpretable. These preliminary results
are encouraging however, because they hold promise that
the method used to prepare and mount the mercury specimen
can yield useable results.

Values are also reported for the energy gaps
in the above metals and for the observed amount of

broadening of the singularity in the density of states
at the edge of the energy gap. The possibility of using
tunnel junctions as thermometers has also been investigated.

TABLE OF CONTENTS

LIST OF TABLES

LIST OF FIGURES

CHAPTER I

INTRODUCTION

A. Motivation

This thesis reports on a continuation of
work initiated at the University of Alberta by J. G.
Adler in 1962. The original motivation for our
electron tunnelling work has been given by Adler in
his Doctoral Thesis (1963).

During the course of Adler's work
instrumentation was developed which enabled us to
observe small deviations in the electronic density
of states of some metals when they became super-
conducting. The cause of these deviations was not
entirely clear at that time, but it has since been
established that they are intimately connected with
the phonon spectrum of the superconductor. Further
investigations of this effect are reported here.

The motivation for the kind of work
described here has been given by Krumhansel (1962).
The argument given is that the phonon field is an
experimentally accessible quantum field with a
natural high frequency cut-off, and as such it
should be an excellent testing ground for quantum
field theories.

It should be pointed out that electron-

tunnelling is not the best method of exploring the phonon field. With specimens involving polycrystalline films, the only type of specimen fabricated to date, one can only obtain one characteristic curve, and any phonon information must be interpreted from this one curve. Peaks in the phonon spectrum cause irregularities in the curve, and these irregularities overlap considerably. Hence the only quantitative information tunnelling gives is a few phonon 'critical frequencies',and one does not know what symmetry direction in the crystal the critical frequencies pertain to. Furthermore we are limited by the technique to a few superconductors. This is to be compared to neutron spectroscopy, which has allowed entire dispersion curves along various symmetry directions to be obtained for several metals to a precision of about one percent (Brockhouse et. al. 1962, Woods et. al. 1962).

However, neutron spectroscopy has its limitations also. The metal studied must be a good neutron scatterer, and the neutron source must be intense. Even with these two demands satisfied, each experiment takes a time of the order of days so that automatic recording systems must be used.

Thus in view of the relative simplicity of electron tunnelling work plus the fact that its basic mechanism involves an electron phonon interaction at $0°K$,

it is desirable to get as much information on phonons
as possible with this method, in spite of the somewhat
limited nature of the information.

Even limited data can be of considerable
value. Consider two phonon calculations based on
elastic constants and a plausible model, one by Bhatia
(1955) for sodium and the other by Musgrave (1963) for
white tin. The phonon spectrum obtained by Bhatia for
sodium predicts a specific heat curve which agrees
with the observed one to within 4 percent. The end point
of this spectrum is at 22.1 mv. The actual end point
determined by neutron scattering is at 15.8 mv.
Musgrave's phonon spectrum for tin gives a specific
heat curve which is 4 percent too high; the calculated
spectrum is complicated with an end point of 21 mv. The
actual spectrum as determined by tunnelling is indeed
complicated with an end point of 17.7 mv. The end point
is unambiguous, and there is no other experimental
source for this information at present.

The calculated phonon spectra mentioned
above are in error because the authors had only zero
frequency information available to them (the elastic
constants) along with integrated information (specific
heat data). Phillips (1959) has outlined a method for
calculating phonon spectra if critical point data are
also available, and these calculations should be far more
accurate.

CHAPTER II

MICROSCOPIC THEORIES OF SUPERCONDUCTIVITY AS RELATED TO ELECTRON TUNNELLING

A. The BCS Theory

The first successful microscopic theory of superconductivity was evolved by Cooper (1956), and Bardeen, Cooper, and Schrieffer (1957 a,b), and is usually referred to as the BCS theory.

While this theory has been superseded in elegance by later works, it nonetheless appears to be correct in its essential features. It will accordingly be taken as the main framework for the descriptions here.

The BCS theory is based on virtual phonon exchange between electron pairs, and is accordingly a many body theory. The Hamiltonian Operator H for the electron is taken to be the sum of a Bloch term H_0, a phonon interaction term H_1, and a coulomb repulsion term H_2. Thus in the BCS theory,

$$H = H_0 + H_1 + H_2 \quad , \tag{2.1}$$

where

$$H_0 = \sum_{k < k_f} |\epsilon_k| \left(1 - \eta(k,\sigma)\right) + \sum_{k > k_f} \epsilon_k \, \eta(k,\sigma) \quad ,$$

$$H_1 = \sum_{k,k',\sigma,\sigma',K} \left\{ \frac{\hbar\omega_K |M_K|^2 C^*(k'-K,\sigma') \, C(k',\sigma')}{(\epsilon_k - \epsilon_{k+K})^2 - (\hbar\omega_K)^2} \right.$$

$$\left. \cdot \; C^*(k+K,\sigma) \, C(k,\sigma) \right\} \quad ,$$

and

$$H_2 = \left\langle \frac{4\pi e^2}{K^2} \right\rangle_{AV} \quad .$$

In these expressions, k is the electron wave vector, k_f is the wave vector of an electron at the Fermi surface, K is the phonon wave vector, σ is the spin index, ϵ_k is the Bloch energy measured from the Fermi energy, $\hbar\omega_K$ is the phonon energy, M_K is the matrix element for the electron-phonon interaction calculated for the zero-point amplitude of the lattice vibrations, $C^*(k,\sigma)$ creates a Block state $|k,\sigma\rangle$, $C(k,\sigma)$ annihilates a Bloch state $|k,\sigma\rangle$, and $n(k,\sigma)$ the single particle number operator is

$$C^*(k,\sigma)\,C(k,\sigma) = \begin{cases} 1, & |k,\sigma\rangle \text{ occupied} \\ 0, & |k,\sigma\rangle \text{ unoccupied}. \end{cases}$$

The symbols e and $\hbar$ have their customary meaning.

The phonon interaction term is attractive for excitation energies $|\epsilon_k - \epsilon_{k+K}| < \hbar\omega_K$.

In order that the C, C^* operators in the H_1 term will not cause contributions to the energy of alternating sign when operating on the various possible wave functions, the BCS theory considers only a sub-set of electron states $|k,\sigma\rangle$ in which the electrons are paired. The pairing is such that if the state $|k,+\tfrac{1}{2}\rangle$ is occupied, the state $|-k,-\tfrac{1}{2}\rangle$ is also. The BCS criterion for super-conductivity is then that the attractive interaction term H_1 dominate the Coulomb repulsion term H_2 for this sub-set of states. Creation and annihilation operators are then defined for the pair states:

$$b^*_k = c^*(k, \tfrac{1}{2}) \, c^*(-k, -\tfrac{1}{2}) \quad ,$$

$$b_k = c(k, \tfrac{1}{2}) \, c(-k, -\tfrac{1}{2}) \quad .$$

In order to simplify the mathematics, the coefficient of the C , C^* operators in H_1 is replaced by a negative constant for excitation energies in the range $|\epsilon| < \hbar \omega_p$ and by zero outside this range, where $\hbar \omega_p$ is a representative virtual phonon energy. The physical justification of this is that the thermal excitation energies in a superconductor will be very small compared to the predominant virtual phonon energies. The H_1 term of the reduced Hamiltonian thus becomes

$$H_{1\,red.} = -V \sum_{k,k'} b^*_k \, b_k \quad , \quad |\epsilon_k| < \hbar \omega_p \quad .$$

It is worth noting at this stage that because of this simplified form for $H_{1\,red.}$, experiments which involve excitation energies of the order of $\hbar \omega_p$ will probably yield results which disagree with those predicted by the BCS theory. This is observed to be the case in electron tunnelling experiments, and the regions of disagreement are of interest because they are connected with the phonon distributions of the metals involved.

It is not possible to generalize the BCS theory to this wider energy range by simply returning to the expression given for H_1 however, because lifetime effects become important for these highly excited

states. The BCS theory has thus been contrived to describe the superconducting state for electron energies close to the Fermi energy. The results of the BCS theory are that

(a) The single-particle-like excitations have the peculiar dispersian law

$$E_k^2 = \epsilon_k^2 + \Delta^2 \quad , \tag{2.2}$$

where E_k is the single-particle-like excitation energy, ϵ_k is the Bloch energy (both measured from the Fermi energy), and Δ is the real, positive half gap energy, which is of course temperature dependent.

(b) The temperature dependence of Δ is given by the integral equation

$$\frac{1}{N(0)V} = \int_0^{\hbar\omega_p} \frac{d\epsilon}{\epsilon^2 + \Delta^2} \tanh\left(\beta \frac{\epsilon^2 + \Delta^2}{2}\right) \quad , \tag{2.3}$$

where $N(0)$ is the density of states at the Fermi energy for electrons in the normal metal, V is the constant appearing in $H_{1red.}$, and $\beta = \frac{1}{k_B T}$, where k_B is Boltzmann's constant and T is the temperature.

With the additional assumption that Δ becomes zero at the transition temperature for the superconductor, it is then possible to tabulate Δ as a function of the reduced temperature $t = T/T_c$, which Muhlschlegel (1959) has done.

An <u>approximate</u> expression for the Muhlschlegel
tabulation is $\frac{\Delta(T)}{\Delta(0)} \simeq (1 - t^4)^{1/2}$. The BCS expression
for $\Delta(0)$ is

$$\Delta(0) = 1.75 \, k_B T_c .$$

(2.4)

(c) The electron density of states for the superconducting
state is obtained by differentiating equation 2.2:

$$\frac{dN(\epsilon)}{dE} = \frac{dN(\epsilon)}{d\epsilon} \frac{d\epsilon}{dE} = N(0) R_p \left(1 - \left(\frac{\Delta}{E}\right)^2\right)^{-1/2} ,$$

(2.5)

where R_p means the 'real part of'.

This new density of states is populated
according to Fermi-Dirac statistics. The electronic
density of states in a superconductor is thus redistributed
near the Fermi energy in the manner indicated in Figure 2.1.

Owing to finite lifetime effects, the singularity
in the density of states at the edge of the energy gap
is not found experimentally, but otherwise the BCS theory
is in excellent accord with experiment for energies within
a few gap widths of the Fermi energy.

B. The Eliashberg Gap Equations and Their Application to
    Tunnelling Results.

As has been indicated in the preceding section,
the BCS theory does not take the explicit form of the
phonon spectrum into account. It is also gauge-variant.
Bogoliubov et al (1959) have succeeded in reformulating
the BCS theory in a gauge-invariant manner. Eliashberg

Figure 2.1

The electronic density of states

near the Fermi energy for a metal

in the superconducting state, and

also for the same metal in the

normal state. The energy origin

is at the Fermi energy. The small

energy range does not permit band

structure to be shown.
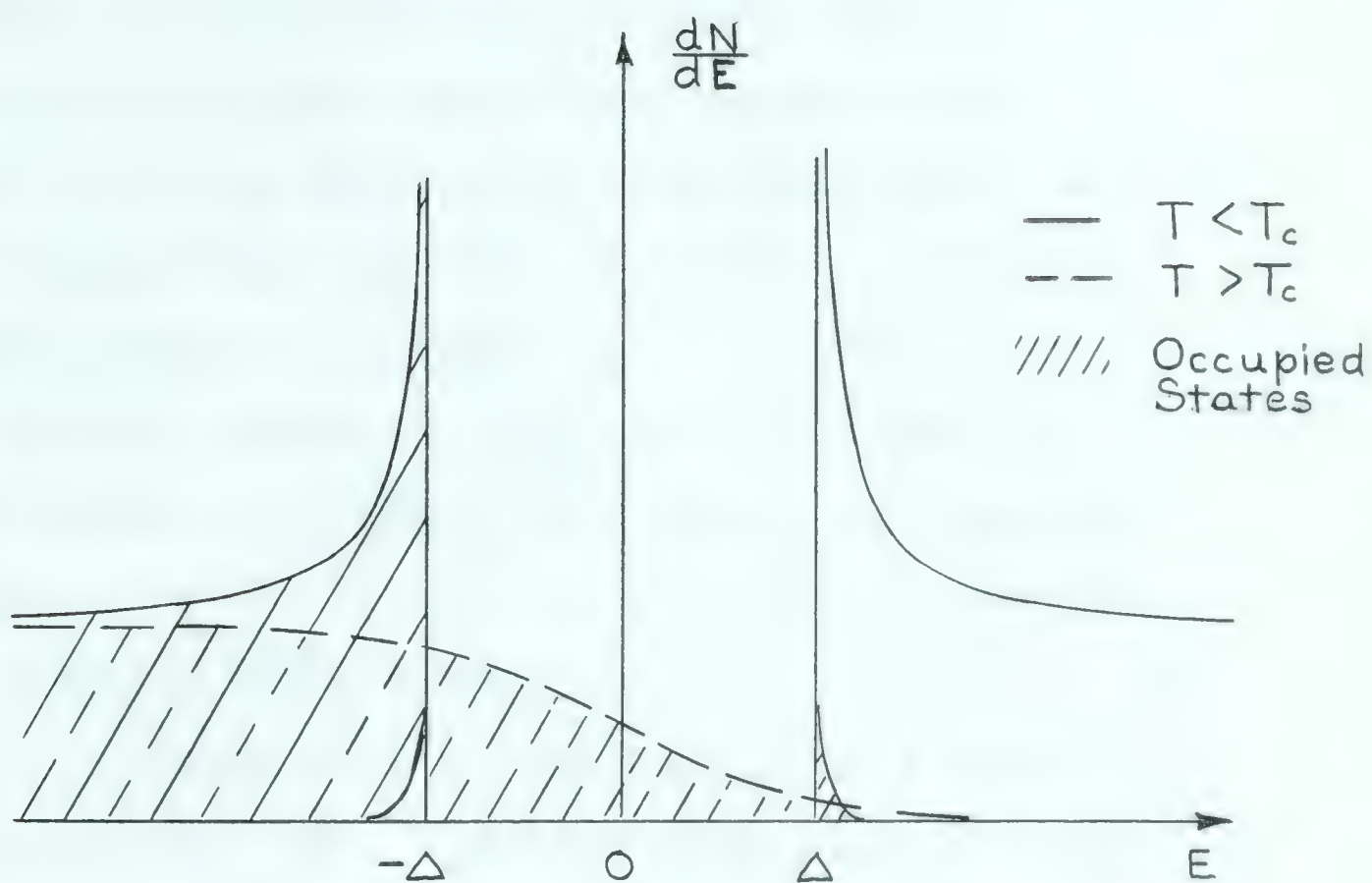
(1960) has in turn succeeded in extending the
Bogoliubov theory to include both lifetime effects
for the excited electrons and an explicit phonon
distribution. Lifetime effects have been included
by using the Green's Function (or propagator)
formalism. In this formalism, energies can be
complex, so that plane waves decay exponentially
in time. One thus expects the Eliashberg theory to
yield an energy gap parameter $\Delta = \Delta(\omega)$ which is
a complex function of energy; ω is taken as the
energy variable since the quasi-particle concept of
the BCS theory is not valid when finite lifetimes are
taken into account. It is also convenient to measure
energy from the Fermi energy.

Throughout the remainder of this thesis,
Planck's constant $\hbar$ will be taken equal to unity,
as will the electron charge e and Boltzmann's
constant k_B. This is common practice in theoretical
papers, and it causes no difficulty in the experimental
work to be described here in that the connection between
natural frequencies, electron energies due to applied
voltages, and thermal energies is readily obtained by
reinserting the appropriate constants. That is, $\omega = V = T$
becomes $\hbar\omega = eV = k_B T$ for purposes of calculation.
Kittel (1960) has given an excellent tabulation of the
various ratios of the physical constants which facilitates

such conversions. The ratio of most interest here is

$$e/k_B = 11.60 \,^\circ K/mv$$

Returning to the Eliashberg theory, it is indeed found that Δ is a complex function of ω, but the equations which determine Δ are not very tractable. In the Eliashberg theory, $\Delta(\omega)$ is given in terms of a gap function $\varphi(\omega)$ and a renormalization function $Z(\omega)$ according to the equation

$$\Delta(\omega) = \varphi(\omega) \Big/ Z(\omega) \ .$$

The equations which determine φ and Z are

$$\varphi(\omega) = \int_{\Delta_0}^{\omega_{cc}} d\omega' \, R_p \left[\left(\frac{Z'\omega'}{\varphi'}\right)^2 - 1\right]^{-1/2} \left\{ \int d\omega_0 \, \alpha(\omega_0)^2 \, g(\omega_0) \right.$$

$$\left. \cdot \left(D_{\omega_0}(\omega'+\omega) + D_{\omega_0}(\omega'-\omega) - U\right) \right\} , \quad \text{and}$$

$$1 - Z(\omega) = \frac{1}{\omega} \int_{\Delta_0}^{\omega_{cc}} d\omega' \, R_p \left[1 - \left(\frac{\varphi'}{Z'\omega'}\right)^2\right]^{-1/2} \left\{ \int d\omega_0 \, \alpha(\omega_0)^2 \, g(\omega_0) \right.$$

$$\left. \cdot \left(D_{\omega_0}(\omega'+\omega) - D_{\omega_0}(\omega'-\omega)\right) \right\} ,$$

where $g(\omega)$ is the normalized phonon spectrum, $\alpha(\omega)$ is an effective electron-phonon coupling parameter, U is a Coulomb pseudo-potential defined to include only the interactions outside a band of energies $|\omega| < \omega_{cc}$ which is large compared to the Debye energy, $\Delta_0 = \varphi(\Delta_0) \Big/ Z(\Delta_0)$ is the gap parameter at the edge of the energy gap,

and $D_{\omega_0}(x) = (x + \omega_0 - i0^+)^{-1}$ is one of the phonon

propagator terms. φ and Z are assumed to be

isotropic and homogeneous.

Once the function $\Delta(\omega)$ has been determined,

it only remains for our purposes to find out how it

affects the single-particle-like density of states in a

superconductor. Schrieffer et al. (1963) have been able

to show, again with the aid of the propagator formalism,

that the effective tunnelling density of states in a

superconductor, $\dfrac{dN}{d\omega} = N_T(\omega)$, is given by

$$N_T(\omega) = N(0)\, R_p \left[1 - \left(\frac{\Delta(\omega)}{\omega} \right)^2 \right]^{-1/2} , \tag{2.7}$$

where as before $N(0)$ is the density of Bloch states at

the Fermi energy for a normal metal. For energies where

phonon effects are important, $\omega \gg |\Delta|$, equation (2.7)

may be expanded to first order in Δ^2 :

$$\frac{N_T(\omega)}{N(0)} \doteq 1 + \frac{\Delta_1(\omega)^2 - \Delta_2(\omega)^2}{2\omega^2} , \tag{2.8}$$

where $\Delta(\omega) = \Delta_1(\omega) + i\,\Delta_2(\omega)$,

and $i = (-1)^{1/2}$.

It is perhaps desirable at this stage to show

briefly how electron tunnelling results are connected with

the normalized density of states for a superconductor, $\dfrac{N_T(\omega)}{N(0)}$.

A typical tunnel junction consists of two thin

metallic films and a dielectric layer arranged in the
geometry of a parallel plate capacitor. The dielectric
layer is sufficiently thin that electrons may pass from
one metallic film to the other by 'tunnelling' through
the potential barrier provided by the dielectric layer.
The tunnelling process is that predicted by quantum
mechanics, and it is a temperature independent process.

A simple model for the tunnel current exists
for the case of an n-s system* at absolute zero which
exhibits negligible band structure and also has a
constant barrier transition probability P for energies
near the Fermi energy ω_f .

This model is shown in Figure 2.2 along with
the current-voltage (i-v) diagram and its derivative.
The subscripts a and b refer to the two metals involved in
the tunnel junction.

The current-voltage (i-v) expression for this
case is seen immediately from the diagram to be

$$i(v) = \text{const.} \; P \int_0^{\vee} N_T(\omega)_a \; N(o)_b \; d\omega$$

The derivative of this expression is

$$\frac{di}{dv}\Big|_s = \text{const.} \; P \cdot N_T(\omega)_a \cdot N(o)_b$$

---

* i.e., a tunnel junction in which one metal is in the
  normal state and the other is in the superconducting state.

Figure 2.2

A model for the tunnel current
and the electrical characteristics
resulting from this model. The
distribution $N_T(\omega-v)_b$ is
given by

$$N_T(\omega-v)_b = \begin{cases} N(0)_b, & \omega < v \\ 0, & \omega > v \end{cases}.$$

$N_T(\omega)_a$

$N_T(\omega - v)_b$
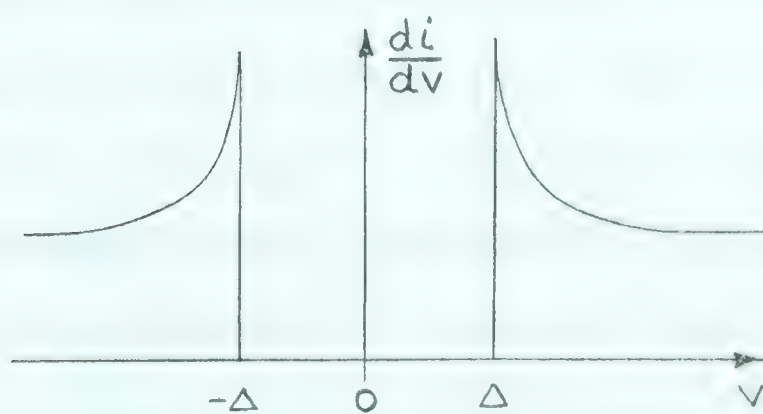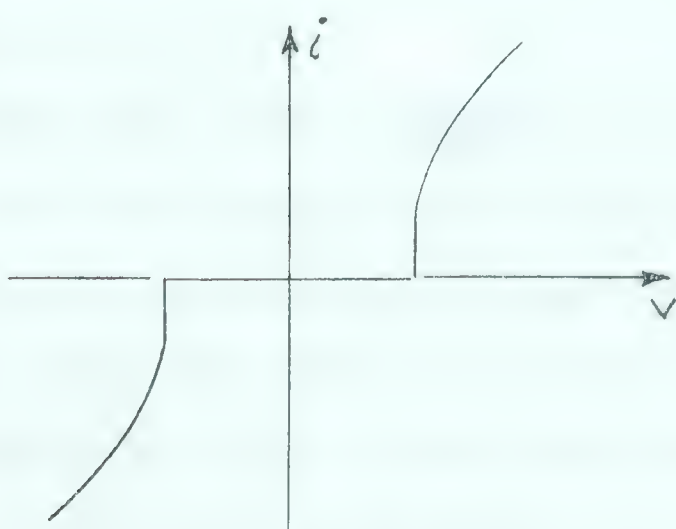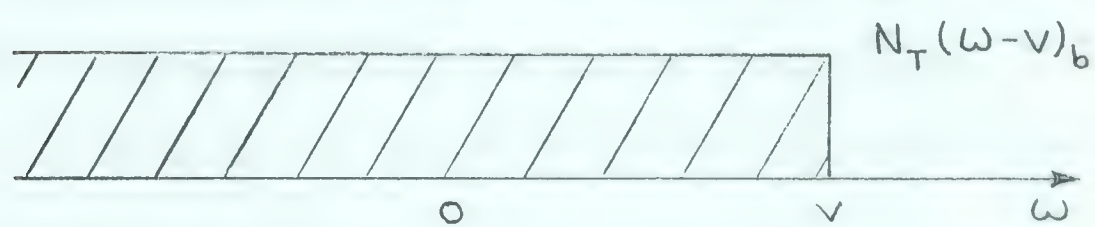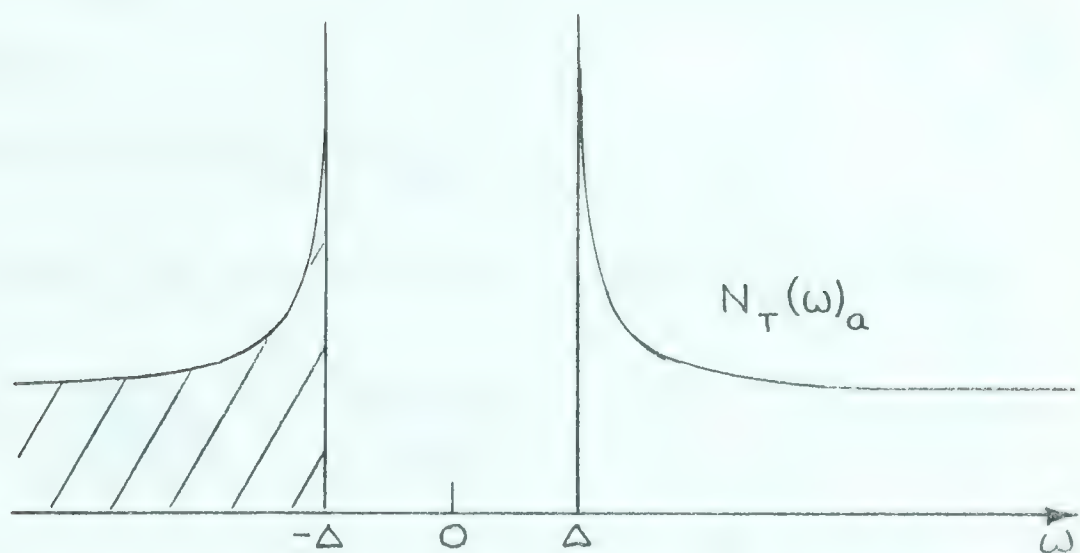
$\dfrac{di}{dv}$

The subscript s has been appended to indicate that one of
the metals involved is in the superconducting state.
Repeating this analysis for the case where both metals
are normal yields

$$\frac{di}{dv}\Big|_n = \text{const} \cdot P \cdot N(0)_a \, N(0)_b \, .$$

The ratio of these two derivatives, $\sigma(v)$, is thus

$$\sigma(v) \equiv \frac{di}{dv}\Big|_s \Big/ \frac{di}{dv}\Big|_n = \frac{N_T(v)_a}{N(0)_a} \, ,$$

so that in this approximation the normalized dynamic
conductance σ for a tunnel junction is equivalent
to the normalized density of states in the superconductor.
A more detailed analysis of this equivalence will be
given in later sections.

Having thus shown that $\frac{N_T(\omega)}{N(0)}$ is a directly
measurable quantity, we now return to equation 2.8. It is
immediately clear that the equations 2.6 must be solved if
equation 2.8 is to be compared with experiment.

Schrieffer et al. have solved the Eliashberg
equations 2.6 numerically for a model chosen to represent
lead. In this model the parameters $\alpha(\omega)$ and U were
taken to be constants and $g(\omega)$ was taken to be the sum
of two Lorentzian-shaped peaks* centered at energies
corresponding to the predominant transverse and longitudinal

---

* A derivation of the Lorentz line-width expression is
given in Dicke and Wittke (1960).

phonon energies. The phonon model distributions are
shown in Figure 5.3 along with our observed σ results
for lead. It may be seen from Figure 5.3 that the σ
characteristic shows a pronounced decrease at the phonon
energies measured from the gap edge singularity. This
experimental behaviour is in excellent agreement with
the machine calculations of Schrieffer et al. Their
computations show a sharp increase in $\Delta_2(\omega)$ and a less
rapid decrease in $\Delta_1(\omega)$ at an energy just beyond each
peak in the phonon distribution. (i.e., at an energy

$$V = \omega_p^+ + \Delta_o \, , \qquad \text{where} \quad \omega_p^+ \quad \text{is slightly larger}$$

than the phonon peak energy).

At these energies it will be noticed that
excited electron states may readily decay by phonon
emission to the states available at the gap edge sing-
ularity. Thus as the voltage applied across a tunnel
junction is increased past a predominant phonon energy,
the decay rate for the excited electrons being injected
into the metal increases and this in turn causes a
decrease in the σ characteristic due to the increase
of the Δ_2 term in the density of states
expression.

An alternative method of solving the Eliashberg
equations 2.6 has been given by Scalapino and Anderson (1964).
These authors have obtained approximate solutions of
equations 2.6 by using a re-iterative procedure based on

singularities. The first iteration consisted of using
an Einstein phonon distribution $g(\omega, \omega_0) = \delta(\omega - \omega_0)$
in the gap equations 2.6. The resulting functions

$\varphi(\omega, \omega_0)$ and $Z(\omega, \omega_0)$ were found to
be singular at $\omega = \omega_0$. The second iteration then
consisted of using the singular parts of the Einstein
results $\varphi(\omega, \omega_0)$, $Z(\omega, \omega_0)$ in equations 2.6
along with a more plausible phonon distribution in order
to calculate new values of φ and Z. The forms
of phonon distribution used were those predicted by
Van Hove (1953) for phonon energies close to the critical
point energies ω_c. The critical point energies are
those at which the $\omega(\vec{q})$ surfaces for the phonons
have a maximum, a minimum, or a saddle point. (The

$\omega(\vec{q})$ surfaces are just the three dimensional version
of the usual phonon dispersion curve $\omega(q)$ versus q for
a given direction of the phonon wave vector $\vec{q}$).

Scalapino and Anderson found that certain of
the Van Hove forms for $g(\omega)$ gave φ and Z functions
in their second iteration that produced logarithmic
singularities in the derivative $\frac{d\sigma}{dv}$ of the σ character-
istic*, at voltages $V = \omega_c + \Delta_0$. These authors state
that their second iteration results are exact as to the form

---

* i.e., the σ characteristic for the model given earlier
  in this section.

of the singularities and nearly so as to their magnitude.

One of the Scalapino and Anderson results of particular interest to us is that at a voltage corresponding to the end point of the phonon spectrum one should find

$$\lim_{V \to \Delta_0 + \omega_c} \frac{d\sigma}{dV} \doteq - \frac{\gamma C}{\omega_t} \ln |\omega_c + \Delta_0 - V| \tag{2.9}$$

and

$$\lim_{\epsilon \to 0} \left(\frac{d\sigma}{dV}\bigg|_{\Delta_0 + \omega_c + \epsilon} - \frac{d\sigma}{dV}\bigg|_{\Delta_0 + \omega_c - \epsilon} \right) \doteq \frac{\pi \beta C}{\omega_t} ,$$

where C is a constant, β and γ are slowly varying functions related to ω_t , ω_t is the predominant transverse phonon energy, Δ_0 is the energy gap at absolute zero, measured at the edge of the gap for the superconducting member of the n-s tunnel junction, and ω_c is the end point energy for the phonon spectrum of the superconductor involved.

Equations 2.9 may be viewed as a quantitative description of the behaviour of the experimentally obtained σ characteristics for applied voltages corresponding to the end point of the phonon spectrum. If there is a logarithmic singularity in the $\frac{d\sigma}{dV}$ characteristic near the end point of the phonon spectrum, then one can determine the end point energy unambiguously. It is unfortunate that the σ characteristics currently being obtained experimentally do not exhibit well-developed singularities,

so that the Scalapino and Anderson analysis may not be exploited to the extent that one might desire.

It is of course impossible for the observed characteristics to be truly singular when the observed $\frac{d\sigma}{dv}$ characteristics do not exhibit well developed singularities at the edge of the energy gap.

It is because of this lack of well developed singularities that we limit our analysis to the end point of the total phonon spectrum if further data is not available. One might, for example, expect singularities of the form (2.9) to occur at the end point of each polarization branch of the phonon spectrum. Such a result is not guaranteed however because the effect of a saddle point in one branch of the phonon dispersion surface may cancell the effect of a maximum in another branch (Van Hove). Conversely, the observation of a singularity of the form (2.9) in observed $\frac{d\sigma}{dv}$ characteristics at an energy corresponding to an intermediate point in the total phonon spectrum need not indicate the end point of one of the polarization branches, since such a result could equally well be due to a saddle point. The problem is further complicated by the possibility of surface maxima which do not admit a quadratic term in their Taylor expansions.

The only completely general result which we have for our tunnelling results then is equation (2.9) for the end point of the total phonon spectrum.

If information is available from other sources
however one may be able to make more extensive critical point
analysis of tunnelling data. An example of this possibility
may be seen in the results obtained for aluminum (Figure 5.11).
In this case one has Walker's x-ray results for reference, and
the end points of the three polarization branches may be
identified in the tunnelling results. The tunnelling results
thus complement the x-ray results very nicely, in that the
energy scale for the x-ray results is the most uncertain
feature of that method, whereas it is the most certain feature
of the tunnelling method.

CHAPTER III

ANALYSIS OF ELECTRON TUNNELLING RESULTS

In the preceding section a tunnel integral was solved for a restricted case. We now wish to obtain solutions to tunnel integrals which are subject to fewer restrictions.

Harrison (1961) has shown that band structure effects should not be observed in electron tunnelling characteristics for two normal metals. The argument given by Harrison is based on an independent particle model, and he finds that density-of-states terms (proportional to V_g , where V_g is the group velocity) cancel current terms (proportional to V_g^{-1}) in the tunnel current integral. The density of states distributions which we observe with electron tunnelling into superconductors arise from the subtleties of the many-particle system. According to the arguments of Bardeen (1961), and Harrison, the density of states observed with electron tunnelling into superconductors is that of the quasi-particles only. When calculating tunnel current integrals, we may use models that are free of band structure, and replace the density of states in the normal metal, $N(\omega)_n$, by the density of states at the Fermi surface, $N(0)$. Obviously, interesting results will only be obtained when at least one of the metals is superconducting.

Two such cases are illustrated in Figures 3.1 and 3.2. The first line of these figures depicts the normalized tunnelling density of states $\rho_s = \dfrac{N_T(\omega)_s}{N(o)}$ as functions of energy. The subscripts s and n refer to the superconducting and normal states respectively, and $\rho_n = 1$.

The distributions ρ_s are populated according to Fermi-Dirac statistics. The number of thermally excited electrons in aluminum is negligibly small at the lowest temperatures available in the present apparatus, so, by varying the temperature, the number of thermally excited electrons in the aluminum may be changed at will.

Figure 3.1 shows some thermally excited electrons, and it may be seen that the small peak which they produce in the current-voltage (i-v) characteristic provides a means of determining the values of the energy gap parameters Δ_a and Δ_b .

It is possible in certain cases to relate the distribution ρ_{sa} to the observed i-v characteristics without knowing the explicit distribution ρ_{sb} . For example, consider the situation shown in Figure 3.2. Here there are no thermally excited electrons and the ρ_{sb} distribution is taken to be free of phonon structure. Both these conditions may be met quite well with a sufficiently low temperature and a suitable choice of metals. The Fermi function $f(\omega, T)$ may accordingly be replaced by a unit

Figure 3.1

Illustration of the use of

thermally excited electrons

for determining energy gap

values.
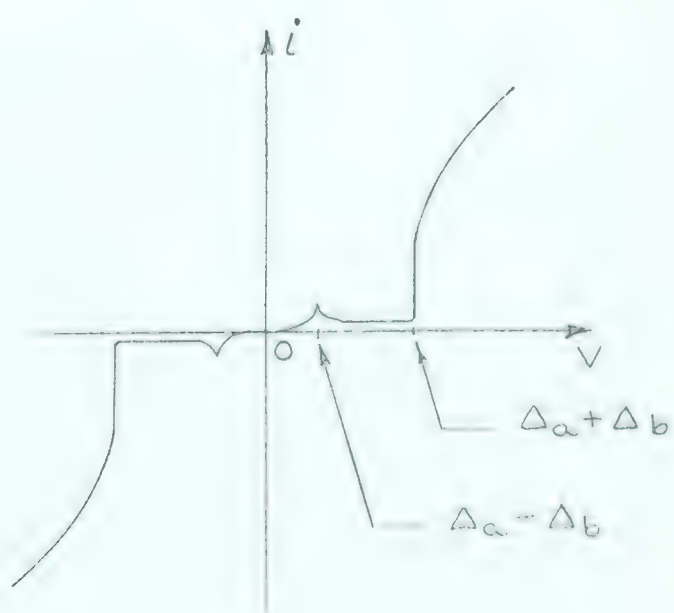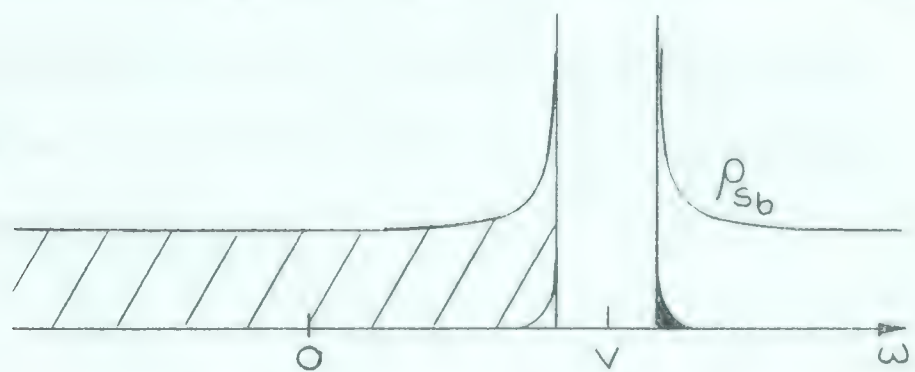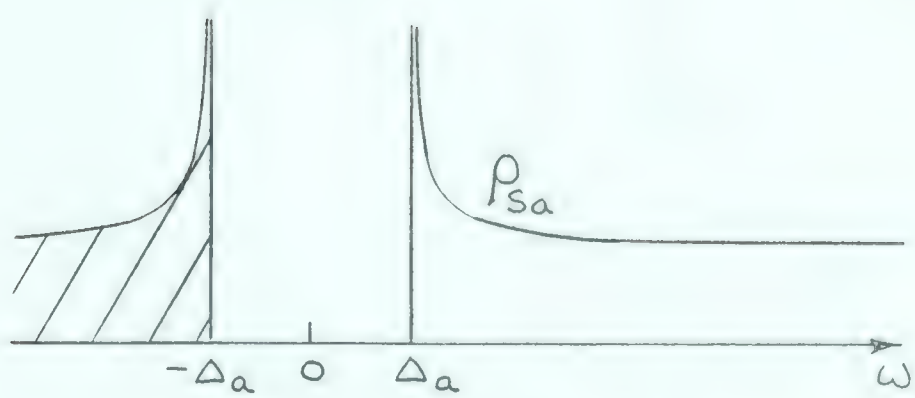
Figure 3.2

Illustration of a method of observing

phonon structure effects in tunnelling

characteristics.
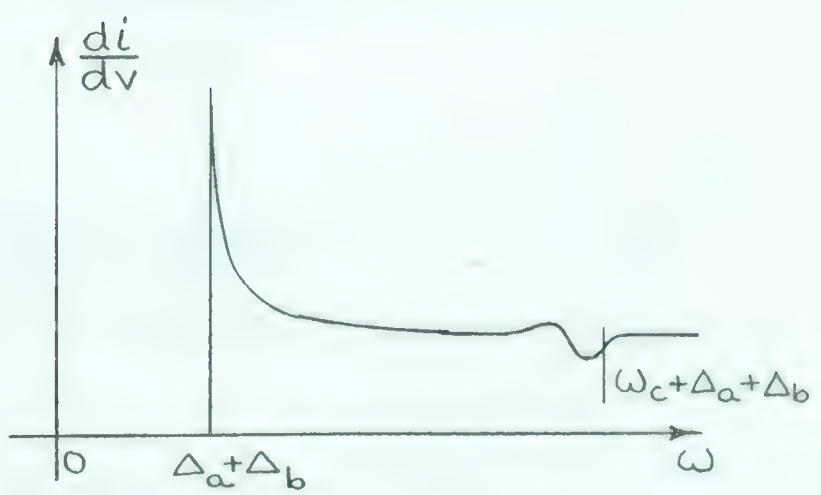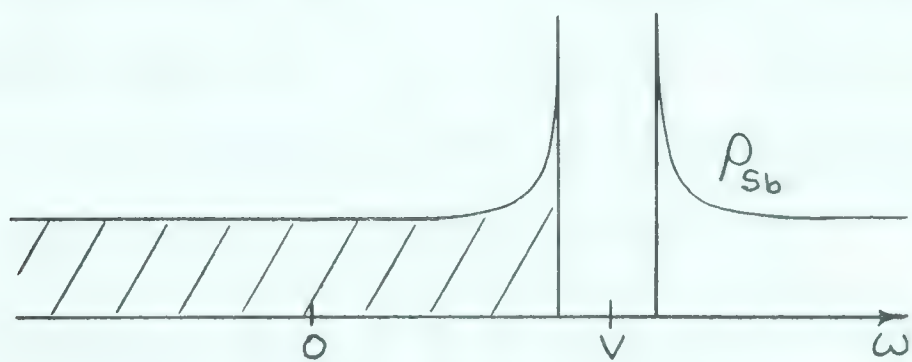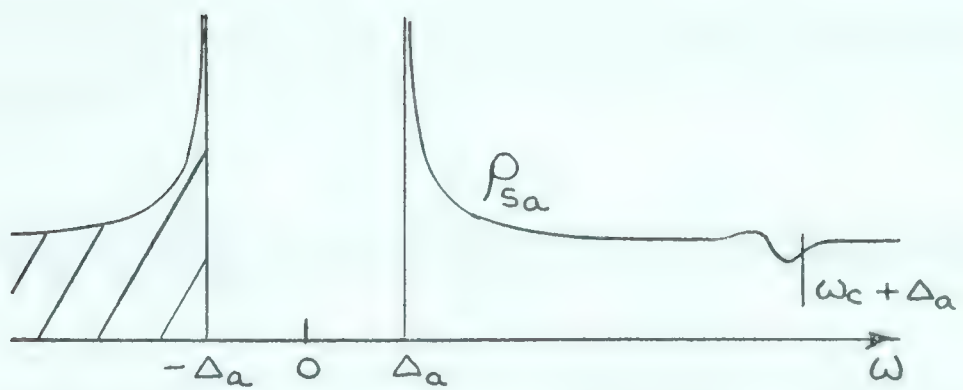
step function:

$$f(\omega, T) = \Theta(\omega) = \begin{cases} 1 & , \omega < 0 \\ 0 & , \omega > 0 \end{cases} .$$

The expression for the current is readily seen from the diagram* to be

$$i = c \int_{-\infty}^{\infty} P(\omega, v)\, \rho_{Sa}(\omega)\, \rho_{Sb}(\omega - v)\left\{\Theta(\omega - v) - \Theta(\omega)\right\} d\omega,$$

where $P(\omega, v)$ is the probability of an electron crossing the potential barrier, and C is a constant. Upon taking the derivative of this expression with respect to voltage, and noting that $\rho_S(0) = 0$, one obtains

$$\frac{1}{c}\frac{di}{dv}\Big|_{SS} = \int_0^v \frac{\partial P(\omega, v)}{\partial v}\, \rho_{Sa}(\omega)\, \rho_{Sb}(\omega - v)\, d\omega$$

$$+ \int_0^v P(\omega, v)\, \rho_{Sa}(\omega)\, \frac{\partial \rho_{Sb}(\omega - v)}{\partial v}\, d\omega$$

$$= I_1 + I_2 .$$

Noting further that $\displaystyle\int_0^v \frac{\partial \rho_{Sb}(\omega - v)}{\partial v}\, d\omega = 1$ and

that $\dfrac{\partial \rho_{Sb}(\omega - v)}{\partial v}$ is zero except near $\omega = v - \Delta_b$,

one obtains

$$I_2 \doteq P(v - \Delta_b, v)\, \rho_{Sa}(v - \Delta_b)$$

If a similar analysis is performed when two normal

---

* or, alternatively, see Shapiro et al (1962).

metals are involved it yields

$$\frac{1}{c} \frac{di}{dv}\Big|_{nn} \doteq \int_0^{\overset{\vee}{v}} \frac{\partial P(\omega,v)}{\partial v}\, d\omega \;+\; P(v,v) \quad .$$

Denoting the ratio of $\dfrac{di}{dv}\Big|_{ss}$ to $\dfrac{di}{dv}\Big|_{nn}$

by σ , one thus obtains

$$\sigma(v) \doteq \frac{P(v-\Delta_b,v)\,\rho_{sa}(v-\Delta_b) + \int_0^{\overset{\vee}{v}} \frac{\partial P}{\partial v}\,\rho_{sa}(\omega)\,\rho_{sb}(\omega-v)\,d\omega}{P(v,v) + \int_0^{\overset{\vee}{v}} \frac{\partial P}{\partial v}\,d\omega}$$

and

$$\sigma - 1 \doteq \frac{P(v-\Delta_b,v)\,\rho_{sa}(v-\Delta_b) - P(v,v) + \int_0^{\overset{\vee}{v}} \frac{\partial P}{\partial v}\big(\rho_{sa}(\omega)\,\rho_{sb}(\omega-v)-1\big)\,d\omega}{P(v,v) + \int_0^{\overset{\vee}{v}} \frac{\partial P}{\partial v}\,d\omega} \quad .$$

$$(3.1)$$

Since $\rho_{sa}(v) - 1$ may be quite small (of the order of

10^{-3}) and still be of interest, it is not at all clear that

$P(\omega,v)$ may be treated as a constant in this

expression. Information about the behaviour of $P(\omega,v)$ may

be obtained from $\dfrac{di}{dv}\Big|_{nn}$. For example, expanding

$P(\omega,v)$ about the origin yields

$$P(v,v) + \int_0^{\overset{\vee}{v}} \frac{\partial P}{\partial v}\,d\omega \;=\; P(0,0) + v\,\frac{\partial P}{\partial \omega}\Big|_{0,0} + 2v\,\frac{\partial P}{\partial v}\Big|_{0,0} + \cdots$$

It is not possible to evaluate $\dfrac{\partial P}{\partial \omega}\Big|_{0,0}$ without some

knowledge of the potential barrier, but it might be expected

to be of the same order of magnitude as $\dfrac{\partial P}{\partial v}\Big|_{0,0}$. Therefore

$$\frac{\dfrac{di}{dv}\Big|_{nn,v=v}}{\dfrac{di}{dv}\Big|_{nn,v=0}} \;\doteq\; 1 + 3 \cdot \frac{v}{P(0,0)}\,\frac{\partial P}{\partial v}\Big|_{0,0} \quad .$$

Figure 3.3 shows this ratio for an Al-Al$_2$O$_3$-In tunnel junction and it may be seen that the neglect of higher order terms in the above expression is not serious since the curve is reasonably linear. In this particular case one obtains

$$\frac{1}{P(0,0)} \left. \frac{\partial P}{\partial v} \right|_{0,0} \doteq 2 \times 10^{-4} /mv$$

Since Figure 3.3 is reasonably linear, one may replace $\dfrac{\partial P(\omega, v)}{\partial v}$ by the constant $\left. \dfrac{\partial P}{\partial v} \right|_{0,0}$ in the integrals in equation 3.1. The integral in the numerator then becomes negligible* as does the integral in the denominator. Expanding $P(v, v-\Delta_b)$ about $P(v,v)$ then yields

$$\sigma - 1 \doteq \rho_{Sa}(v - \Delta_b) -1 - \frac{\Delta_b}{P(v,v)} \left. \frac{\partial P}{\partial \omega} \right|_{v,v} .$$

For the case being considered (Al-In), $\Delta_{Al} \doteq 0.2 \, mv$, so that

$$\sigma - 1 \doteq \rho_{S_{In}}(v - \Delta_{Al}) - 1 - 4 \times 10^{-5} .$$

The contribution due to the variation of the potential barrier is thus negligible since σ may only be measured to a few parts in ten thousand with the present apparatus.

The major limitation on the expression

---

* The energy states which in the normal metal would be in the energy gap region form the gap edge singularity in the distributions, and $\rho_S \doteq 1$ for $\omega \gg \Delta$ since phonon effects are generally small.

Figure 3.3

Transition probability test for

specimen In-38 at 4.6°K

$$\frac{\frac{dI(v)}{dv}\Big|_n}{\frac{dI(0)}{dv}\Big|_n}$$

In-38(4·6°K)
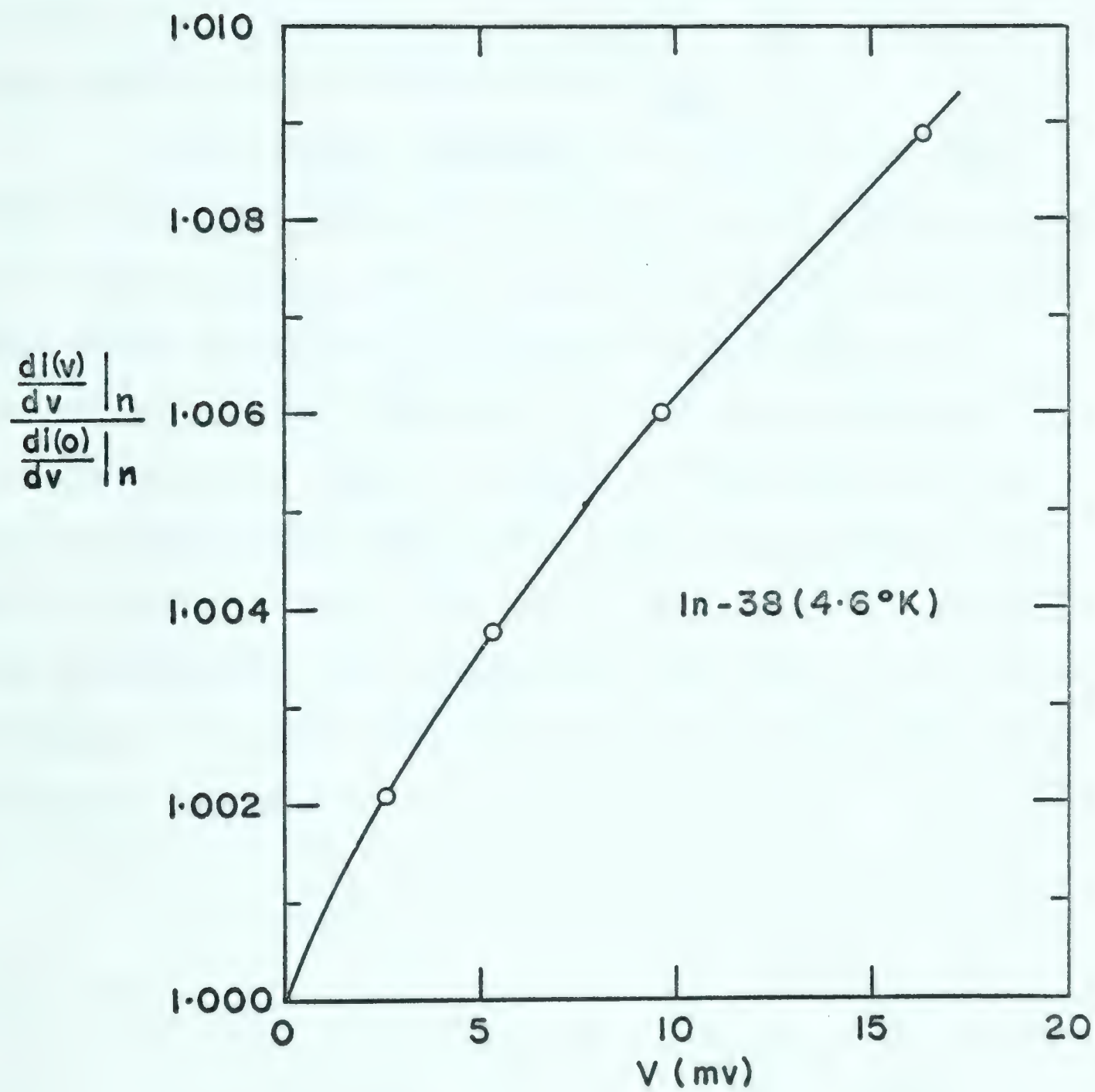
$$\sigma(\nu) \doteq \rho_{sa}(\nu - \Delta_b)$$ for the situation depicted in Figure 3.2 is in the assumption about $\dfrac{\partial \rho_{sb}(\omega - \nu)}{\partial \nu}$ being localized. It is only valid if this derivative is non-zero over a region small compared to that occupied by the variations being observed in ρ_{sa}.

Distributions performing the function of ρ_{sb} in the foregoing example will be called probe distributions. It is readily apparent that either a superconducting or a normal probe distribution at non-zero temperatures will distort the observed distribution. The superconducting probe distribution tends to exaggerate variations in the observed distribution while the normal probe distribution tends to diminish them. For this reason superconducting probe distributions have frequently been used for this work. An attempt to evaluate the distortion which they introduce is given in Appendix IV.

CHAPTER IV

EXPERIMENTAL METHOD

A. Specimen Preparation and Mounting

Tunnel junction specimens have been prepared, and mounted in the He^3 cryostat, in the manner described in detail by Adler (1963). This method of specimen preparation results in a four terminal tunnel junction on a glass substrate. The prepared films have been from 300 to 600 $\overset{o}{A}$ thick, and have been polycrystalline, the crystallites being less than 3000 $\overset{o}{A}$ in size according to x-ray transmission photographs.* The tin films have shown some preferred orientation of crystallites. The substrate is enclosed in a small, gas-tight specimen chamber containing one atmosphere of helium gas at room temperature, and this chamber is attached to the He^3 chamber of the cryostat with a 0.040" diameter copper wire. Electrical leads to the specimen chamber are of lead coated 0.0025" manganim wire. A 220 ohm Speer carbon resistor is mounted on the He^3 chamber to serve as a thermometer.

Some particular aspects of specimen preparation will now be discussed. It will be convenient to designate the first metallic film deposited on the glass substrate, the base layer; the dielectric layer formed on the base layer, the barrier layer; and the metallic film deposited across the barrier layer, the cover layer. The cover layer will sometimes be designated M_α , when it may be any metal.

---

* The author is indebted to Dr. S. S. Sheinin for the x-ray results.

B. The Base Layer Metal

Al-Al$_2$O$_3$-Ma systems have been the only type studied here. The reasons for choosing aluminum as the base layer are that a film of it is easily evaporated, its surface can readily be oxidized to form the barrier layer, and it has been studied extensively by other workers. Aluminum also becomes superconducting at 1.20°K, so that aluminum base layers give a superconducting probe distribution at lower temperatures. This is an advantage for preliminary phonon work in that such a distribution tends to exaggerate any phonon effects that may be present. It is a disadvantage for critical point analysis, but perhaps not a serious one.

Of the other metals available for a base layer, tin appears, from the literature, to be the next most suitable. However, the transition temperature of tin is 3.73°K, so that it offers an advantage over aluminum as a base layer for the observation of phonon effects only if it is also the metal being examined.

Magnesium has been used as a normal base layer by Giaever. It is not as readily handled in an evaporator because the magnesium atoms do not appear to stick readily to anything but the very cleanest surfaces. Greater care must be exercised in masking and surface preparation procedures than with aluminum. Also magnesium oxide in bulk has about one half the volume of the magnesium from

which it was formed (Holland (1961), page 451), so that
magnesium oxide layers might be porous and contain
filamentary bridges connecting the cover metal to the base.
Such bridges of the superconducting metal may completely mask
the tunnel current but weak filamentary bridges of
magnesium might be quite tolerable since they would
remain normal at all temperatures. Magnesium could perhaps
prove to be a very useful base layer for the observation of
phonon effects.

C. The Barrier Layer

An extensive study of $Al-Al_2O_3-Al$ tunnel junctions
has been made by Fisher and Giaever (1961). The most
striking feature of their results is the large scatter on
their graphs of tunnel resistance as a function of barrier
thickness. The barrier thicknesses were determined by
capacitance measurements. The observed scatter of about
20% in the thickness (or the capacitance) could be
readily explained by an oxide layer of non-uniform thickness,
since the capacitance depends on the average of the
reciprocal of the barrier thickness while the tunnel
resistance depends on the average of an exponential of
the barrier thickness. A non-uniform oxide layer would
also be consistent with the filamentary bridges which are
often observed.

Capacitance measurements would thus appear to be

a poor way of determining the effective tunnel thickness
of a barrier layer, but they do at least give some
additional information when used in conjunction with
the tunnel resistance measurements. A small R-C bridge
has accordingly been devised which is suitable for
measuring both the resistance and the capacitance of
our tunnel junctions. This bridge is described in
Appendix II. It covers a larger dissipation range than
commercial bridges and cannot subject the tunnel junction
to more than 50 mv. The first feature is desirable
because of the strong exponential dependence of the
tunnel resistance on the barrier thickness, while the
second is necessary because voltages of the order of one
volt will exceed the dielectric strength of the thin
barrier layer and destroy the tunnel junction. In addition
to these features, a display mode is used which allows
small deviations from a linear current-voltage characteristic
to be observed. The major limitation of the bridge circuit
is that it only provides a two terminal measurement, so that
for accurate results the film resistance must be negligible
compared to the tunnel resistance.

It is possible to make four terminal resistance
measurements using the curve tracer described in Appendix I.
The display available with this apparatus can be quite
sensitive, so that the voltage dependence of the tunnel
resistance may be clearly exhibited.

Unfortunately, specimens with weak filamentary bridges will appear good when subjected to any of the above measurements at temperatures where both metals are normal conductors. The final test of a prepared specimen is thus only obtained after it has been mounted in the cryostat and cooled down to about $0.5°K$. At this temperature any filamentary bridges of aluminum will be superconducting and their effect will be readily apparent at the origin of the current-voltage characteristic.

D. Barrier Layer Formation

A trial-and-error procedure has been adopted for oxidizing the surface of the aluminum base layer because:

1. the effective barrier thickness is strongly dependent on the metal of the cover layer (Handy 1962),

2. the thickness of the oxide layer on the aluminum appears to be dependent upon the moisture content of the air, and

3. the oxidation time and temperature do not appear to be critical.

The third reason may appear surprising, particularly when these are the variables used by experimentalists to control the barrier layers they obtain. Our results indicate that an Al_2O_3 layer approaches a saturation thickness that is

very near that required for good tunnel junctions. Controlling
the time and temperature to within ten percent seems to
give reproducible results for a given cover layer on a
given day. The results vary from day to day in a way that
appears to be associated with the humidity of the air;
however attempts to use deliberately moistened air
produced more consistent barrier layers but ones through
which temperature dependent (i.e., non-tunnelling)
conduction processes were large. Further work might
develop a consistent procedure that would avoid the
filamentary bridges that we sometimes obtain.

E. Alternative Barrier Layers

        Shapiro et al (1962) have reported successful
tunnel junctions using barium stearate as the dielectric
layer. They have since indicated* that such barriers have
a tendency to rupture at low temperatures.

        We have tried evaporating SiO and MgF_2 dielectric
layers but have not been able to obtain tunnel junctions in
this manner. It is quite easy to prepare capacitors in this
way, but as the dielectric layer is decreased in thickness
below a few hundred Å (as given by the capacitance), short
circuits appear. Since layers about 50 Å thick are

* private communication

required before appreciable electron tunnelling can occur
it has not been possible to use these materials as barrier
layers.

F. Lead Connections

The method, described by Adler, of soldering
leads to the substrate before the tunnel junction is made
requires an oxidation temperature lower than 140°C so that
the indium solder will not melt. The surface of the indium
contact must be scraped off before the film is deposited
in order to get an oxide-free indium interface.

The connections were made somewhat differently for
specimen Sn-41. Copper contacts were deposited on the
substrate by evaporation ahead of the base layer. Leads
were then indium soldered to the copper areas after the
specimen was completed. This procedure allowed us to use
a higher oxidation temperature (220°C). The specimen which
resulted was free of filamentary conduction at 0.5°K, but
this could be a fortuitous result.

Several attempts were made to prepare mercury
specimens. A different arrangement was adopted so that
the mercury could be deposited in the evaporator onto a cold
barrier layer (T$\approx$ 80°K) and be kept cold thereafter. It
was found that unusually thick oxide layers were necessary
in order to get a useable specimen. This is rather
surprising in view of Handy's (1962) work in which the cover
layer atoms were found to penetrate the oxide layer in

accordance with their atomic diameters.

Only one specimen was obtained in this way which appeared useable at 80°K, but when it was mounted in the cryostat, it showed excessive filamentary conduction at 4°K.

G.   Thermometer Calibration

Temperatures quoted in this thesis are those of the He^3 chamber inferred from the resistance of a 220 ohm 'Speer' carbon resistor. The experimental arrangement has been described by Adler (1963). Adler's method of calibrating the resistance thermometer consisted of using the He^3 gas as a thermal link between the He^3 and He^4 chambers of the cryostat. The vapour pressure of the liquid in the He^4 chamber then gave the temperature of the resistor. This method of calibration requires that the He^3 chamber be isothermal with the He^4 chamber.

As an alternative to this method we mounted pure aluminum and cadmium wires on the He^3 chamber in order to get calibration values for the resistor at 1.20°K and 0.52°K where the resistance of the wires dissappeared. Another calibration value was obtained at the boiling temperature of the helium in the dewar with exchange gas in the vacuum jacket of the cryostat. The calibration points obtained in this way should be reasonably accurate, yet using these points in the Clement-Quinnell (1952) interpolation equation $T^{-1} = a(\ln R)^{-1} + b + c \ln R$

produced resistance-temperature relations similar to the one shown in Figure 4.1.

The reversal of the interpolation curve at 7.3°K suggests that the interpolation formula is not well suited to this resistor over this temperature range. A further calibration value at 80°K has enabled a visual estimate of a more plausible resistance-temperature behaviour to be made (see Figure 4.1). From this estimate we assign an uncertainty of 0.2°K to our interpolated temperatures in the 4°K to 1°K range, the uncertainty diminishing near calibration points. It will be seen in the following chapter that this rather large uncertainty in temperature does not affect our results due to the nature of the experiments.

It has also been possible to directly determine the temperature of $Al-Al_2O_3-Al$ tunnel junctions at low temperatures (0.6 to 0.3°K). The current observed at applied voltages $V < 2\Delta$ for such a tunnel junction is due to electrons which are thermally excited across the energy gap. In principle at least, its magnitude gives an absolute measurement of the temperature of the junction since the width of the energy gap is also in direct evidence on the current-voltage characteristics. Preliminary calculations of this nature are discussed in Appendix III. The results obtained are in agreement with the thermometer to within 0.1°K in the 0.3 to 0.6°K temperature range.

Figure 4.1

Interpolation results for a 220 ohm

carbon resistance thermometer.
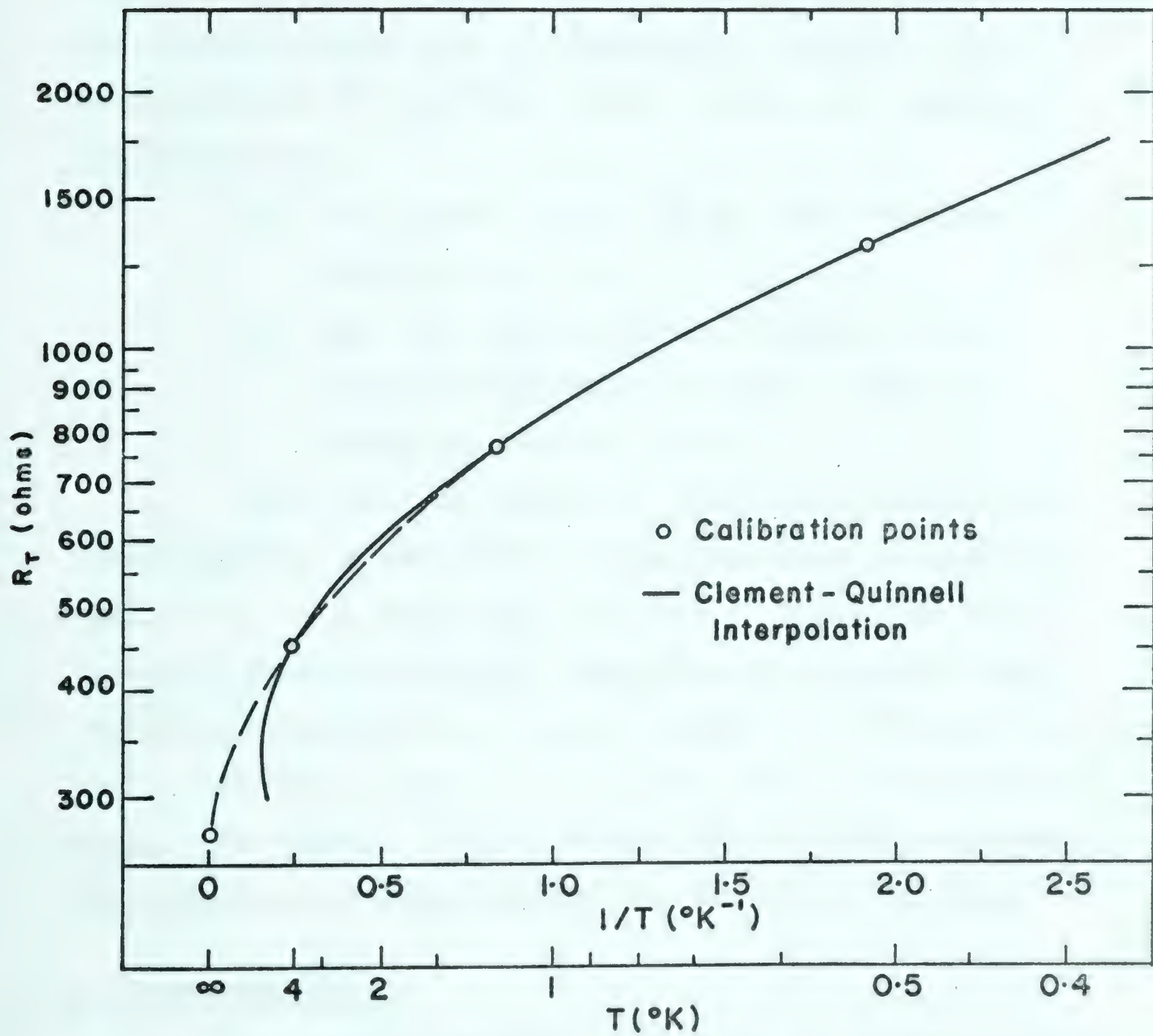
As before, this uncertainty in temperature does not affect our experimental results. The result is interesting however because it indicates that the active part of the tunnel junction is slightly warmer than the He^3 chamber. The author believes that the temperature gradient occurs mainly between the specimen chamber and the He^3 chamber, indicating that

a)   the vacuum chamber has not been evacuated sufficiently, and

b)   that the specimen chamber has not been thermally anchored to the He^3 chamber as firmly as one might desire.

More reliable methods of temperature measurement should shortly be available in this laboratory through the work of Dr. F. D. Manchester and Miss J. Gould, who are currently investigating the properties of semiconducting resistance thermometers. A major source of difficulty with carbon resistance thermometers is that their characteristics change with thermal cycling between 4°K and room temperature. Semiconducting thermometers are not expected to do this.

H.   Instrumentation

The phonon structure present in σ characteristics is usually very weak, so that it is desirable to observe the dynamic conductance $\frac{di}{dv}$ in as sensitive a manner as possible. Appendix I is a reprint of an article which describes apparatus developed for this purpose. Since the

$\frac{di}{dv}$ characteristics are time independent, any assessment of equipment sensitivity is somewhat arbitrary. It appears however that the noise level of the detecting amplifier affords a reasonable basis for comparing systems which utilize bridge circuits, and on this basis the system described here is competitive with the system described by Thomas and Klein (1963) and used by Rowell et al (1963) in similar work.

It is worth noting that the instrumentation is not the only factor which determines the uncertainty in the observed σ characteristics. Any non-tunnelling conduction present in the specimen will usually be erratic, and this will also cause an uncertainty in the observed σ values. It is thus possible to have a 'noisy' specimen, and a rather ideal specimen is required if the specimen noise is to be much smaller than the noise level of our present instrumentation.

CHAPTER V

EXPERIMENTAL PHONON STRUCTURE RESULTS

A. Probe Distribution Details

The base layer metal used for all specimens studied to date has been aluminum, so that we wish to justify the use of the density of states distribution of aluminum as a probe distribution.

The observed σ characteristic for an Al-Al tunnel junction is shown in Figure 5.11. The coordinates for this figure have been chosen to emphasize phonon effects. The effects in evidence are twice as strong as they would be for an n-s tunnel junction, so that it may be seen that the use of a superconducting aluminum probe distribution has contributed a negligible amount of phonon structure to the σ characteristics observed for lead, tin, indium, and mercury. These metals also have larger energy gap values than aluminum, so that the density of states distribution of aluminum in the superconducting state satisfies our probe distribution requirements for these metals reasonably well.

It will sometimes be convenient to refer to the normalized dynamic conductance characteristic,

$\sigma = \left.\frac{di}{dv}\right|_s \bigg/ \left.\frac{di}{dv}\right|_n$, as the first derivative of the

i-v characteristic of the tunnel junction when one or both of the metals involved is superconducting. Similarly, the

derivative of the σ characteristic, $\dfrac{d\sigma}{dv}$, will

sometimes be referred to as the second derivative

characteristic.

In order that phonon structure energies may be

read directly from the energy coordinate, the figures

emphasizing phonon structure will have their energy

origin at $\triangle_{Al} + \triangle_{Ma}$, where Ma is the cover

layer metal involved.

Figure 5.1 shows the current-voltage (i-v)

characteristic and the first derivative characteristic

in the energy gap region for specimen Al-42. The energy

half-gap value has been determined by extrapolating

the linear part of the 'current jump' on the i-v

characteristic to the zero current axis. The half-gap

value so obtained was corrected to absolute zero

using the Muhlschlegel tabulation (the correction was

negligible in this case). The result is given in the

figure as $\triangle(0)_{Al}$ and is also listed in Table 6.2,

along with other half-gap values obtained in a similar

manner.

This extrapolation method for obtaining the
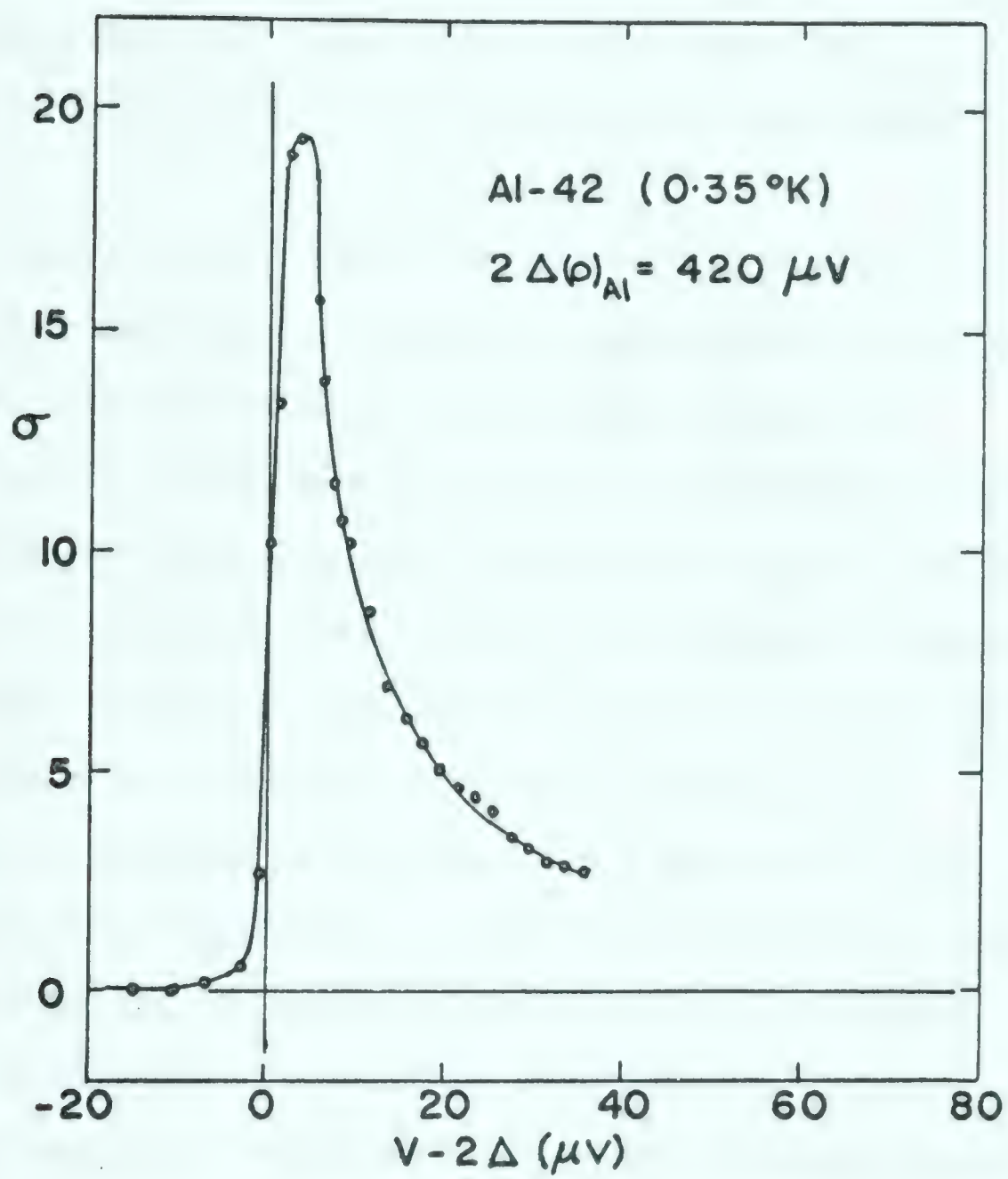
energy gap value is the one prescribed by Giaever et al

(1962). The prescription is somewhat arbitrary but

experimentally convenient.

B. Phonon Effects for Lead, Tin, Indium and Aluminum

1. Lead. Phonon effects were first observed in

Figure 5.1

First derivative results for aluminum

showing the gap edge singularity.

Al-42 (0.35°K)

$2 \Delta(\varphi)_{Al} = 420 \, \mu V$

lead by Giaever et al (1962). These authors suggested that the variation which they observed in their first derivative characteristic was due to an energy-dependent gap parameter, and they also pointed out that the variations occured in a voltage region near the Debye energy.

Rowell et al (1963) subsequently published detailed first and second derivative experimental results for lead in conjunction with theoretical articles by Schrieffer et al (1963) and Scalapino and Anderson (1964).

We have only studied two lead specimens, and in both cases the observed results were in excellent agreement with published results. The results obtained for one of these specimens are shown in Figures 5.2 and 5.3. Appreciable broadening of the gap edge singularity for lead is evident in Figure 5.2. The slight 'overshoot' of the observed points relative to the BCS curve at 0.4 mv may be due to the superconducting probe distribution. The maximum amplitude value of 4.5 for the characteristic at the gap edge for this specimen is typical of the results obtained for most of the specimens studied here. The largest maximum value obtained for any specimen studied to date has been 20. These values are comparable to the few that have been reported in the literature. The broadening of the gap edge singularity may be due to the thin films used for specimens.

Figure 5.2

First derivative results for lead

showing the gap edge singularity.

Pb-39 (0·35°K)

$\Delta(o)_{Pb} = 1·31 \pm 0·02$ mv

$\Delta(o)_{Al} = 0·18 \pm 0·02$ mv

— BCS
o Observed
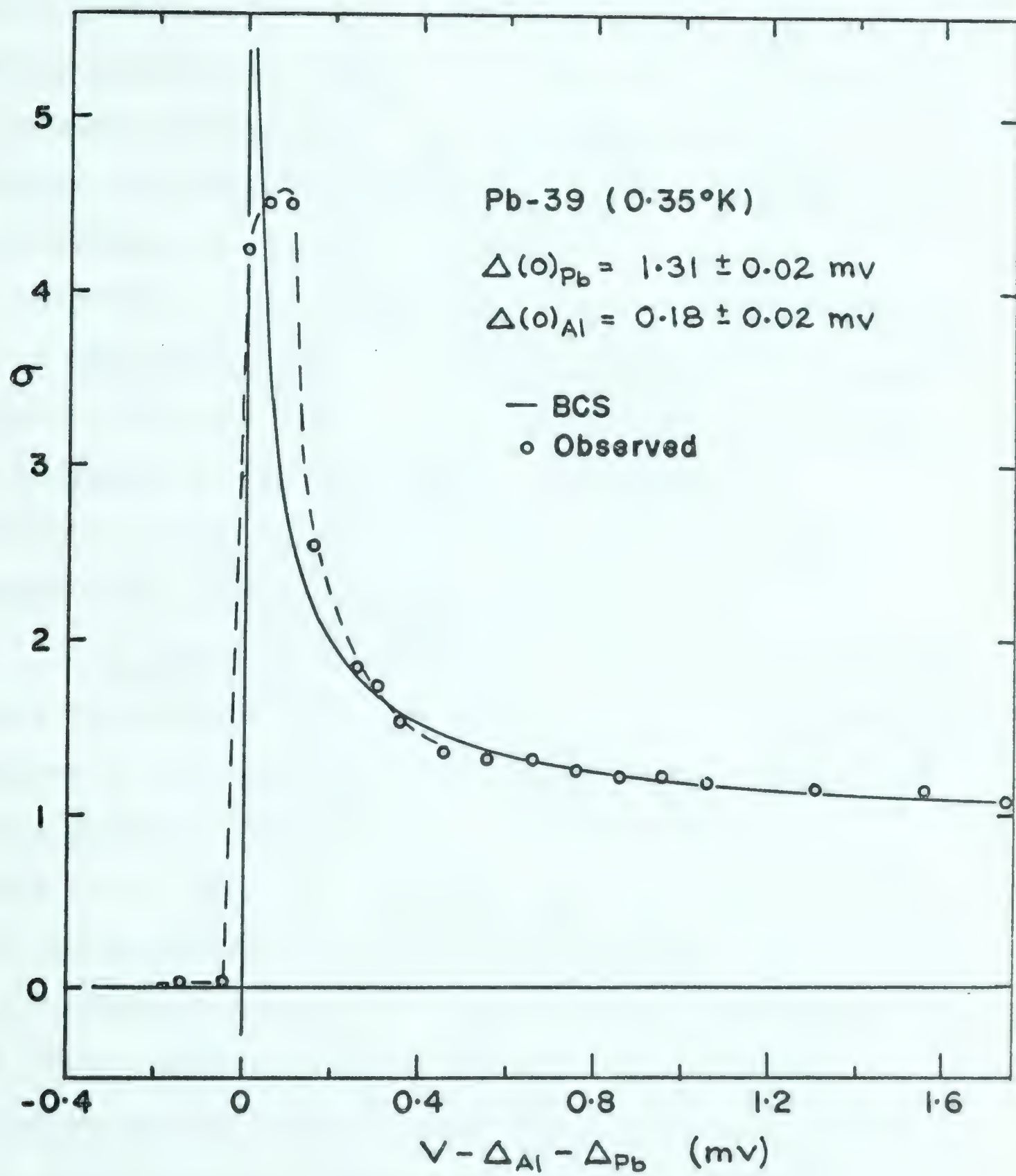
The effect of the transverse and longitudinal phonon groups on the σ characteristic for lead is readily apparent in Figure 5.3. The arrows correspond to predominant transverse and longitudinal phonon energies along symmetry directions for lead observed by Brockhouse et al (1962) with neutron scattering. The Lorentzian shaped curves shown below the experimental points are proportional to the phonon distributions used by Schrieffer et al (loc cit) in their model calculation. The structure at energies above 12 mv appears in Schrieffer's model calculation also and is therefore assumed to be sum and harmonic structure.

2. Tin. First derivative results showing phonon effects for tin have not been published to our knowledge, but Rowell et al have published second derivative results for $Sn-SnO_x-Sn$ tunnel junctions on two separate occasions (Rowell et al (1963) and Scalapino and Anderson (1964)). Three tin specimens have been investigated here and the results obtained from two of them are shown in Figures 5.4 to 5.7. Figure 5.4 shows the normalized first derivative results obtained from specimen Sn-40 at 2.2°K. Phonon deviations are clearly evident at voltages of 4 mv and 16 mv, and smaller deviations are discernible throughout the 4 to 16 mv region. The results shown in Figure 5.5 were obtained with a different specimen and a superconducting probe distribution. It may be seen that

Figure 5.3

First derivative results for lead

showing phonon structure.

Pb-39 (1.2°K)

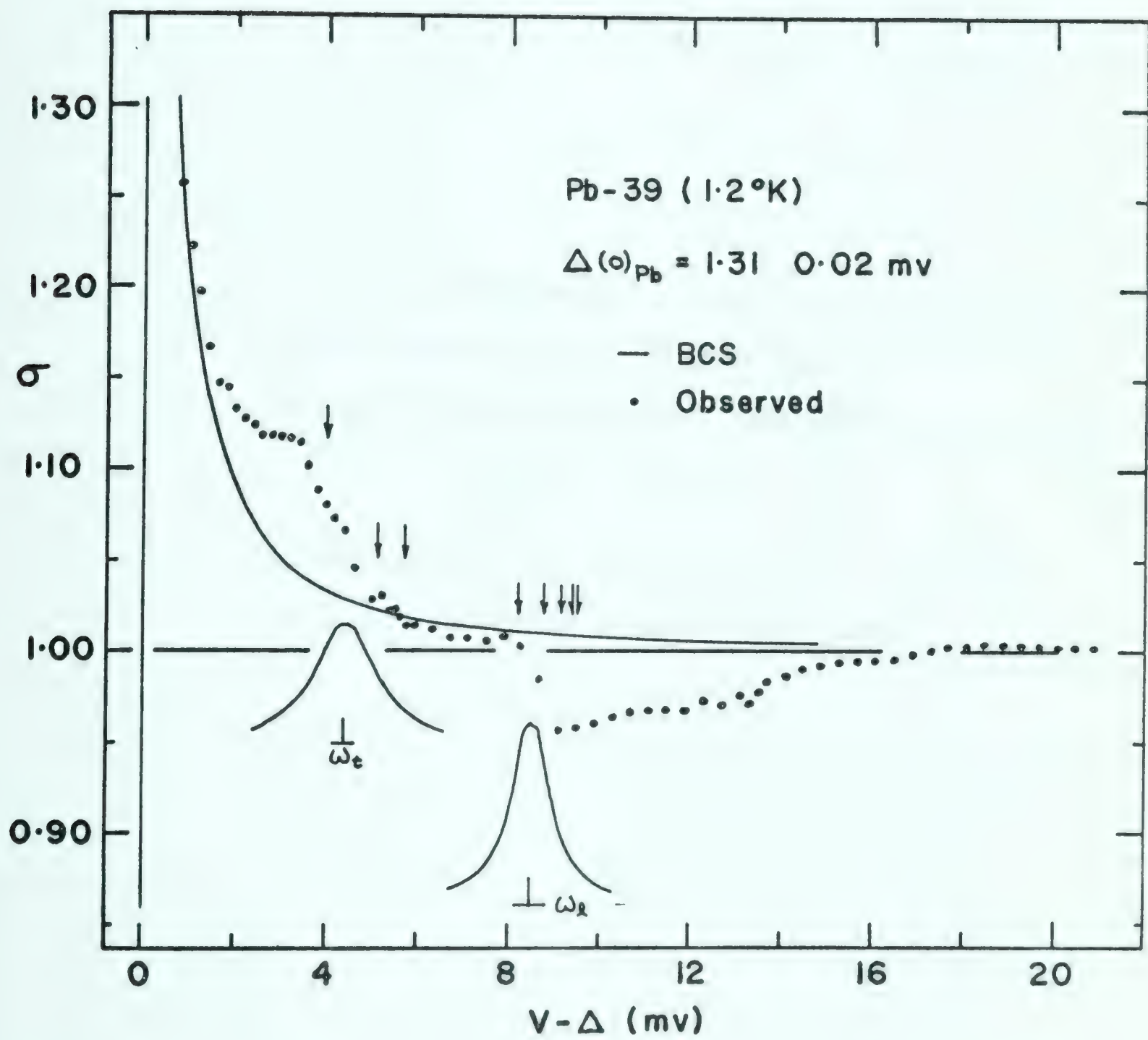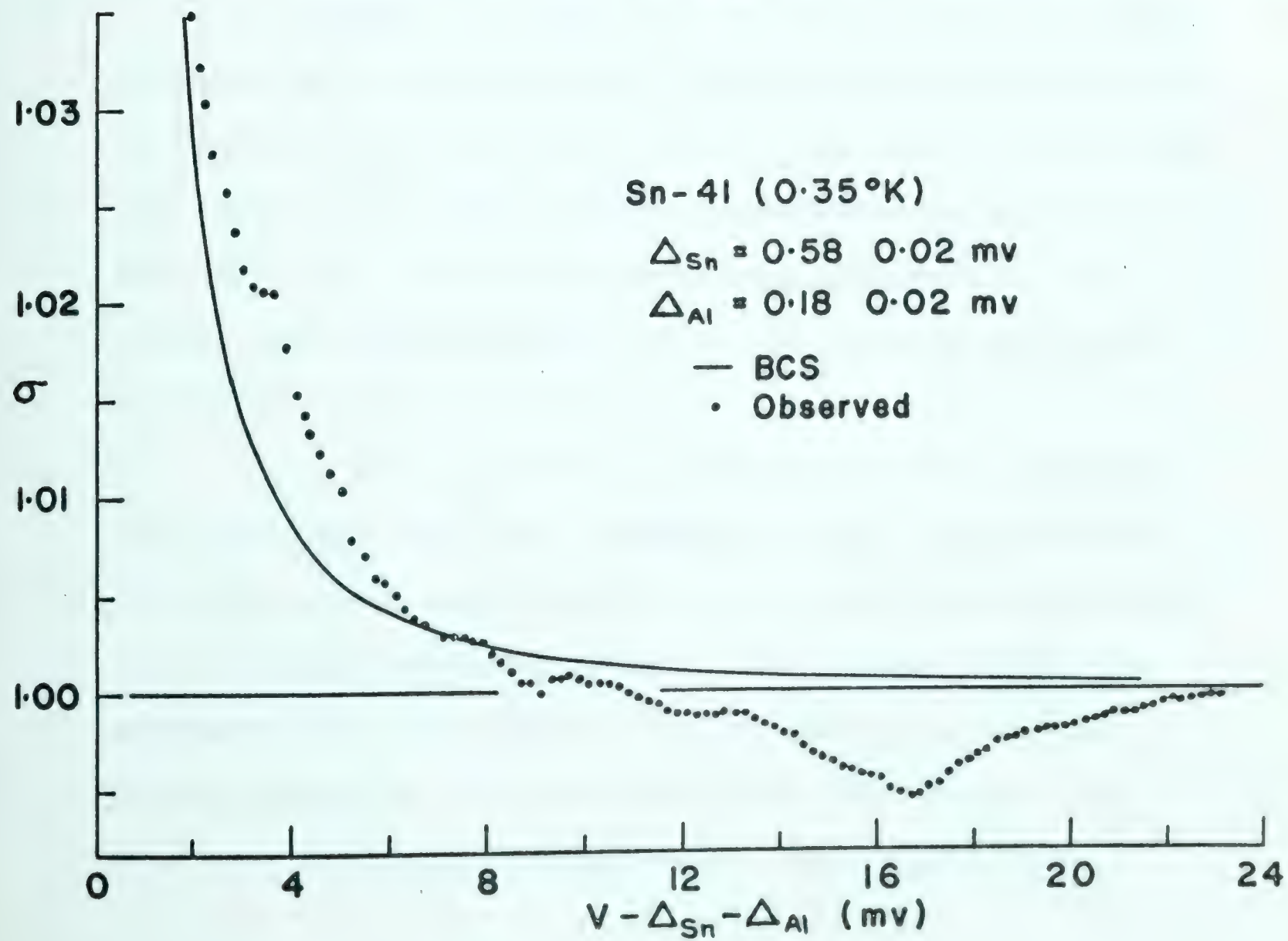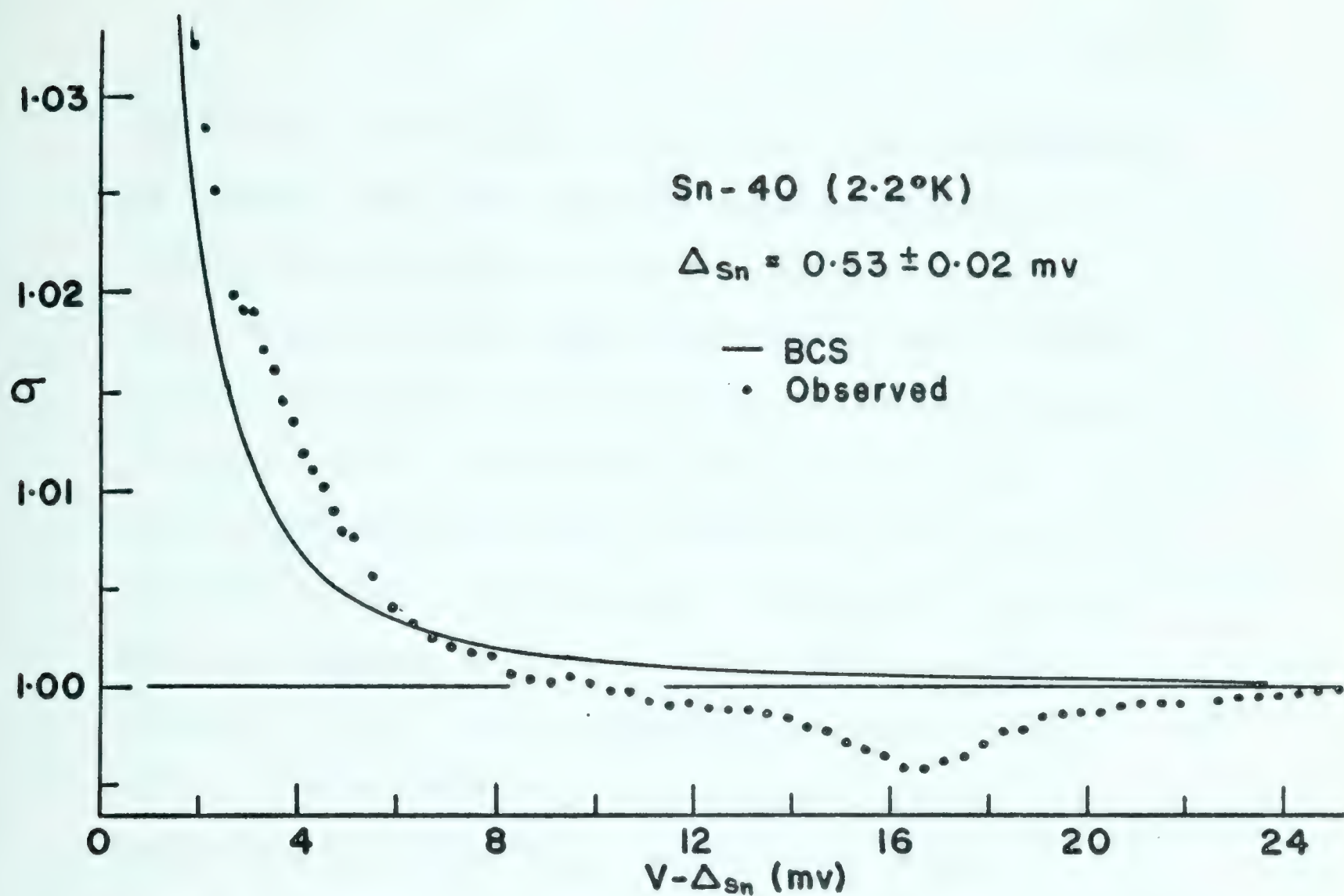$\Delta(o)_{Pb} = 1.31 \quad 0.02$ mv

— BCS
• Observed

Figure 5.4

First derivative curve for tin

at 2.2° K showing phonon structure.

Figure 5.5

First derivative curve for tin

at 0.35°K showing phonon structure.

Sn-40 (2·2°K)

$\Delta_{Sn} = 0.53 \pm 0.02$ mv

— BCS

• Observed

Sn-41 (0·35°K)

$\Delta_{Sn} = 0.58 \ 0.02$ mv

$\Delta_{Al} = 0.18 \ 0.02$ mv

— BCS

• Observed

the phonon effects are reproducible from one specimen
to another, and that the superconducting probe
distribution enhances the small variations. It is
also clear that the phonon spectrum of tin is quite
complex relative to that of lead, as one would expect
from the crystal symmetries (white tin has an
interlinked body centered tetragonal structure, while
lead has a face centered cubic structure). The tin
spectrum appears to have a broad transverse group
at about 4.5 mv, and a longitudinal group at about
16 mv. These energies are $0.3 \omega_D$ and $1.2 \omega_D$
respectively, where ω_D is the Debye energy.

Figure 5.6 shows the second derivative results
obtained by taking first differences from the data shown
in Figure 5.5. This method introduces undue scatter into
the results, so that a visually estimated smooth curve has
been drawn in. The gross structure indicated by the
arrows is in good agreement with the results published
by Rowell et al (loc cit).

A small portion of the original data obtained
from specimen Sn-41 was re-analysed with a protractor-
like instrument which enabled us to read slopes directly
from the projected photographs. The slopes taken were
estimated best fits over a 0.3 mv interval, so that
noise present in the recordings with this period or
less was in effect filtered out. The results were

Figure 5.6

Second derivative curve for

tin at 0.35°K.

Figure 5.7

Expanded portion of Figure 5.6

showing critical point curve fit.
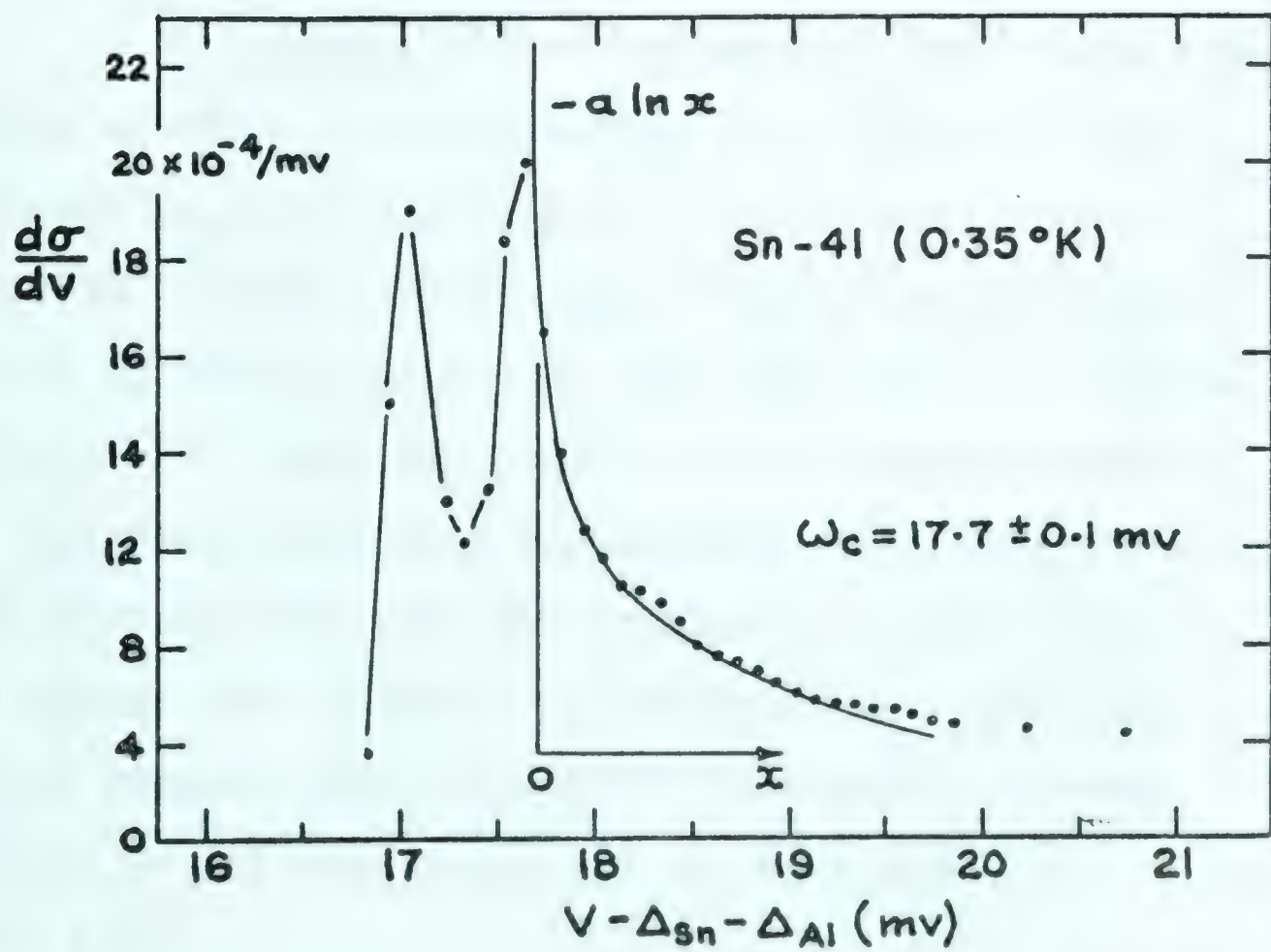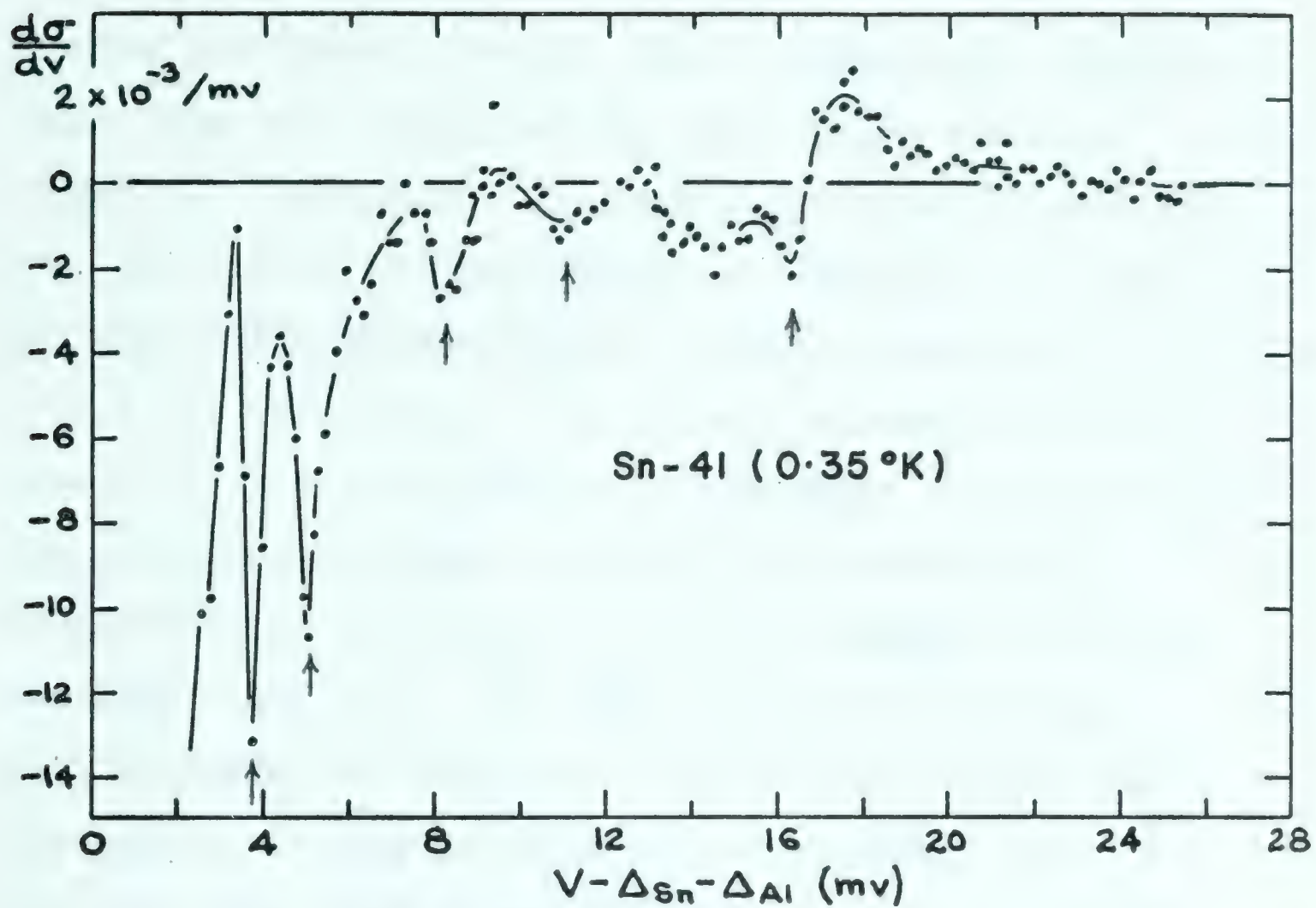
plotted and formed a smooth curve. Tangential slopes were
taken from this curve, and the results are shown in
Figure 5.7 as points. A curve of the form $-a \ln|x|$
has been fitted to these points (cf. page 18). The
critical point energy obtained in this manner is
17.7 $\pm$ 0.1 mv*(1.3 ω_D) and it is in agreement with the
value 17.7 $\pm$ 0.1 mv reported by Scalapino and Anderson
for a $Sn-SnO_x-Sn$ tunnel junction. The absence of a
well-developed singularity on the low energy side of the
critical point (i.e., x negative) is also in accord
with Scalapino and Anderson's results, indicating that
the end point singularity is not sufficiently well
isolated from other phonon effects.

3. Indium. Some preliminary first derivative
results showing phonon structure for indium have been
published by Adler and Rogers (1963). Three indium
specimens have been investigated since then, and the
results obtained from one of them are shown in Figures
5.8 to 5.10. While the quality of the characteristics
has varied slightly from one specimen to the next for a
given type of specimen, the predominant phonon effects
have always been found to be reproducible. The data
for the critical point fit shown in Figure 5.10 were
obtained in the same manner as the data shown in
Figure 5.7.

---

* Uncertainties quoted throughout this work are estimated
  outside limits for a given measurement. Insignificant
  figures will be denoted with a bar.

Figure 5.8

First derivative results for indium
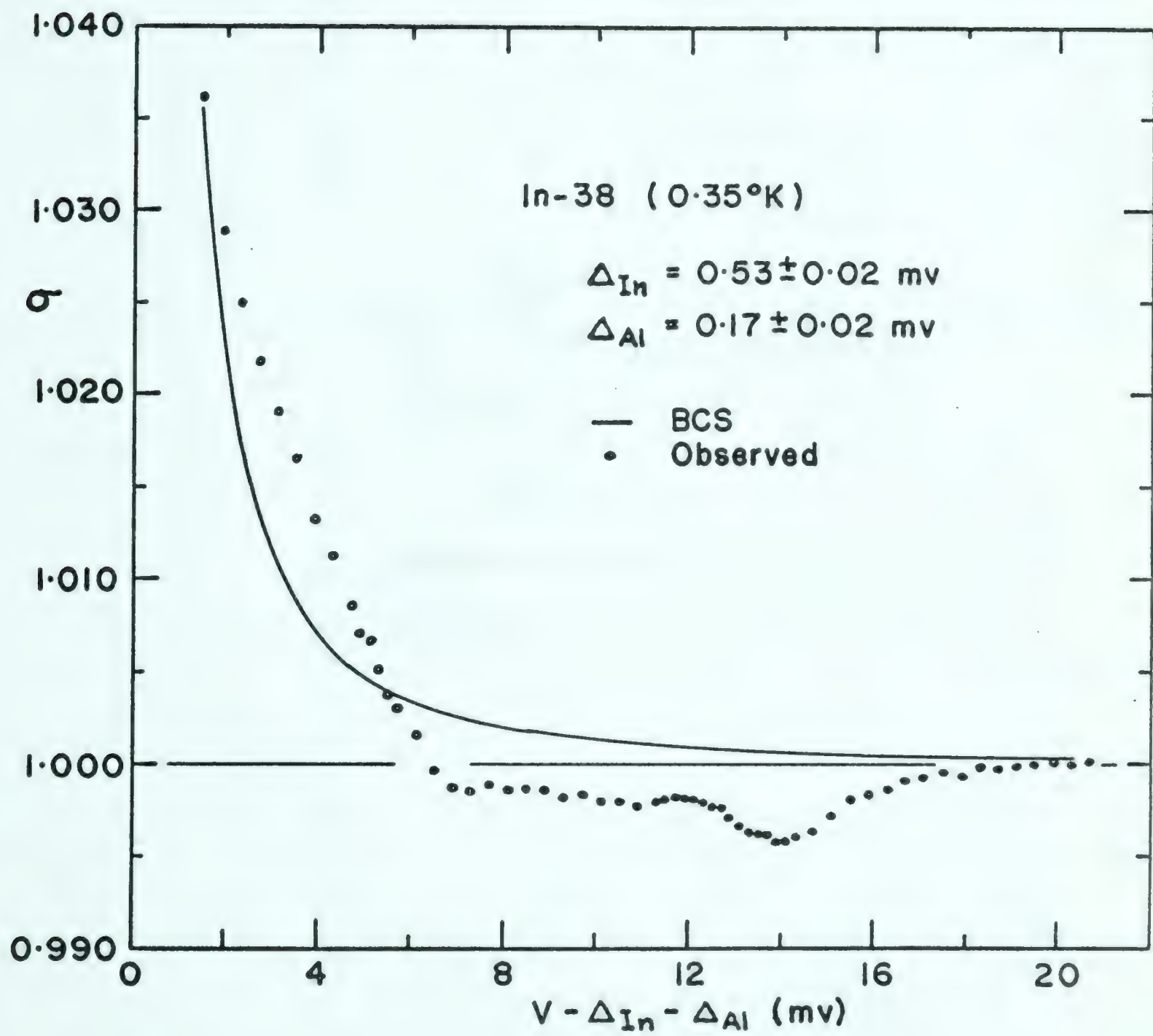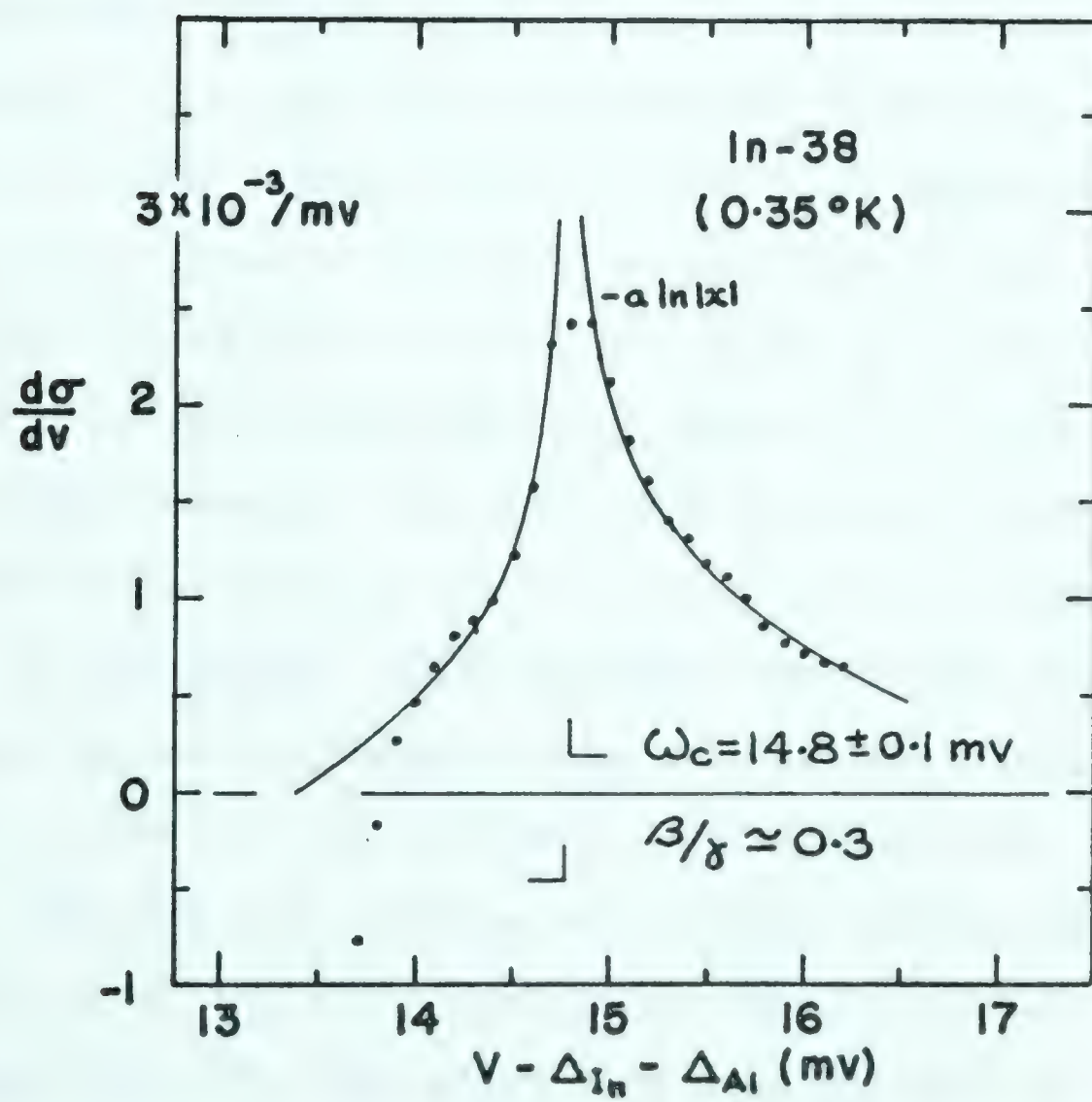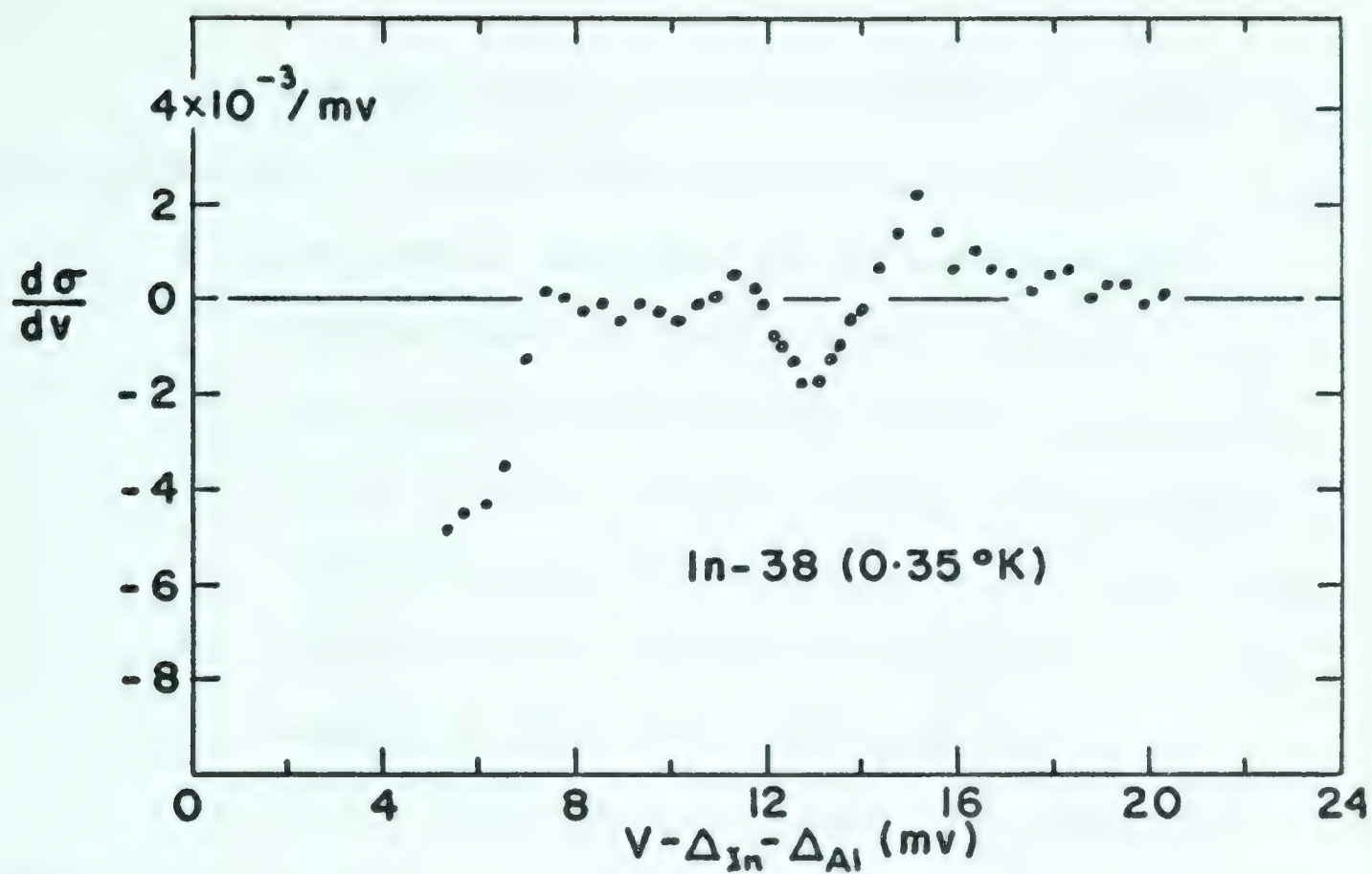
at 0.35°K showing phonon structure.

Figure 5.9

Second derivative results for

indium at 0.35°K.

Figure 5.10

Expanded portion of Figure 5.9

showing critical point curve fits.

One may draw the following conclusions about the
phonon spectrum of indium from Figures 5.8 to 5.10:

 a) the phonon spectrum is of a complexity
      intermediate to that of lead and tin,

 b) the phonon spectrum has a broad transverse
      group at about 5 mv ($0.5\,\omega_D$) and a long-
      itudinal group at about 13 mv ($1.4\,\omega_D$), and

 c) the end point of the phonon spectrum has an
      energy of 14.8 ± 0.1 mv ($1.56\,\omega_D$).

A critical point curve (Figure 5.10) has been
fitted to both sides of the 'singularity' observed in the
second derivative results at 14.8 mv. The fit to the low
energy side of the singularity is somewhat uncertain, but
the critical point energy coincides with that obtained
from the curve fitted to the high energy side of the
singularity. It is thus possible to assign an approximate
value of 0.3 to the ratio β/γ (cf. page 18). The β
and γ curves given by Scalapino and Anderson for lead
suggest that this ratio is of the correct order of magnitude.

     4. Aluminum. Three specimens have been studied
to voltages beyond the Debye energy, but phonon effects
were only observed in one of these. The effects are
very small and are only visible under ideal conditions.
Figure 5.11 shows the first derivative results obtained
for specimen Al-42*. The solid line labeled 'BCS' is

---

* The author wishes to thank Mr. D. W. Penner for
  preparing and mounting this specimen.

Figure 5.11

First derivative results for

aluminum at 0.35°K showing

phonon effects.

AI-42 (0·35°K)

$2\Delta(\circ) = 0.42 \pm 0.01$ mv

$\left.\begin{array}{c}\circ\\ \bullet\end{array}\right\}$ Observed (see Appendix I, Fig·11)
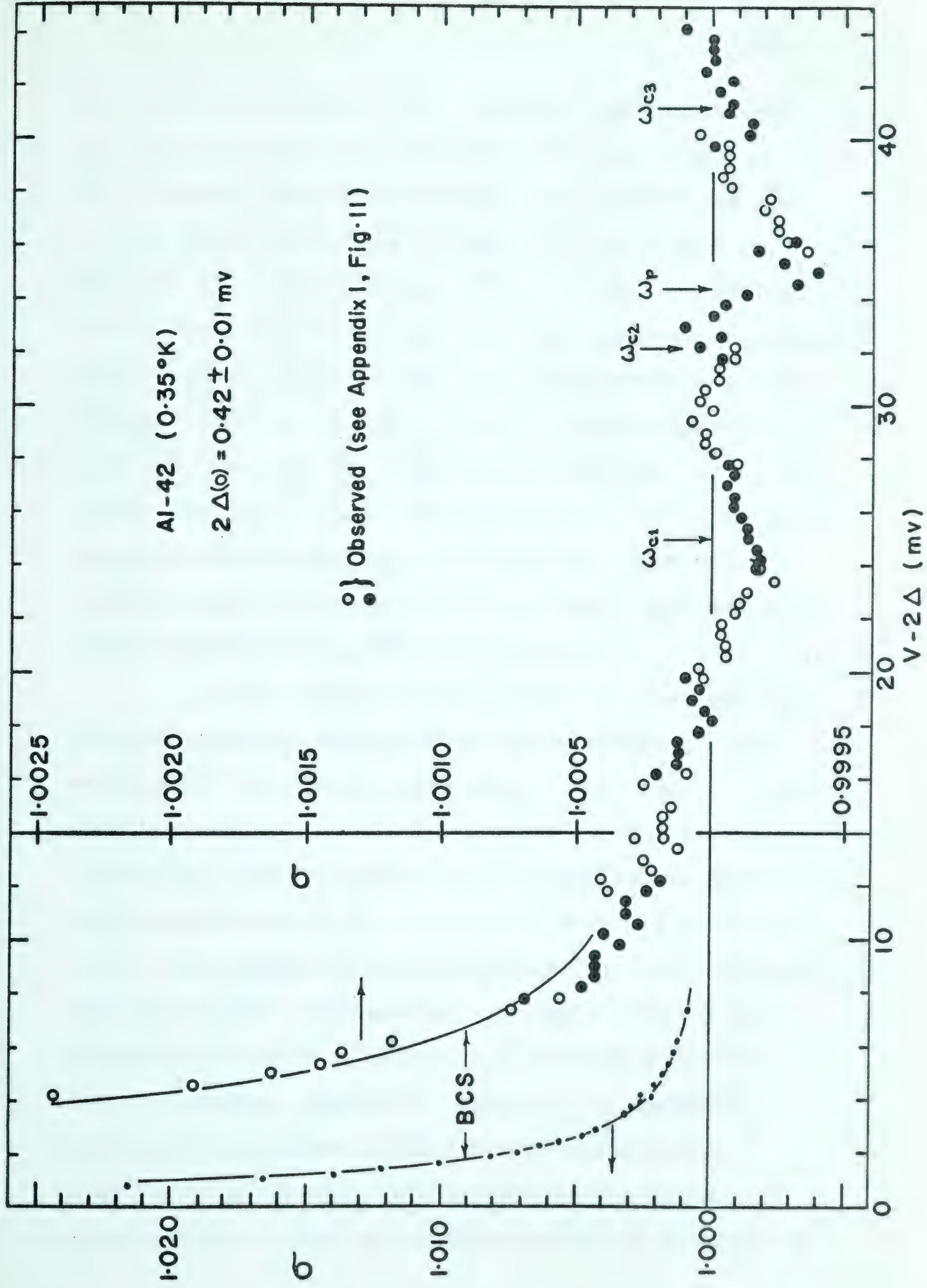
the characteristic for two identical superconductors

as calculated from the BCS theory by Adler (1963).

The agreement between calculated and observed results

is very good for applied voltages of less than 8 mv.

Although it is perhaps speculative to base conclusions

on the results obtained from only one specimen, the small

deviations at higher energies are very probably phonon

effects. The uncertainty in the σ characteristic is

somewhat less than the nominal $\pm$ 0.0003 which we usually

obtain with our present instrumentation. The excellent

behaviour of the specimen is responsible for this low

noise because it allowed us to use higher gain and the

lower attendant bandwidth for recording.

If one estimates the actual σ characteristic

from the observed data, then definite trends are in

evidence at the arrows ω_{c1}, ω_{c2}, and ω_{c3} . These

energies correspond to the end points of the lower

transverse, upper transverse, and longitudinal modes of

the phonon spectrum for aluminum as obtained by Walker

(1956) with diffuse x-ray scattering. At each of these

energies the σ characteristic should be recovering

from the minimum that occurs at a lower energy, and

such a behaviour appears in Figure 5.11. Walker's

results also indicate a strong peak in the phonon

spectrum at an energy corresponding to the arrow

labelled ω_p . The σ characteristic is observed to

decrease rapidly as expected at this energy.

Our results for aluminum are thus in good
qualitative agreement with Walker's x-ray results.
Tunnelling methods may provide more precise values
of the end point energies than are available from
x-ray methods, should a method of lowering the
uncertainty in the observed σ results be devised.
Modest improvements in the techniques of preparing
specimens and recording the results should accomplish
the necessary improvement.

C. Preliminary Results for Mercury

It should be possible to observe phonon effects
in tunnel junctions involving mercury, but such specimens
are difficult to prepare since mercury melts at -40°C.
One such specimen has been obtained in the manner described
on page 35 but the results are unclear due to an
excessive amount of filamentary conduction.

The σ characteristic obtained for this specimen
is shown in Figure 5.12.

The violent flucuations in evidence are definitely
not phonon effects, so that one may only conclude from
Figure 5.12 that the phonon effects in mercury are less than
0.03 in magnitude. This is not a very informative conclusion
as we expect the phonon effects in mercury to have an
amplitude of about 0.01 (see Table 5.1). However, the
BCS trend is clearly in evidence, so that this method of

Figure 5.12

First derivative results for mercury

at 0.35°K. Phonon structure has not

been resolved.

Hg-1 (0.35°K)

$\Delta_{Hg} = 0.82 \pm 0.02$ mv

$\Delta_{Al} = 0.18$ mv (assumed)

— BCS
• Observed
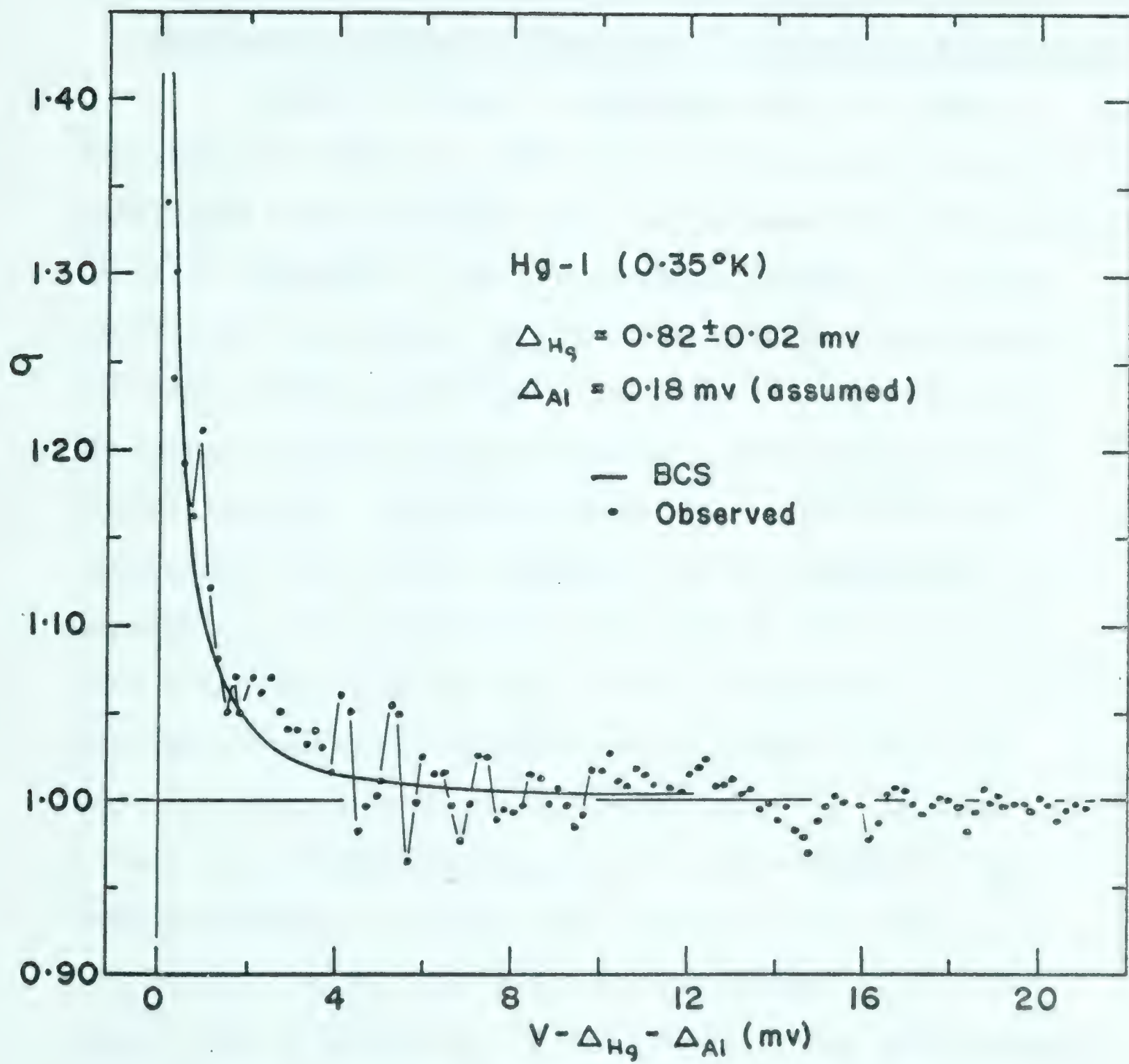
specimen preparation should be capable of yielding good results.

D.   Semi-empirical Equations for the Strength and Temperature Dependence of Phonon Structure in Tunnelling Experiments

Phonon structure experiments are not readily executed, so that it is desirable to know which metals might give phonon effects that can be resolved with a given piece of apparatus. The two limiting factors of primary importance are perhaps the lowest temperature that can be achieved in the cryostat and the resolving power of the apparatus used to obtain the dynamic conductance of the tunnel junction. Empirical knowledge at least of the strength of the phonon structure and its temperature dependence for a given metal in terms of available data would therefore be very useful. Reasonable available data might be taken as the Debye energy ω_D and the energy gap at absolute zero $2\Delta_0$. In order to set up an empirical equation for the strength of the phonon structure, consider the structure for lead. Schrieffer's model predicts a strong minimum in σ just beyond ω_ℓ , where ω_ℓ is the energy of the longitudinal phonon group. The exact nature of the minimum for Schrieffer's model depends on the ratio ω_ℓ/ω_t , the electron-phonon interaction strength, and the Coulomb pseudo-potential. However, since Δ_0 also depends on the latter two quantities and since ω_ℓ/ω_t will not

be widely different for various metals, one might expect the energy dependence of $\triangle_1$ and $\triangle_2$ to be roughly universal from Schrieffer's model. Taking $\omega_t \doteq \omega_D$ and noting that

$$\sigma \doteq \rho_s \doteq 1 + \frac{\triangle_1^2 - \triangle_2^2}{2\omega^2}$$

for

$$\omega \gg \triangle = \triangle_1 + i\triangle_2 ,$$

one might then expect

$$S_0 \equiv 1 - \sigma_{min} \doteq C\left(\frac{\triangle_0}{\omega_D}\right)^2 ,$$

(5.1)

where S_0 is the strength of the phonon structure at 0°K, σ_{min} is the normalized dynamic conductance at the minimum of the predominant structure appearing at perhaps 1.2 ω_D , and C is a proportionality constant which we shall assume is the same for both strong and weak-coupling superconductors.* If one assumes further that the temperature dependence of $\triangle_1$ and $\triangle_2$ is the same as that of the BCS half gap energy $\triangle(T)$, then

$$\frac{S(T)}{S_0} \doteq \left(\frac{\triangle(T)}{\triangle(0)}\right)^2 .$$

(5.2)

This equation gives the temperature dependence of $S(T)$ in terms

---

* The weak coupling superconductors are those for which $N(0)V \ll 1$, where $N(0)$ and V have the same meaning as in section II A. While the BCS theory is restricted to the weak coupling limit in some cases, Schrieffer's approach is believed to be free of this restriction.

of that given by the BCS theory for the energy gap, so that

$\dfrac{S(T)}{S_0}$ may be exhibited directly as a function of the

reduced temperature $t = T/T_c$.

Since the energy gap in lead, tin, indium and aluminum is developed essentially to its zero temperature value at the lowest temperature available in the He^3 cryostat, it has been possible to evaluate C in equation 5.1 for these four metals. The results are shown in Table 5.1.

Table 5.1

Observed Phonon Structure Strengths

Metal	S (x 10-3)	C
	observed	
Pb	43	1.9
In	4.5	1.5
Sn	5.1	2.9
Al	0.17	4.2
	estimated	
Hg	8.5	2

The value of S_o observed for an Al-Al specimen was 3.5×10^{-4}. This value is expected to be more than twice the value which one would obtain with an n-s system, and since the values for lead, indium, and tin correspond to those for n-s systems, the value $S_o = 1.7 \times 10^{-4}$ has been entered for aluminum in Table 5.1. The values obtained for C may be seen to be essentially constant relative to the large variation of S_o .

The value of S_0 may be calculated for mercury using this value for C, and we see that the phonon structure in mercury should be readily resolved with the apparatus used here.

The temperature dependence of $S(\tau)$ has been observed for lead and indium. The results obtained are shown in Figure 5.14, and are in reasonable agreement with equation 5.2.

Equations 5.1 and 5.2 would thus appear to be useful empirical guides for proposed phonon structure experiments on weak-coupling superconductors.

Figure 5.13

Observed temperature dependence
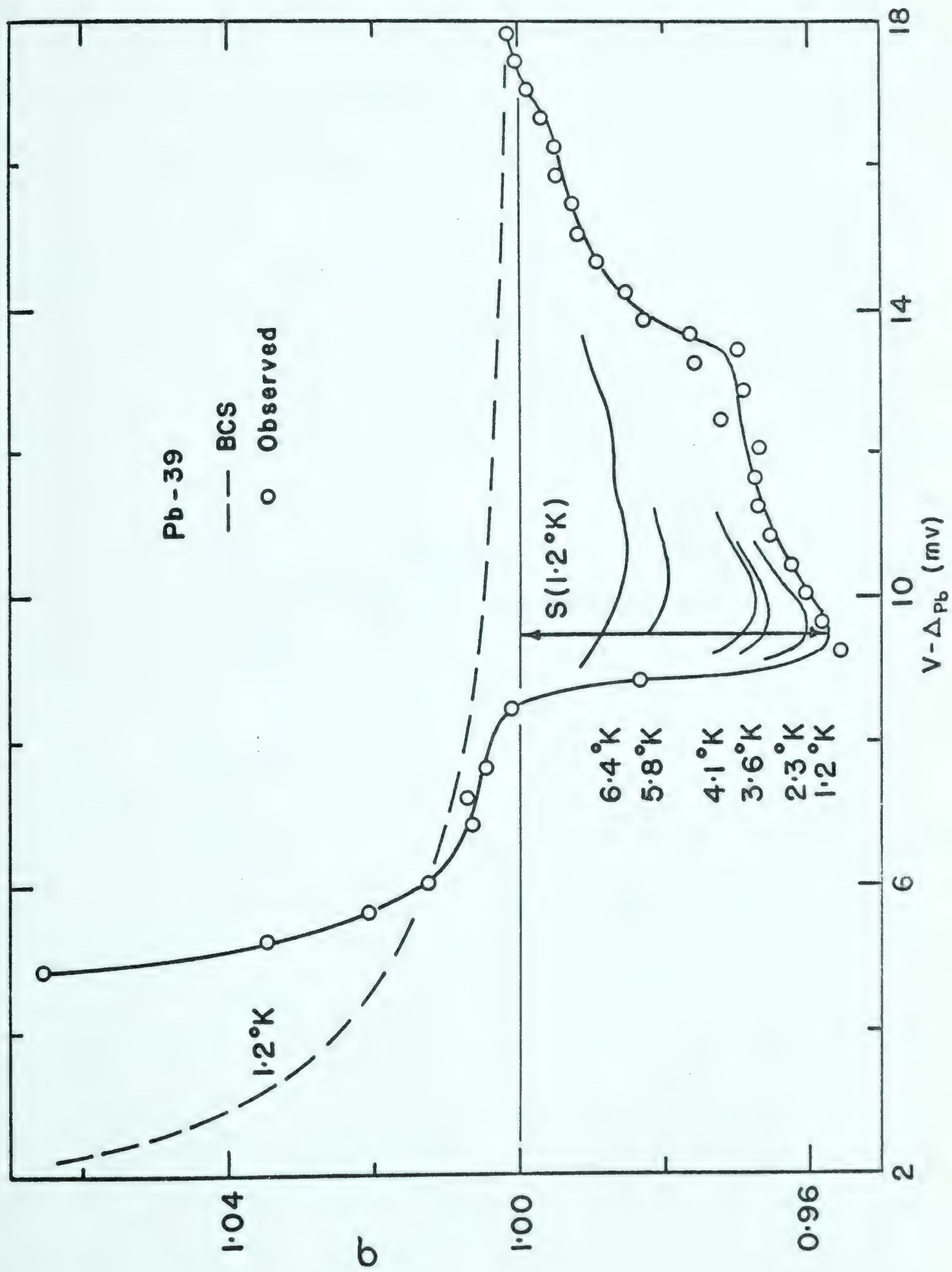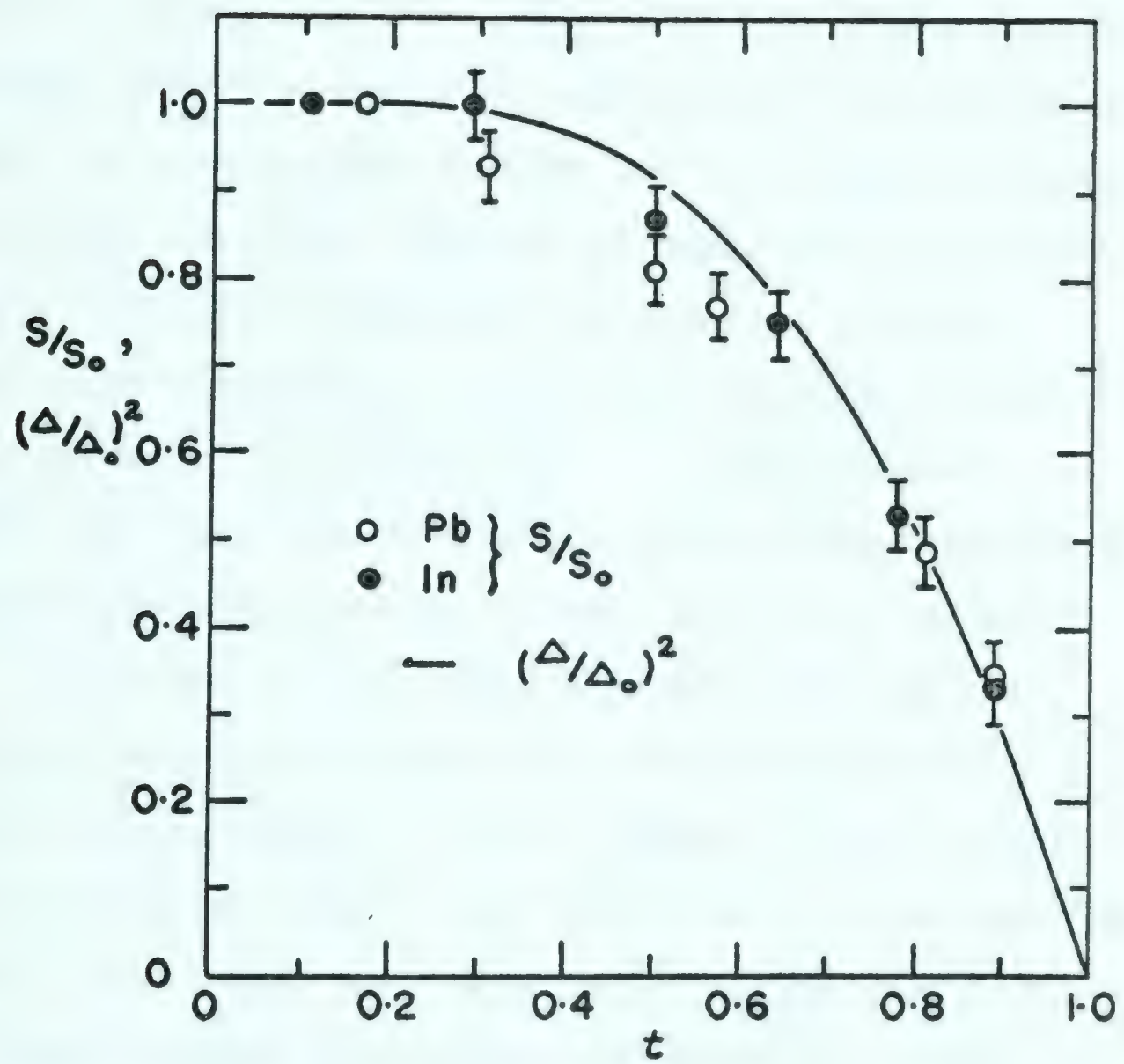
of the first derivative curve for lead.

Figure 5.14

Experimental test of equation 5.2

CHAPTER VI

TUNNELLING CHARACTERISTICS IN THE ENERGY GAP REGION

A. Josephson Currents and Double Particle Tunnelling.

Two mechanisms are known to exist for conduction within the energy gap (i.e., for $V < \Delta$). These are the Josephson current mechanism[1], which gives rise to a d.c. current for zero applied voltage and to a high frequency a.c. current for small applied voltages; and the double particle tunnelling mechanism[2] which gives rise to a current jump followed by a conduction increase at each of the voltages Δ_a and Δ_b . Both processes require that both metallic layers of the tunnel junction be superconducting, and are favored by a thin barrier layer. Since we have not used unusually thin barrier layers for the phonon experiments described here one would not expect either of these effects to be strongly evident in the gap region characteristics for our specimens. However, the current that appears in the gap region of the current-voltage characteristics shown in Figures 6.1 and 6.2 may be attributable to double particle tunnelling if one assumes that the current jump at Δ_{Al} has not been resolved. The temperature-independent linear

1. Josephson (1962)
2. Schrieffer and Wilkins (1962), Taylor and Burstein (1962), Adkins (1963).

Figures 6.1 to 6.4

Current-voltage characteristics which
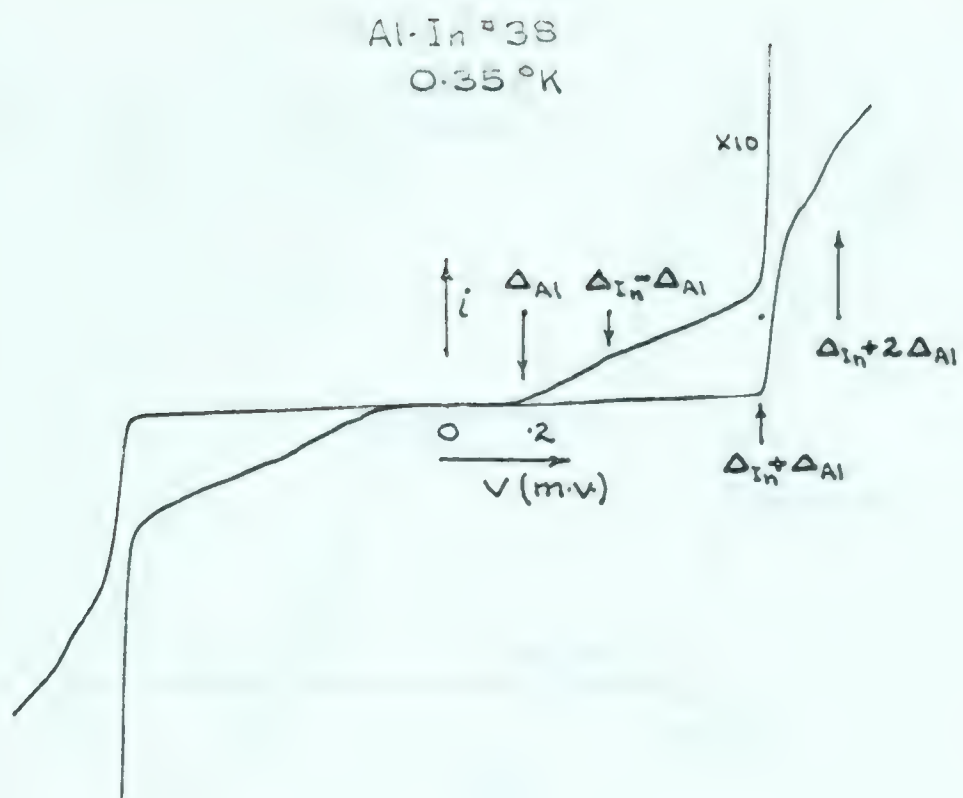exhibit double particle tunnelling
effects.

Figure 6·1
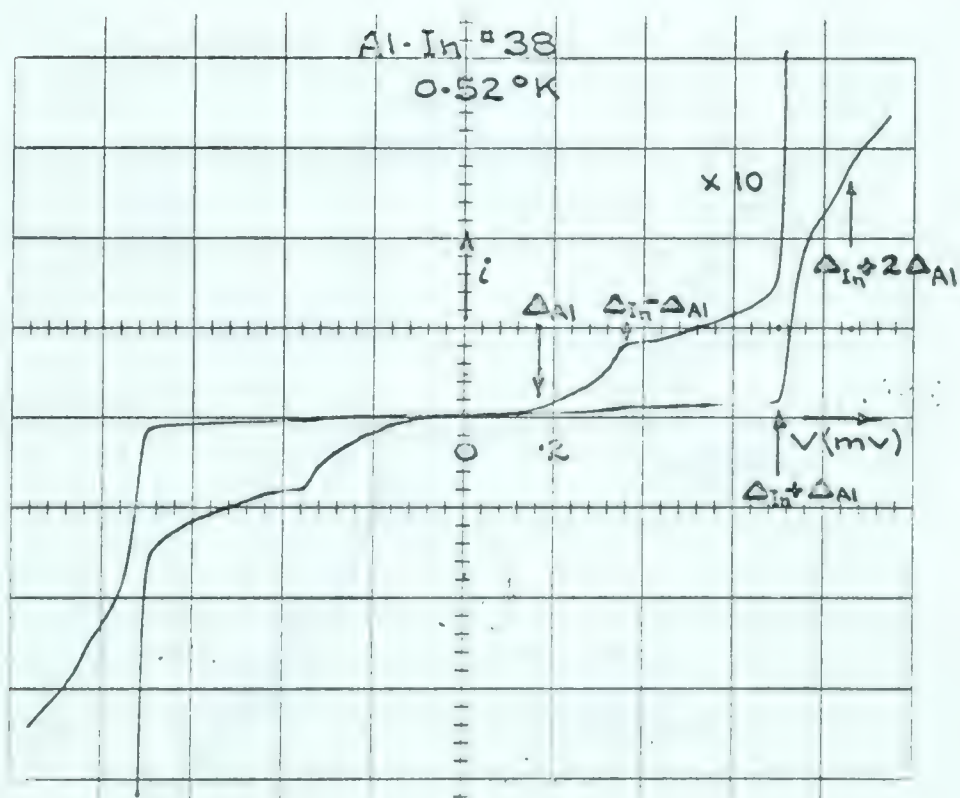
Figure 6·2
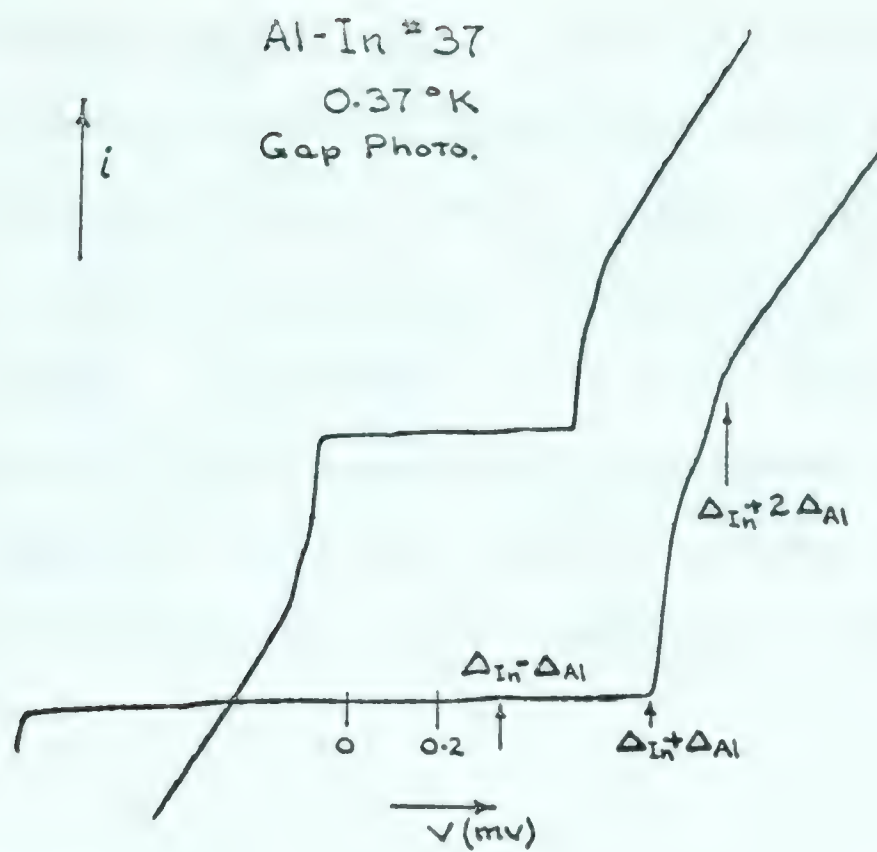
Figure 6·3
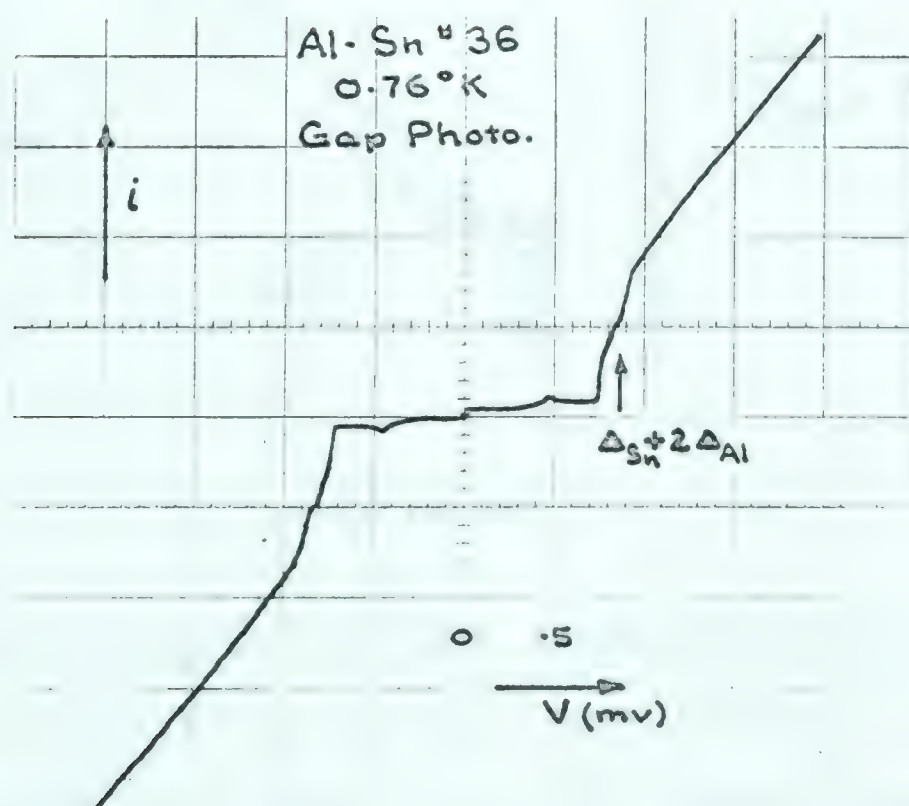
Figure 6·4

increase in current beyond Δ_{Al} is in qualitative
agreement with double particle tunnelling results obtained
by Taylor and Burstein using a Sn-Tl tunnel junction. One
may also see a further increase in conduction at

$V = \Delta_{Ma} + 2\,\Delta_{Al}$ in Figures 6.1 to 6.4. This is the
energetic threshold for a double particle tunnelling process
in which two electron pairs are broken up in M_a and two
excited pairs are produced in the aluminum, as indicated in
Figure 6.5.
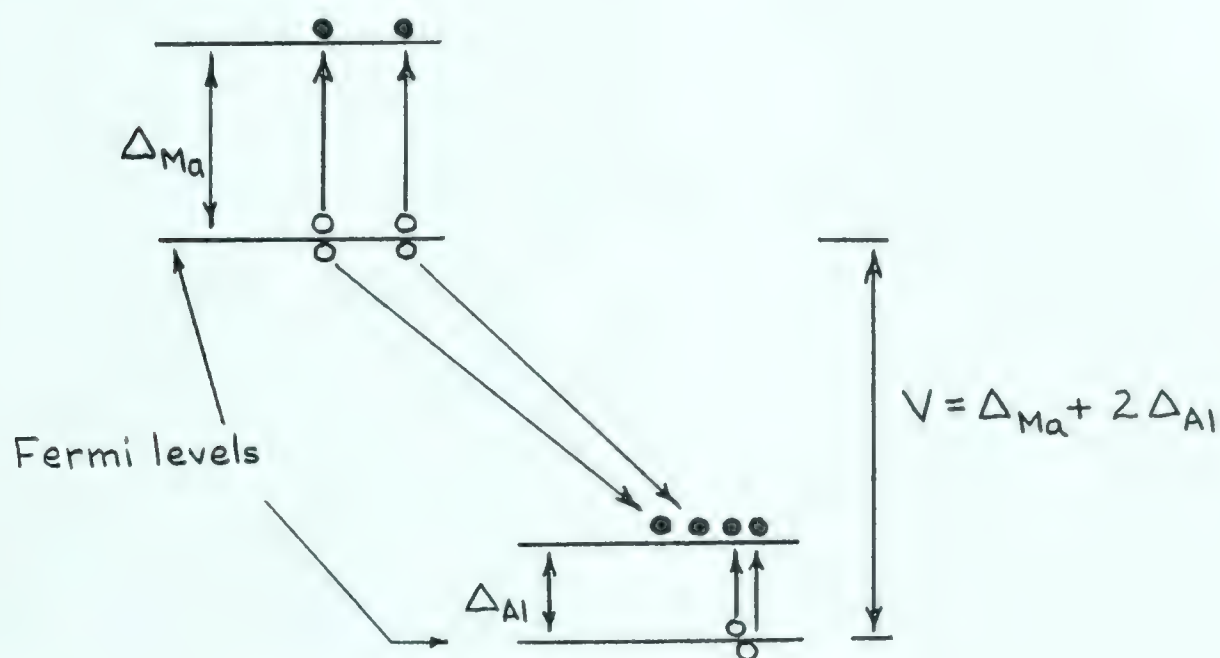
Figure 6.5

A possible double particle tunnelling process. The
initial states are shown as open circles, and the
final states as filled circles. Energy conservation
requires that the energy gained by the two electrons
in crossing the potential difference V be equal to
or greater than the energy of the final excited states.

It is not clear however why such a mechanism should produce effects in the current-voltage characteristic which are much stronger than the double particle tunnelling effects in the energy gap region.

As one would expect, Josephson currents have not been observed.

B. Filamentary Conduction

Figures 6.6 and 6.7 show current-voltage characteristics in the gap region which display a current jump at the origin as is expected for the d.c. Josephson current. However, the characteristics do not drop to zero just off the origin, so that some other conduction mechanism must be responsible. Giaever (1960) has explained a similar behaviour in an $Al-Al_2O_3-In$ tunnel junction by assuming a metallic bridge pierces the oxide layer. The bridge was assumed to contribute negligible conduction in the normal state. An order-of-magnitude estimate for one of our specimens based on the bulk resistivity of aluminum at room temperature gave a bridge diameter value of 0.1 $\overset{o}{A}$. A bridge would only be conceivable if it had a diameter about two orders of magnitude greater than this, which is still plausible for this model. It does suggest that the bridges are very fine filaments.

The behaviour of the Pb-39 characteristic shown in Figure 6.7 might then be explained as follows:

The barrier layer was pierced by two aluminum filaments with different cross-sections. The resistance-current characteristic for the filaments is assumed to have a broad transition at the critical current. As the voltage across the junction was increased the current in the filaments would remain relatively constant near the critical value, but once the filaments became normal the heat

Figure 6.6

The current-voltage characteristic

for a tin specimen showing filamentary

conduction.

Figure 6.7

The current-voltage characteristic

for a lead specimen showing filamentary
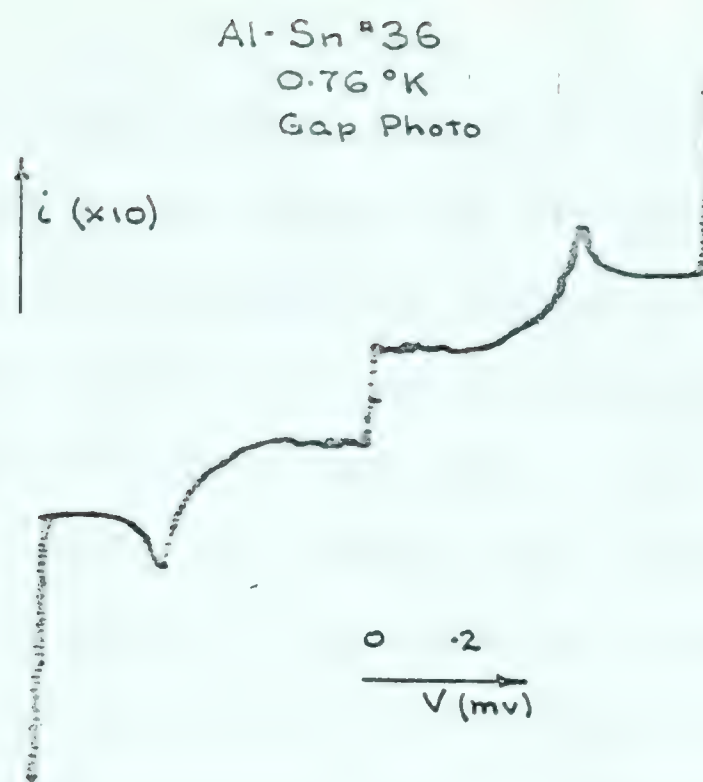
conduction.

Al·Sn #36
0·76 °K
Gap Photo

i (×10)

0   ·2
V (mv)

Figure 6·6

Al·Pb #39
0·34 °K

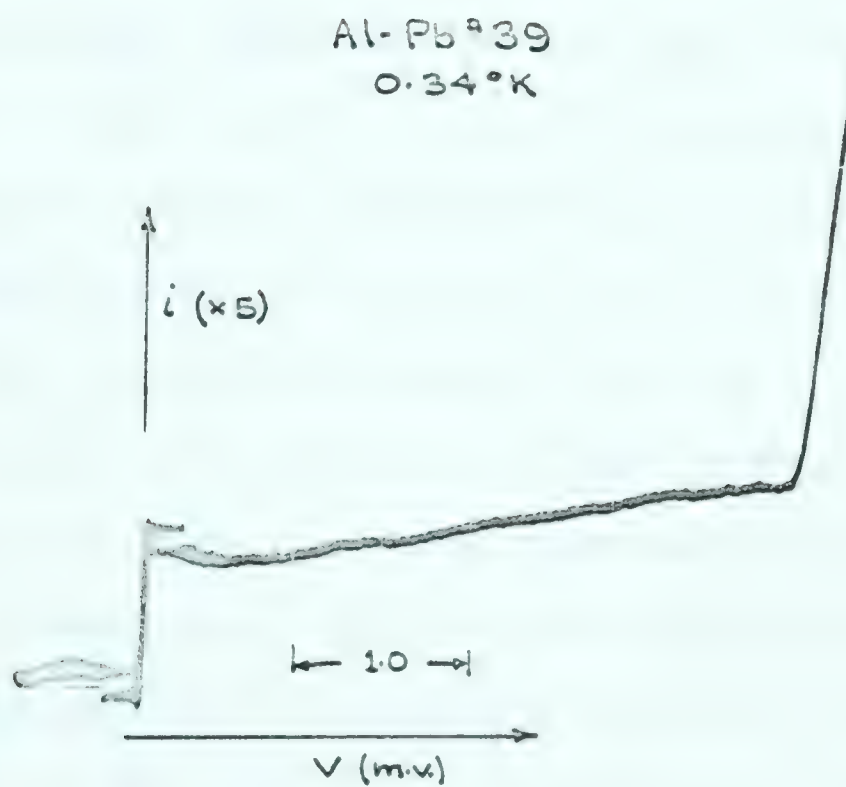i (×5)

|← 1·0 →|

V (m.v.)

Figure 6·7

generated in them would prevent them from becoming

superconducting until the voltage was reduced well

below that for which the filaments became normal. The

smaller of the two filaments in the characteristic shown

in Figure 6.7 thus appears to have had an upper critical

voltage of 0.2 mv, while the stronger one persisted in

the superconducting state for voltages in excess of the

gap voltage. It must eventually have become normal

however since at large voltages the σ characteristic

for this specimen normalized to unity. The choice of

two filaments for the explanation of Figure 6.7 is quite

artificial. It would seem more reasonable to assume

that there are either a great many filaments or none at

all in a particular specimen. A multiply bridged specimen

should have a large number of small discontinuities through-

out its current-voltage characteristic. These small

discontinuities should be apparent on our δv-v recordings

because of the large gains employed for δv . This was

in fact where we first encountered this type of specimen

fault. Figures 6.8 to 6.10 show this behaviour for specimens

Sn-36, Pb-39, and Hg-1. The filaments in the tin and lead

specimens appeared to be aluminum, since the current jumps

at the origin of the current-voltage characteristics

disappeared near the transition temperature for aluminum.

Useable phonon characteristics were thus obtainable for

these specimens at 2°K. The filaments in the mercury

Figures 6.8 to 6.10

$\delta v - v$ recordings showing erratic

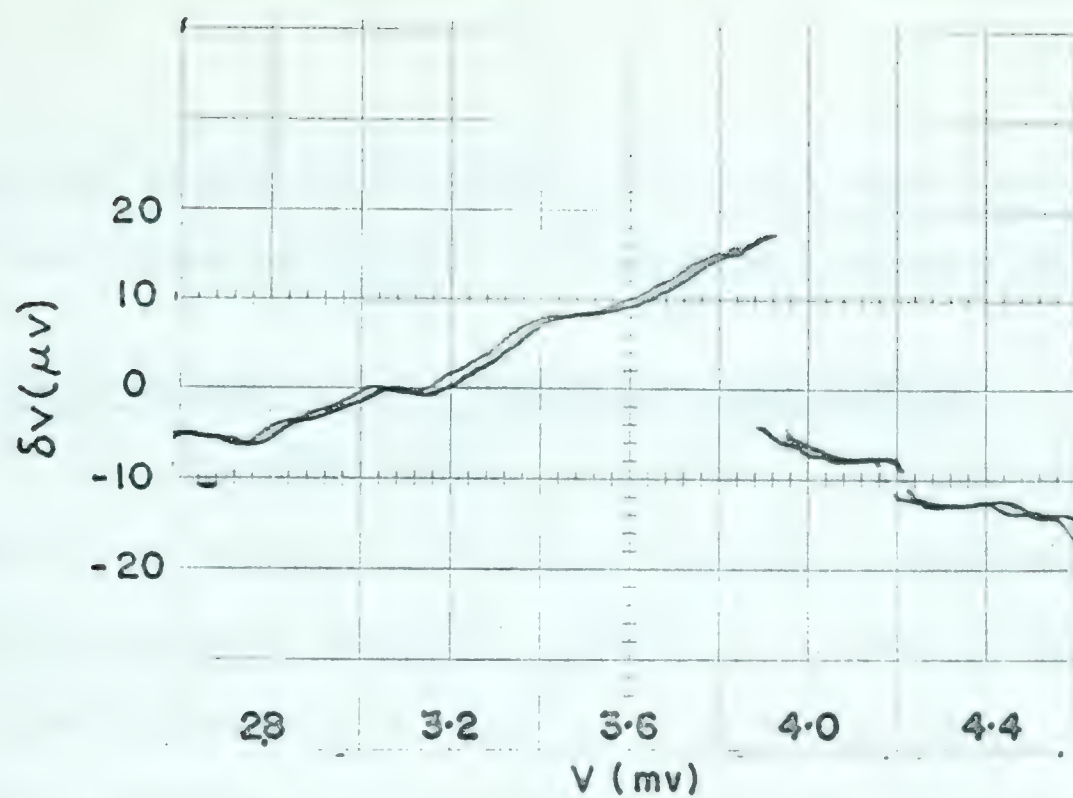behaviour due to filamentary conduction.

Figure 6·8

Hg-1
(0·35°K)
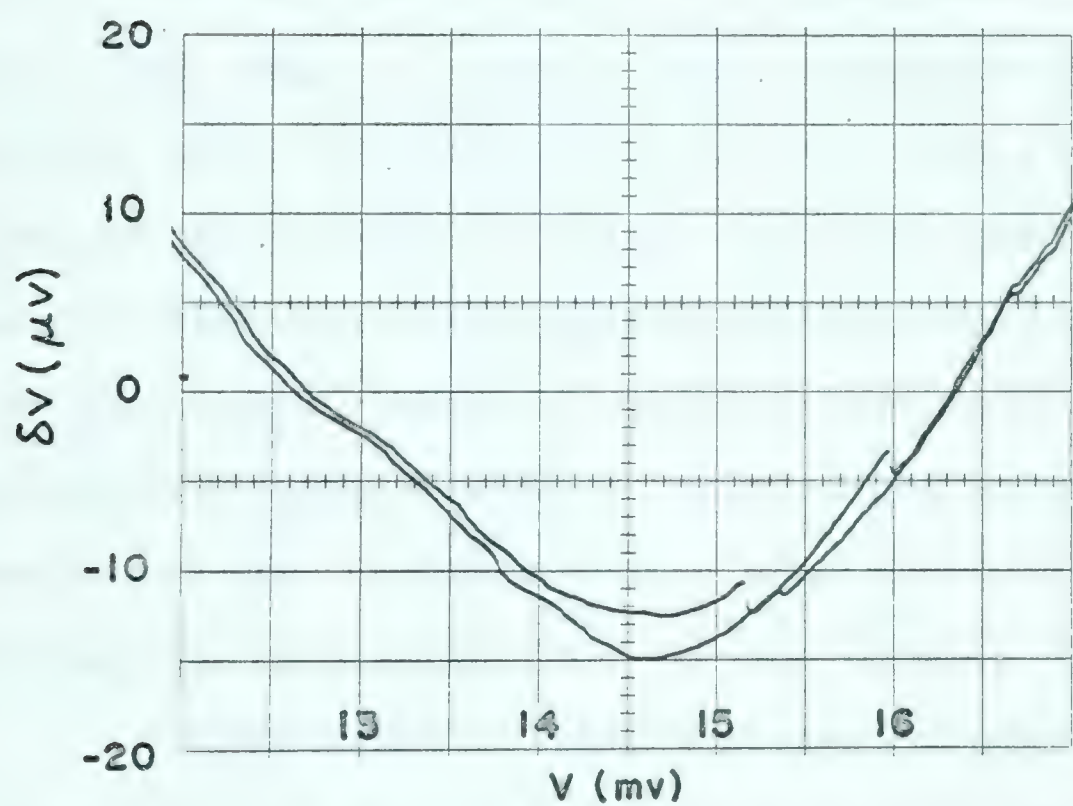
Figure 6·9

Pb-39
(0·35°K)
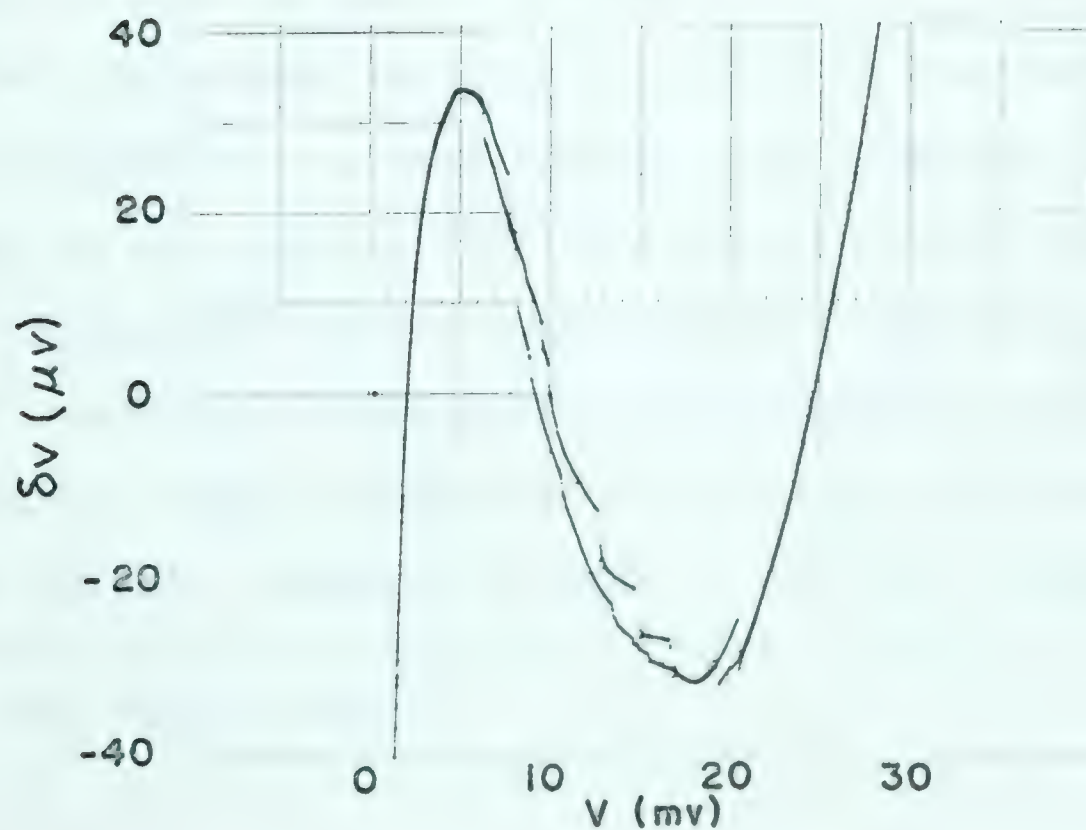
Figure 6·10

Sn-36
(0·8°K)

specimen appeared to be mercury, and were quite strong,
so that useable phonon characteristics were not obtained.

C. Broadening of the Gap-edge Singularity

The BCS theory predicts a singularity in the
density of states at the gap edge of a superconductor,
and this should manifest itself as a jump discontinuity
in the current at a voltage $V = \Delta_a + \Delta_b$ for a
tunnel junction consisting of two superconducting metals
M_a and M_b. Such a jump discontinuity is never
observed, which indicates that the gap edge singularities
in the actual density of states functions are 'smeared.'
Giaever (1962) has investigated the gap edges using a
$Sn-SnO_x-Sn$ tunnel junction, and has been able to get
reasonable agreement between observed and calculated
current-voltage characteristics when Hebel-Slichter
smearing* is introduced into the BCS density of states.

Other forms of smearing might produce agreement
that is just as good. In fact the major contribution of the
Hebel-Schlichter smearing according to Giaever's calculations
is to produce a linear current rise from zero instead of a
jump at the gap edge and this result may be obtained simply
by truncating the BCS distribution. The calculations with
the truncated distribution are immensely simpler than
Giaever's and we shall now outline them in order to compare
the smearing observed in some of our Al-Al junctions to that

---

* See Adler (1963).

observed by Giaever for tin.

In order to set up the truncation we denote the BCS distribution factor by G, where

$$G = R_p \left(1 - \left(\frac{\Delta}{\omega} \right)^2 \right)^{-1/2} .$$

Measuring energy from the gap edge in units of yields

$$G \doteq (2x)^{-1/2} ,$$

where $\quad x = \frac{\omega - \Delta}{\Delta} .$

The area under this curve between zero (the gap edge) and α is $2(2\alpha)^{1/2}$. Thus we are led to adopt the truncation form

$$G_s = \begin{cases} 0 & , \quad x < -\alpha \\ (2\alpha)^{-1/2} & , \quad -\alpha < x < \alpha \\ (2x)^{-1/2} & , \quad \alpha < x \ll 1 \end{cases} .$$

where G_s is to represent the smeared BCS density of states factor. The current-voltage characteristic for a symmetrical tunnel junction* is then calculated as the convolution of G_s with itself. This produces a linear increase in the current when only the truncated portions of G_s are effective, and the resulting normalized dynamic conductance is readily calculated to be

$$\sigma = \frac{1}{2\alpha} \quad \text{for} \quad 2\Delta(1-\alpha) < V < 2\Delta .$$

---

* A symmetrical tunnel junction is one in which the two metals are the same.

We can apply this result directly to our aluminum results, since we have always used aluminum as our base layer. Three Al-Al specimens have so far been recorded in this laboratory. The current-voltage characteristic of one of them (Al-26) has already been reported by Adler (1963). Approximate values for α are listed in Table 6.1.

Table 6.1

Values of the Gap Edge Broadening Parameter

Specimen	Reference	α
Al-Al 26	Adler	0.10
Al-Al 34	This work	0.03
Al-Al 42	"	0.03
Al-400 Å-Al-500 Å	Giaever (1961	0.02
Al-400 Å-Al-270 Å	"	0.05
Sn-Sn	"	0.03

The α-values for Giaever's specimens were obtained by reading slopes directly from his published current-voltage characteristics. The dimensions shown are the film thicknesses. The α-value which we have taken from Giaever's tin results agrees with the corresponding value for Hebel-Schlichter smearing which Giaever found to give the best fit to his experimental data. Thus our trucation parameter α bears a reasonably close resembence to the Hebel-Schlichter smearing parameter δ . The

rather large α value for our Al-26 specimen may have
been due to a.c. pick-up in our early measuring circuits.
A.C. pick-up from the 60 cycle mains is always present
and it causes our current-voltage characteristics to
be averaged over a voltage width V_p about the applied
voltage V , where V_p is the unwanted a.c. voltage.
The peculiar grounding arrangement of our present
circuitry has been evolved as a direct attempt to
minimize V_p , which we believe is now about 1 μv
or less. We should thus be able to detect α values down
to 0.01 or perhaps less, but a problem will undoubtedly
arise with the present instrumentation if gap smearing
is to studied in detail.

The mechanism for gap smearing is not clear.
Giaever has suggested that strained films are the cause,
while Adler suggests that the thinness of the films is
responsible. Adler's suggestion would appear to receive
some support from a recent theoretical article by Blatt
and Thompson (1963). These authors find that the energy
gap undergoes resonances as a function of film thickness.
The resonance period is of the order of 10 $\overset{o}{A}$, and the
gap averaged over a few periods becomes larger than the
bulk value as the film thickness is decreased. Since
our films are both thin and not uniform in thickness, we
have here a possible explanation for both gap smearing and
for the increased gap value observed for thin films by

Giaever et al (1962) and others. A direct check on the
Blatt-Thompson theory might be effected by measurements
on a series of tunnel junctions prepared with very thin
metal films. A study along these lines is currently
being undertaken by Mr. D. Penner in this laboratory.

D. Some Further Energy Gap Values for Aluminum, Lead,
   Tin, Indium, and Mercury

Table 6.2 shows some energy gap values corrected
to absolute zero obtained during the course of this work.
The ratio $\frac{2\Delta(0)}{T_c}$, where T_c is the bulk transition
temperature and $2\Delta(0)$ is the energy gap value at $0°K$,
is also shown in this table. Some values reported by
other workers for this ratio are included for comparison.
It may be seen that the results obtained by various workers
are not consistent to within the stated uncertainties in
measurement. Part of this inconsistency may be due to the
use of thin film specimens, since Giaever et al (1962)
and others have found that a decrease in film thickness
causes an increase in the energy gap and the film transition
temperature. A more suitable transition temperature for
the ratio $\frac{2\Delta(0)}{T_c}$ might therefore be the value obtained
directly from the tunnelling characteristics*. However,
Douglas and Meservey (1962) have found the ratio $\frac{2\Delta(0)}{T_c}$

---

* The transition temperature determined from the resistance
  of the film itself is probably meaningless due to edge
  effects.

Table 6.2

Energy Gap Values

Reference	Metal	$2\Delta(0)$ (mv)	$\dfrac{2\Delta(0)}{T_c}$ ($\pm$ 0.1)
Giaever et al. (1962)	Pb	2.68	4.3$\overline{3}$
	Sn	1.20	3.7$\overline{3}$
	In	1.05	3.6$\overline{1}$
	Al	0.40	3.8$\overline{7}$
Douglass and Meservey (1962)	Pb	–	4.2$\overline{0}$
	Al	–	3.3 *
Zavaritskii (1961)	Pb	2.66	4.2$\overline{6}$
	Sn	1.12	3.4$\overline{7}$
	In	1.01	3.4$\overline{5}$
	Al	–	3.3$\overline{7}$ *
Bermon and Ginsberg (1963)	Hg	1.61 $\pm$ 0.04	4.5
This work	Pb	2.64 $\pm$ 0.05	4.2$\overline{7}$
	Hg	1.63 $\pm$ 0.04	4.5$\overline{1}$
	Sn	1.16 $\pm$ 0.03	3.6$\overline{1}$
	In	1.09 $\pm$ 0.03	3.7$\overline{5}$
	Al	0.42 $\pm$ 0.02	4.0$\overline{5}$

* Calculated on the basis of the film transition temperature which varied from 1.3 to 1.5°K for different specimens. The remaining ratios are based on the bulk transition temperatures.

where T_c is the "film transition temperature", is still dependent upon film thickness for aluminum films. We have accordingly used the bulk transition temperature for our ratios shown in Table 6.2.

This convention which is also adopted by Giaever et al., is experimentally convenient, since temperatures need not then be measured with precision.

The ratio $\frac{2\Delta(0)}{T_c}$ given in Table 6.2 for aluminum is abnormally high. In this case the transition temperature of the films as observed from the tunnelling characteristics was $1.40 \pm 0.05°K$, giving a ratio

$$\frac{2\Delta(0)}{T_c} = 3.5 \pm 0.1$$. This rather large discrepancy between the film transition temperature and the bulk transition temperature for aluminum appears from the literature to be a characteristic of that metal in that the corresponding effect is observed to be far less pronounced for lead, tin, and indium.

CHAPTER VII

CONCLUSION

A. Results for Lead, Tin, and Indium

The phonon structure effects observed in lead and
tin have been in agreement with similar results published
in the literature, while our results for indium cannot
be compared with other published data, observed or
calculated, in that we have not been able to locate any
such data. Some end point energies for the phonon spectrum
of aluminum have been estimated from our aluminum results,
and our estimates agree with Walker's x-ray results to
within the uncertainty of about 3% in the x-ray data.

The values which we have obtained for broadening
of the gap edge singularity and for the energy gaps of the
various metals studied are in good agreement with the
corresponding values which have appeared in the literature,
indicating that the specimens which we have prepared are
comparable to those prepared by other workers in this field.

B. Thermometry Results

Some preliminary work has been done in the use of
tunnel junctions as thermometers, and the results appear
quite promising in that the observed discrepancies are
believed to be due to the experimental arrangement, and
not the tunnel junction itself. For example we find that
it is not possible to lower the temperature of the He^3

chamber below 0.5°K when the indicated vacuum space pressure is above 5×10^{-6} mm Hg., but that temperatures of 0.35°K may be attained for a pressure of 1×10^{-6} mm Hg. Since the specimen chamber has a surface area comparable to that of the He^3 chamber, it is quite plausible that there is still enough heat leak to the specimen chamber at an indicated pressure of 1×10^{-6} mm Hg. to cause our observed discrepancies in temperature.

APPENDIX I

APPARATUS FOR MEASURING CHARACTERISTICS OF SUPERCONDUCTING

TUNNEL JUNCTIONS

The notation $\triangle v$ has been used in this paper for one of the voltages observed. This voltage has been referred to as δv in the preceding text in order to avoid possible confusion with the gap parameter $\triangle$.

Apparatus for Measuring Characteristics of Superconducting Tunnel Junctions*

J. S. ROGERS, J. G. ADLER, AND S. B. WOODS

Department of Physics, University of Alberta, Edmonton, Alberta, Canada

(Received 8 October 1963; and in final form, 4 November 1963)

Much information about the density of electron states in a superconductor may be obtained using electron tunneling techniques. It is of particular interest to measure the normalized dynamic conductance of superconducting tunnel junctions as a function of applied voltage. This quantity is the ratio of the dynamic conductance $(di/dv)_s$ when one or both metallic members of the tunnel junction are in the superconducting state, to the dynamic conductance $(di/dv)_n$ when both members are normal. A new method has been developed which enables measurements to be made of $(di/dv)_s/(di/dv)_n$ to a few parts in ten thousand. With this method only a bridge circuit, a galvanometer amplifier, and an oscilloscope are used. The galvanometer amplifier has a passband from dc to a few cps and an input noise voltage of about 3×10^{-8} rms V. The circuits of the bridge and amplifier are presented and analyzed. The operation of the circuits for measuring the characteristics of low resistance specimens ($\lesssim 500\,\Omega$) is described.

INTRODUCTION

MUCH information about the density of electron states in a superconductor may be obtained using electron tunneling techniques.[1–3] It is of particular interest to measure the normalized dynamic conductance of superconducting tunnel junctions as a function of applied voltage. This quantity is the ratio of the dynamic conductance $(di/dv)_s$ when one or both metallic members of the tunnel junction are in the superconducting state, to the dynamic conductance $(di/dv)_n$ when both members are normal. Those variations in the effective density of electron states in a superconductor which mirror the phonon spectrum can be extremely small in some metals,[2,4] but they have been described theoretically[3] and can be charted experimentally with sensitive conductance measurements. Two methods of making conductance measurements with the requisite sensitivity have been described[1,5] recently. The bridge method described here, although somewhat less direct, is much simpler to construct and is capable of yielding the normalized dynamic conductances

of suitable specimens with an accuracy of a few parts in ten thousand.

A typical tunnel junction between two normal metals is not strongly nonlinear in the region of interest, since the junction resistance only decreases by a factor of two as the applied voltage is increased from 0 to about 250 mV. If such junctions are cooled so that one of the metals becomes superconducting, a strong nonlinearity develops at the origin in the i-v characteristic due to the energy gap in the density of electron states of the superconductor. Also, far weaker deviations from the characteristic obtained for normal metals occur at voltages corresponding to the energies of the transverse and longitudinal phonons in the metal lattice. It is these small deviations that are of specific interest here. They generally occur in the voltage range between 5 and 50 mV where the i-v characteristic is approximately linear. This near linearity is exploited by our bridge but, since highly nonlinear regions can be approximated as closely as one wishes by a succession of sufficiently short linear relations, the apparatus may be used, with a little extra patience, to investigate the energy gap region as well.

THE BRIDGE

Principle of the Method

In Fig. 1 a bridge is shown, one arm of which contains a nonlinear passive element R_x, having a voltage v across it. As long as the input resistance R_g of the preamplifier is large enough, the current through it will be negligible and

* This work was supported by the National Research Council of Canada.
† Present address: Department of Physics, Dalhousie University, Halifax, Nova Scotia, Canada.
[1] I. Giaever, H. R. Hart, and K. Megerle, Phys. Rev. **126**, 941 (1962).
[2] J. M. Rowell, P. W. Anderson, and D. E. Thomas, Phys. Rev. Letters **10**, 334 (1963).
[3] J. R. Schrieffer, D. J. Scalapino, and J. W. Wilkins, Phys. Rev. Letters **10**, 336 (1963).
[4] J. G. Adler and J. S. Rogers, Phys. Rev. Letters **10**, 217 (1963).
[5] D. E. Thomas and J. M. Klein, Rev. Sci. Instr. **34**, 920 (1963).

determination of the current i through R_x becomes a load-line problem involving the i-v characteristic of R_x, the bridge voltage V, and R_a. The right-hand-side of the bridge may be viewed as a load-line problem as well; in particular, if the two upper arms of the bridge are equal, the two load lines will coincide as shown in Fig. 2. If, in addition, a constant voltage V_y is subtracted from the bridge unbalance voltage, a new voltage Δv is obtained. A suitable choice of R_d and V_y will permit Δv to be the voltage difference between the i-v characteristic of R_x and a tangent line to it, as indicated in Fig. 2. It is clear that Δv will be small in the region of v_0 and so may be amplified considerably in presentation. A sequence of such $\Delta v - v$ presentations thus becomes a sensitive map of the nonlinearity of the specimen R_x.

Bridge Equation for a Three Terminal Specimen

The bridge in Fig. 1 uses a three-terminal connection to R_x. In practice, however, four terminal connections to R_x are necessary as lead resistance changes can be appreciable when the specimen changes from the normal to the superconducting state. However, for simplicity the analysis of the three-terminal system will be considered first.

FIG. 1. Bridge circuit with 3-terminal connection to R_x, the nonlinear resistance.
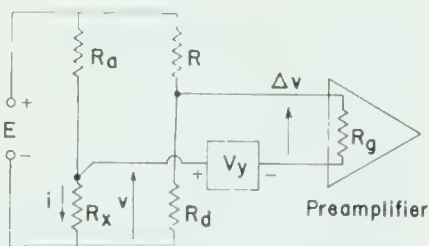
Let R_a in Fig. 1 include the resistance of the upper current lead to R_x, and assume R_g to be large enough that the resistance of the upper potential lead to R_x may be neglected. On the lower end of R_x only one lead is used whose resistance then is part of R_x. On writing three suitable loop equations and solving for i, one obtains

$$i = R(R_a R_d)^{-1}\{v + [1 + R_d R^{-1} + (R_a + R)R_d(R_g R)^{-1}]\Delta v\} + (R + R_d)(R_a R_d)^{-1}V_y. \quad (1)$$

This expression may readily be differentiated with respect to v. If we append subscripts n and s to distinguish between measurements on R_x when both metals are in the normal state and when one is in the superconducting state, respectively, then for $R_d \ll R_g$ and $R_a \approx R$, we may write for the normalized dynamic conductance,

$$g \equiv \frac{(di/dv)_s}{(di/dv)_n}$$

$$= \frac{R_{an}R_{dn}\{1 + [1 + (R_{ds}/R) + 2(R_{ds}/R_g)][d(\Delta v_s)/dv]\}}{R_{as}R_{ds}\{1 + [1 + (R_{dn}/R) + 2(R_{dn}/R_g)][d(\Delta v_n)/dv]\}}.$$

$$(2)$$

FIG. 2. Superimposed load line graphs.
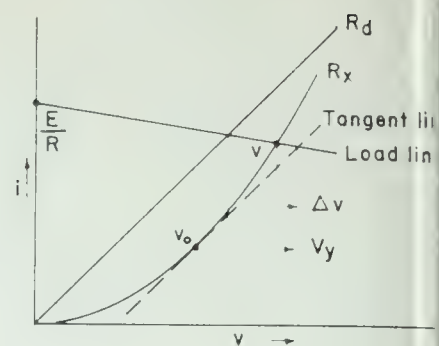
For regions not too close to the energy gap $R_{dn} \approx R_{ds}$ and if $R_a \gtrless 10 R_d$, we can expand (2) and obtain

$$g \approx 1 + [d(\Delta v_s - \Delta v_n)/dv] + [(R_{an} - R_{as})/R_{as}] + [(R_{dn} - R_{ds})/R_{ds}]. \quad (3$$

Let R_u be the resistance of the upper current lead when the specimen is in the normal state. Then it can be seen from (3) that the error $\delta_u g$, introduced in g due to R_u becoming zero (superconducting) will be $\delta_u g = R_u/R$. This error can be made negligible by choosing a large enough value for R. Similarly, denoting the lower current lead resistance by R_l, then if it becomes superconducting, $R_{dn} - R_{ds}$ will be in error by an amount R_l so that $\delta_l g \approx R_l/R_{dn}$. This error can not be made negligible in practice since there is an upper bound to R_{dn} imposed by leakage conduction across the specimen and by requirements of the preamplifier to be described later.

Bridge Modification for a Four Terminal Specimen

As indicated above, difficulty is encountered in the bridge of Fig. 1 when part of R_l becomes superconducting. This problem is avoided when R_l is the normal lead of a specimen with only one metal superconducting, but measurements in which both metals are superconducting are also of interest. The bridge shown in Fig. 3. avoids the difficulty by making R_l effectively part of R_b. In order to see how resistances of the potential leads affect the bridge operation, let us first consider a bridge which has been balanced with $R_l = R_p = 0$. This balance condition, of course, is dependent on the current through the nonlinear specimen resistance. If R_l and R_p become nonzero, a small unbalance current will flow through the lower potential lead R_p. Neglecting changes in the other loop currents, one
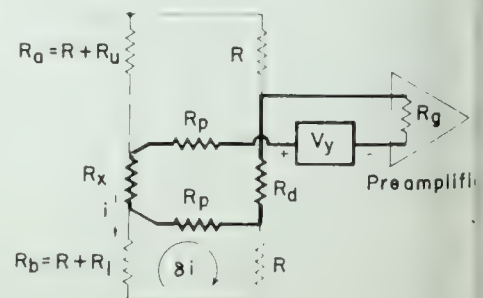

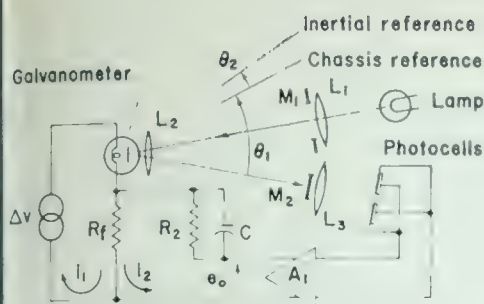FIG. 3. Bridge circuit with four-terminal connection to R_x.

FIG. 4. Galvanometer preamplifier.

obtains from the lower current loop

$$\delta_l i \approx i R_l / 2R.$$

This unbalance current causes an error in the measurement of Δv of $R_p \delta i$, which is equivalent to a change in R_d of

$$\delta R_d = R_p \delta i / i \approx R_l R_p / 2R,$$

so that the error in g due to a change in R_l is now

$$\delta_l g = R_p \delta R_l / 2R R_d.$$

This error may be made negligible.

It is essential for the Δv-loop indicated by heavy lines in Fig. 3 to be free of thermal voltages[6] since the value of Δv is required with a precision of about 10^{-8} V. Thermal voltages elsewhere in the bridge do not affect the measurements because the specimen resistance and R_d are small compared to the other bridge resistances. It should also be remarked that the low impedance of the Δv-loop is essential to the operation of the preamplifier described in the following section. For this reason a Kelvin bridge is not suitable for these measurements.

THE PREAMPLIFIER

From the foregoing it is clear that the amplifier must have a low noise level, and the input impedance should be high. The passband must include dc but need not exceed a few cycles per second. A modification of the galvanometer amplifier described by MacDonald[7] has been developed which satisfies these requirements quite well. A simplified diagram of this amplifier is shown in Fig. 4.

The optical arrangement shown differs from the symmetric arrangement recommended by Jones[8] only in the placement of the photocells. Here the photocells are placed in front of the symmetry position of the lamp. Lens L_1 forms an image of the lamp filament on the galvanometer mirror. Lens L_2 forms an image of mask M_1 in the plane of mask M_2. This image is a vertical rectangle of light a little wider than M_2 and positioned so that some light passes each side of M_2. Since the lens arrangement is symmetric, L_3 would cause the light passing M_2 to reform into an

image of the lamp filament at the symmetry position of the lamp were the light beam not intercepted by the photocells. The position of the photocells is chosen so that two small, separated, vertical strips of light fall on them. The widths of these strips are modulated by the motion of the galvanometer mirror. Since the photocells are connected in parallel but with opposite polarity, they generate either a positive or a negative signal which is fed back to the input after amplification.

Analysis of the Preamplifier Circuit

(a) *Input impedance.* Since the galvanometer acts as an error sensing element, and since $i_1 \ll i_2$, one obtains for the dc input resistance,

$$R_g = \Delta v / i_1 \approx R_f i_2 / i_1 \equiv \alpha R_f,$$

where α is the current gain. Typically, $\alpha \simeq 10^4$ and R_f is between 20 and 2000 Ω, so that R_g is of the order of 10^6 Ω.

(b) *Gain.* Retaining the approximation that negligible error signal appears across the galvanometer, one obtains for the over-all dc gain

$$A_0 = e_0 / \Delta v \approx (R_2 + R_f) / R_f.$$

Since $R_2 = 200$ kΩ, the gain is very nearly linear in R_f^{-1}.

(c) *Dynamic stability, vibrational noise.* A good deal of information may be obtained about the galvanometer amplifier by determining its transfer functions in the open-loop condition.[9] One may show from the differential equations for the closed-loop circuit of Fig. 4 that the currents i_1 and i_2 are summed in effect in the resistor R_f, so that the equivalent open-loop circuit is that shown in Fig. 5. The corresponding block diagram for the closed-loop system is shown in Fig. 6. In this diagram e_n is a voltage equivalent of the noise induced by vibrations and introduced into the amplifier by horizontal rotations of the chassis relative to an inertial system. It may be evaluated from the differential equations for the closed-loop system. If I is the moment of inertia of the galvanometer coil, R_{in} is the total resistance of all elements in the i_1-loop indicated in Fig. 5, φ is the flux linkage of the galvanometer coil, D is the differential operator with respect to time, and θ_2 is the angle the amplifier chassis makes with a suit-
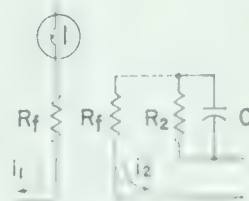

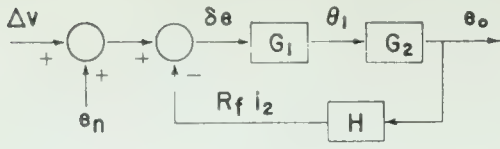FIG. 5. Open-loop circuit for the preamplifier

[6] F. K. Harris, *Electrical Measurements* (John Wiley & Sons, Inc., New York, 1952), pp. 180–185.

[7] D. K. C. MacDonald, in *Handbuch der Physik*, edited by S. Flügge (Springer-Verlag, Berlin, 1956), Vol. 14, p. 159.

[8] R. V. Jones and J. C. S. Richards, J. Sci. Instr. 36, 90 (1959).

[9] J. J. D'Azzo and C. H. Houpis, *Control System Analysis and Synthesis* (McGraw-Hill Book Company, Inc., New York, 1960).

FIG. 6. Block diagram for the closed-loop system.

to the amplifier performance. The approximations are excellent for the dc behavior.

(d) *Noise level.* Vibration appears to make the major contribution to the noise level of the amplifier. From the central term of Eq. (4) it will be noticed that the vibration noise voltage e_n is independent of the stiffness constant of the galvanometer suspension, so that using a rigid suspension does not help. From the right hand side of Eq. (4) it is evident that a galvanometer should be chosen for which $M \equiv T^2 R_{in}/S$ is a minimum. In this merit figure, T is the free period of the galvanometer and S is its current sensitivity expressed in, say, mm/μA at one meter. The use of a high resistance galvanometer increases the tolerance of the merit figure to high resistance specimens.

It is also evident from Eq. (5) that a galvanometer with a high current sensitivity is desirable so that the photocells will be preceded by sufficient gain to make their drift negligible when referred back to the input.

able inertial frame of reference, then

$$e_n = R_{in} I D^2 \theta_2 / \varphi = R_{in} K D^2 \theta_2 / \omega_n^2 \varphi, \qquad (4)$$

where ω_n is the natural resonance frequency of the galvanometer in rad/sec, and K is the stiffness constant of its coil suspension. It is clear that if $R_{in} \ll R_{cd}$, where R_{cd} is the damping resistance specified for the galvanometer, then G_1 is the transfer function of a highly overdamped second-order system. Denoting the damping constant for the G_1 system by ξ, one obtains

$$G_1^{-1} = (K R_{in}/\varphi)(1 + 2\xi D \omega_n^{-1} + D^2 \omega_n^{-2})$$
$$\approx (K R_{in}/\varphi)(1 + 2\xi D \omega_n^{-1})[1 + (2\xi)^{-1} D \omega_n^{-1}], \quad (5)$$

where $2\xi \approx \sqrt{2} R_{cd}/R_{in} \gg 1$. Since $R_{cd} = 10$ kΩ for the galvanometer used here, the overdamped condition is appropriate. If the frequency dependent loading of the R_2-C network on the photocell post-amplifier A_1 is neglected, a suitable choice of θ_1, the angle that measures the rotation of the galvanometer mirror relative to the amplifier chassis, may be made so that $e_0 = k\theta_1$, where k is a constant. Thus $G_2 = k$.

The forward transfer function of the system is then constant to a corner frequency ω_1 with the value

$$\omega_1 = \omega_n/(2\xi) = 0.7 \omega_n R_{in}/R_{cd},$$

beyond which it decreases with a slope of 20 dB/decade to ω_2, the second corner frequency, located at

$$\omega_2 = 2\xi \omega_n = 1.4 \omega_n R_{cd}/R_{in}.$$

Beyond ω_2 the transfer function decreases at a rate of 40 dB/decade, with an attendant phase lag of 180°. Consequently, phase lead compensation must be introduced if the closed loop system is to be stable. The network shown in the i_2-loop of Fig. 5 is a standard phase lead compensator, so that

$$H = \beta(1 + \tau D)/(1 + \beta \tau D),$$

where $\beta = R_f/(R_2 + R_f)$ and $\tau = R_2 C$. Lead compensation is introduced for frequencies nominally between $\omega_a = \tau^{-1}$ and $\omega_b = (\beta \tau)^{-1}$, but is effective over a much wider range than this for the small values of β obtained here.

The gain of the closed-loop system is

$$A \approx 1/H, \qquad (6)$$

and has the value of β^{-1} up to the corner frequency ω_a after which it decreases at a rate of 20 dB/decade. The actual gain characteristic is somewhat more complicated than Eq. (6) indicates because of the various approximations made in the derivation, but it is a satisfactory guide

OTHER FEATURES OF THE CURVE TRACER

Circuitry

The detailed circuit shown in Fig. 7 contains some further features that require comment. Although standard shielding and construction practice were followed, some undesirable parasitic effects remained until the balance
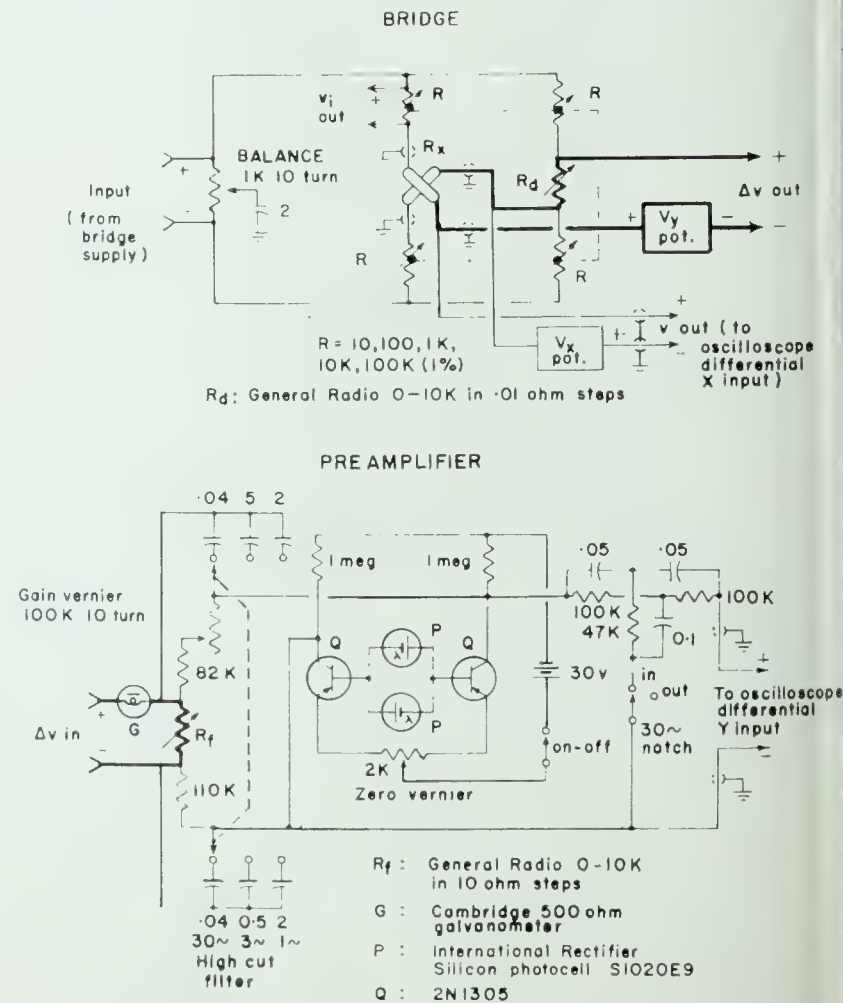

FIG. 7. Bridge and preamplifier circuits. Heavy lines denote thermal-free wiring. Unless otherwise specified, all resistors are $\frac{1}{2}$ W, 5% tolerance, all resistance values are in ohms, and all capacitance values are in μF.
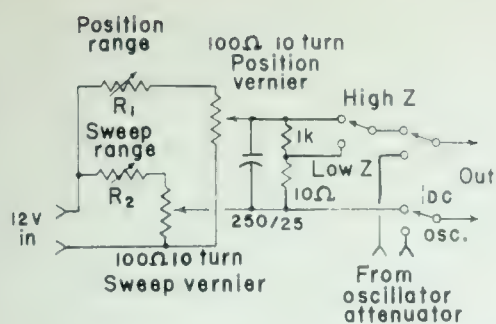
FIG. 8. Bridge supply circuit. R_1, R_2 may be adjusted stepwise to [th]e following values: $R_1 = 0, 470$; $R_2 = 0, 390, 1.5$ K, 4.7 K, 15 K, 47 K, [47]0 K, 470 K. The electrolytic capacitor value is in μF/dcwv.

[co]ntrol and the symmetrical configuration of the pre-[a]mplifier were introduced.

A Tektronix 502 oscilloscope has been used for recording [th]e results. This oscilloscope permits differential dc inputs [to] both X and Y amplifiers, and has a resistance of 1 MΩ [co]nnected from each input terminal to ground. The effect [of] these resistances on the bridge operation, particularly [in] the grounding of undesired signals, must be considered [wh]en choosing the input modes to use. We have used [di]fferential inputs to both channels of the oscilloscope and [th]en provided an ac ground for the bridge through the [ca]pacitor associated with the balance control. Without [th]is a 60 cps signal that was not entirely rejected by the [os]cilloscope input appeared on the entire bridge circuit. [Th]e ac ground is adjusted with the balance control unit [un]til it is at the virtual dc ground point opposite the [os]cilloscope connection to the bridge. The Δv-v trace is [in]dependent of the sweep rate for slow speeds[10] when this [ad]justment is properly made. It is readily seen that with [th]is arrangement feedback may occur from the output of [th]e preamplifier to its input via the oscilloscope input re-[si]stance, the balance control, and the bridge circuit. This [fe]edback is minimized by the symmetry of the circuit [de]sign.

It is interesting to notice that a complete symmetriza-[ti]on of the preamplifier would somehow involve a second [ga]lvanometer. Another advantage might be gained with a [se]cond galvanometer by arranging it so that vibration [no]ise would contribute to a common mode signal and thus [be] rejected. A mechanical filter[11] has been tried to reduce [th]e effect of vibration, but it is difficult to eliminate long
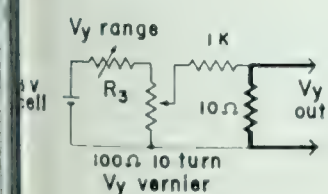

FIG. 9. V_y potentiometer circuit. R_3 may be adjusted stepwise to 0, 1.2, 15, or 150 K.

[10] Slow speeds are those for which the preamplifier can follow the [cha]racteristic without lag.
[11] The preamplifier chassis has been suspended from a spring, so that [it h]as a free period of about 1 sec for vertical oscillations, and of [abo]ut 5 sec for rotations about the vertical axis. Oil damping is [pro]vided for both these degrees of freedom, and a shroud covers the [cha]ssis and suspension to keep out air currents.
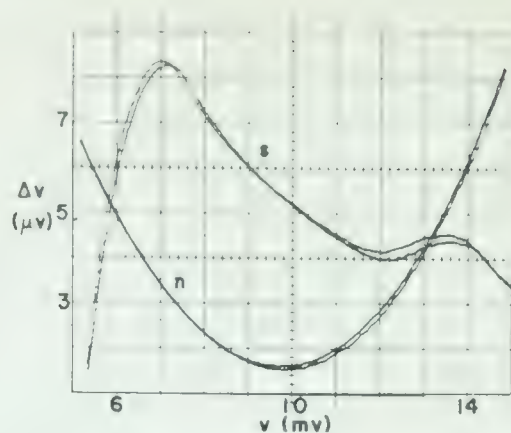

FIG. 10. Δv—v traces obtained from the oscilloscope.

period noise in this manner. The 30 cps "twin-T" notch filter in the output of the preamplifier suppresses a vibrational resonance associated with the galvanometer suspension.

The purpose of the transistor amplifier is to extend the frequency range of the preamplifier. The transistors are operated near cutoff (zero bias) so they require very little power. Some drift results from this unconventional biasing, but it is negligible compared to the photocell drift. The zero adjustment in the transistor amplifier has only a slight effect on the preamplifier zero because of the large gain which precedes the transistors, but it does have a large effect on any common mode ac signal from the photocells.

Operation

Sweep. The oscillator is used mainly for monitoring the specimen characteristics between measurements. The use of the manual sweep instead of the oscillator frees the circuitry from a mains connection, and it is then electrically much quieter. The position (range and vernier, Fig. 8) controls are used to set the high voltage end of the sweep
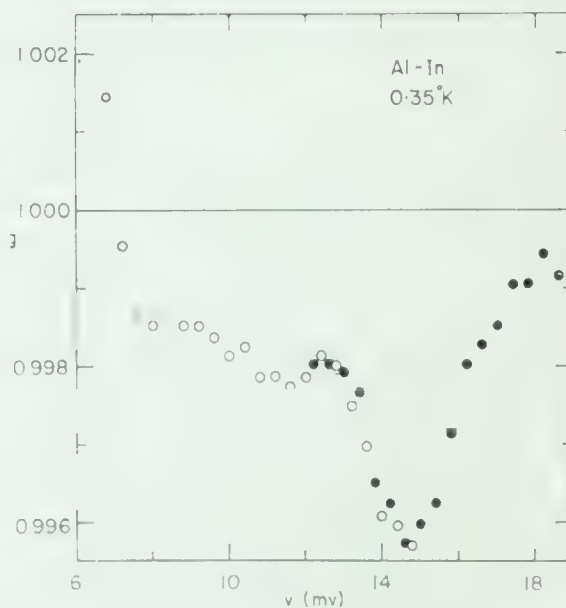

FIG. 11. Normalized dynamic conductance results obtained from the traces shown in Fig. 10 (open circles) along with results obtained from similar adjacent traces (filled circles). The experimental scatter is evident in the overlap region. The characteristic approaches unity to within this experimental error at higher voltages.

range and the voltage is swept downward from this value with the sweep vernier. The sweep range is adjustable in half-decade steps so that any desired sweep may be made to occupy three or more turns of the vernier potentiometer.

Δv-v tracing. The preamplifier must not be subjected to large voltages since the galvanometer receives the full input voltage if the light beam is driven off the photocells. To maintain the preamplifier output within reasonable bounds the R_d and V_y controls are adjusted in conjunction (Fig. 9). Variation of R_d causes the Δv-v pattern on the oscilloscope to skew and shift vertically; V_y is adjusted to oppose the vertical shift. In Fig. 10 a typical Δv-v plot is shown and the analyzed results obtained from it appear in Fig. 11. The plot is simply a photograph of the oscilloscope face. The information is retrieved from the photograph by comparison with a raster generated on the same oscilloscope, so that distortions in the various optical systems utilized cancel out. The data from the Δv-v pl[o] are processed by a digital computer according to Eq. ([2] Little resolution is lost by recording on the oscillosco screen since for a typical preamplifier gain of 10^3, a uni change in the slope of the pattern only causes a change the normalized dynamic conductance of 10^{-3} assuming th equal gains are used on the vertical and horizontal osc loscope channels.

i-v tracing. For cases where negative resistance regio are not required, the galvanometer amplifier may be us to preamplify v while a large value of R_a yields a lar v_i. If a negative resistance region is to be traced, the volta supply for the specimen must be of low impedance. O thus chooses a value for R_a smaller than R_x and uses t low-z mode of the manual sweep. The galvanomet amplifier may then be placed across R_a to amplify t small v_i which results.

APPENDIX II

BRIDGE CIRCUIT FOR DETERMINING THE CAPACITANCE OF TUNNEL JUNCTIONS

An extended Wheatstone bridge with a phase sensitive error signal display has been found useful during the preparation of tunnel junctions.

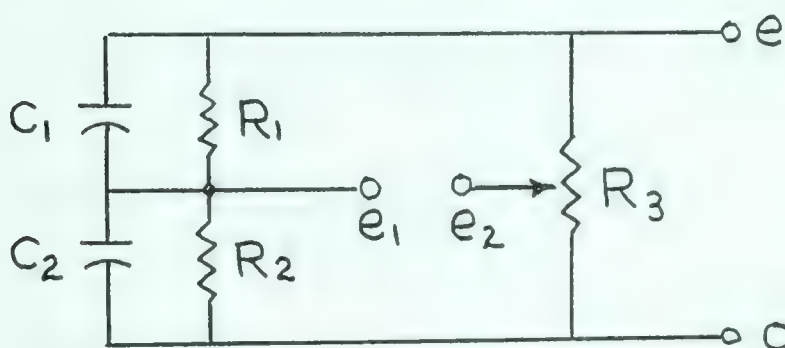Its basic circuit is shown in Figure A 2.1.

Figure A 2.1

Basic bridge circuit for capacitance measurements.

In this figure, $e = e_m \exp. j\omega t$ is a sinusoidal voltage applied to the bridge circuit, $e_1 - e_2$ is the error signal, and the combination $R_1 - C_1$ is to represent the specimen. One may readily derive the equation

$$\beta_1 \equiv \frac{e_1}{e} = \beta \cdot \frac{1 + \omega^2 \tau_1 (\tau_2 + \beta d\tau) + j\omega (1-\beta) d\tau}{1 + \omega^2 (\tau_2 + \beta d\tau)^2}, \quad (A\ 2.2)$$

where $\beta = \dfrac{R_2}{R_1 + R_2}$,

$$\tau_1 = R_1 C_1 \quad ,$$

$$\tau_2 = R_2 C_2 \quad ,$$

$$d\tau = \tau_1 - \tau_2 \quad ,$$

and ω is the frequency in radians per second.

It therefore follows that the null conditions for the bridge are

$$\beta = \dfrac{e_2}{e} \quad \text{and} \quad d\tau = 0 \quad ,$$

or
equivalently,   (A 2.3)

$$R_1 = \dfrac{1 - \beta_2}{\beta_2} R_2 \quad ,$$

and $C_1 = \dfrac{\beta_2}{1 - \beta_2} C_2 \quad ,$ (A 2.4)

where $\beta_2 = \dfrac{e_2}{e}$.

While these null conditions may be more readily obtained by conventional methods, the derivation given above is more closely allied with the actual measurement operation which is now to be described.

Figure A 2.2 shows the operational form of the bridge circuit. It may be seen that the horizontal deflection of the oscilloscope display is proportional to e , while the vertical deflection is proportional to $e_1 - e_2$. The displayed pattern is therefore a straight line for low frequencies ($\omega\tau \ll 1$) as may be seen from equation A 2.2. Suitable values of R_2 and β_2 will

Figure A 2.2

A bridge circuit for measuring the capacity of
a tunnel junction. R_s' may be adjusted step-
wise to the following values in ohms: 10, 31.6,
100,3.16, 1K, 3.16K, 10K, 31.6K, 100K, 500K,
1M, ∞ . The resistors used for R_s' are
$\pm$ 1%, 1/2 W carbon film resistors. The
capacitor C_s is a Heathkit DC-1, and may be
adjusted from zero to 0.1 μf in 100 $\mu\mu$f steps.

R_3: 100 ohm, 10 turn, 1/4 % lin.

✳ : Hewlet-Packard 200 CD
Oscillator

make the straight line horizontal, and the null condition
A 2.3 is then satisfied. An increase in frequency will
cause the displayed pattern to open into an ellipse as a
result of the term $j\omega(1-\beta)d\tau$ in equation A2.2,
so that the value of C_2 which causes the ellipse to
close again satisfies the null condition A 2.4. This
method of null attainment is suitable for specimens having
a characteristic frequency $\omega = 1/\tau_1$ which is at the high
end of the operational frequency range of the bridge
(5 c.p.s. to 50 K.C.S. for the circuit shown in Figure A 2.2.)

If the specimen has a characteristic frequency which
is at the low end of the operational frequency range of the
bridge, it will not be possible to satisfy the condition
$\omega\tau \ll 1$. In this case the initial display pattern
will be a tilted ellipse for the lowest frequency available.
If one then increases the frequency to 50 K.C.S. ,the ω^2
terms in equation A 2.2 should be dominant. Suitable
adjustment of R_2 and β will cause the displayed pattern
to close into a straight line, and finally C_2 may be adjusted
to make the straight line horizontal. The null equations
A 2.3 and A 2.4 may then be applied as before. It will be
noticed that the null conditions are independent of frequency,
so that once a null is obtained, no matter by what means, it
should be independent of the frequency.

The above analysis is based on the ideal circuit
shown in Figure A 2.1, but the actual circuit is a far more

complicated situation which behaves only approximately as the ideal circuit. We now consider the steps taken to bring the actual circuit behaviour into line with the ideal behaviour.

It will first be noticed that an attenuated signal is fed to the horizontal amplifier of the oscilloscope. The attenuation is chosen so that both channels of the oscilloscope may be operated at the same gain, then there is little relative phase shift introduced by the oscilloscope.

A shielded lead, having an appreciable capacitance that must be added to the readings of the decade capacitor box, connects the capacitor C_s to the rest of the circuit. Finally we notice that the resistor R_3 is of the helical coil type, so that it has an appreciable distributed inductance. It has been found convenient to correct for this inductance by making an additional correction to the value C_s . The net correction δc to C_s has been obtained as a function of C_1 , R_s , and β_2 , where R_s is the value of R_s' corrected for the input resistance to the ground of the 'A' terminal of the vertical channel of the oscilloscope. (A suitable dial on the resistor allows β_2 to be read directly to $\pm$ 0.1%). The correction δc has been obtained simply by inserting known values of C_1 and R_1 into the circuit.

A typical set of correction curves for C_s is

given in Figure A 2.3. Two apparently identical bridge

constructions have yielded somewhat different correction

curves, so these curves must be obtained for each bridge

circuit made. It is implicit in the nature of the correction

that δc should be small compared to C_1 . Our

typical specimens have $C_1 \simeq 30\, m\mu f$, and δc

is usually about $2\, m\mu f$, i.e., about 5% of C_1

If the values of δc are appreciable compared to C_1

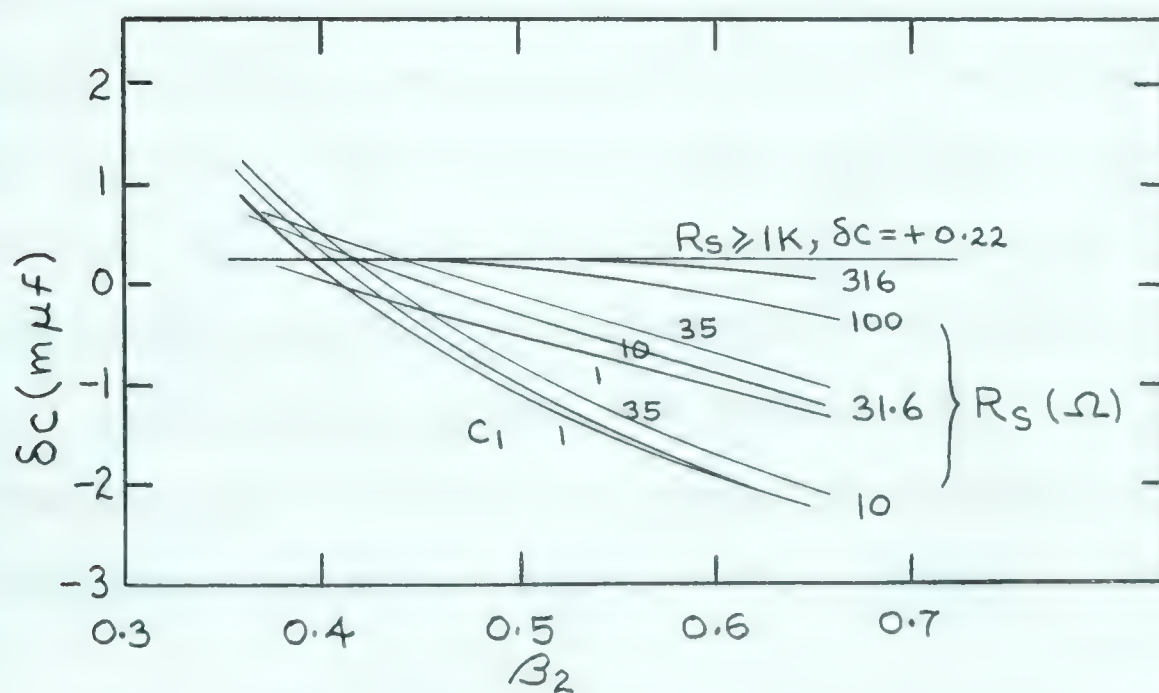the specimen capacitance cannot be determined with this

bridge circuit.

Figure A2.3

Capacitance corrections.

APPENDIX III

TUNNEL JUNCTIONS AS THERMOMETERS

The current-voltage characteristics of a tunnel junction in which at least one of the metallic films is superconducting always possess information relating directly to the temperature of the superconducting member (or members), so that such tunnel junctions may be used as thermometers.

As a simplified example of this application, let $\rho_{S1} = \rho_{S2}$ be the density of states distributions for a symmetric tunnel junction. The distribution diagram corresponding to the tunnel current integral for an applied voltage slightly less than the energy gap voltage* is shown in Figure A 3.1, along with the i-v characteristic in the gap region for this same tunnel junction. The current $i(2\Delta^-)$ is due to thermally excited electrons in the distribution ρ_{S2} tunnelling into the distribution ρ_{S1} and also to the thermally excited holes in the distribution ρ_{S1} tunnelling into the distribution ρ_{S2}. Using the approximation of a constant tunnelling probablility, one may write an approximate expression for $i(2\Delta^-)$ directly:
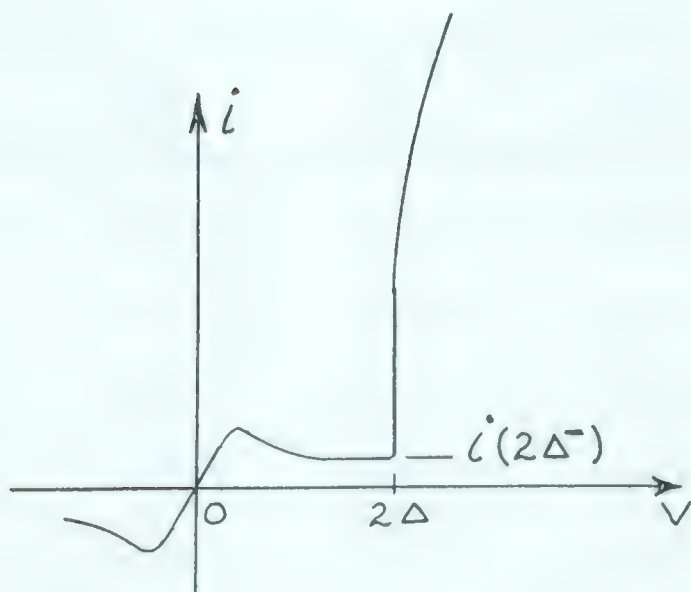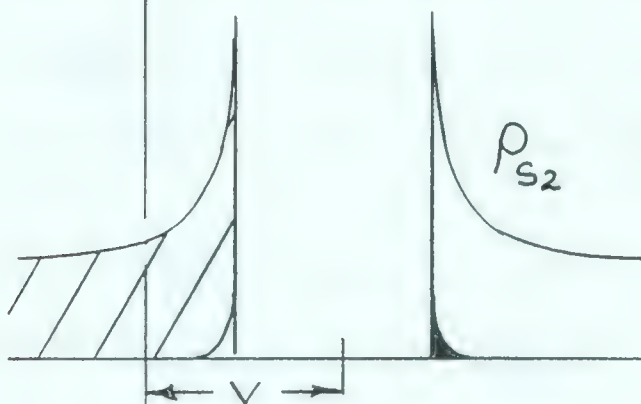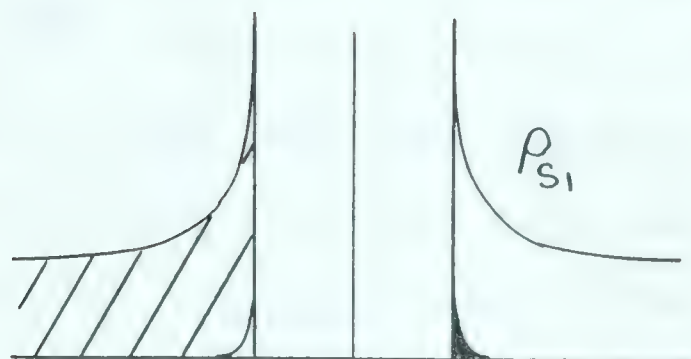
$$i_{ss}(2\Delta^-) \doteq 2c \int_0^\infty e^{-\frac{x+\Delta}{T}} \left(\frac{\Delta}{2x}\right)^{1/2} 1.06 \, dx \quad .$$

The first term in the integrand is the Fermi function

---

* $V = 2\Delta^-$

Figure A 3.1

Illustration of the use of a tunnel

junction as a thermometer.

approximation for $\frac{\Delta + x}{T} \gg 1$, the second term is

the asymptotic form of the BCS function G for $\omega = \Delta^+$,

and the factor 1.06 is the value of $G(2\Delta)$. A proper

derivation of this result will show that a factor

($1 - e^{-\frac{2\Delta}{T}}$) due to the reverse current has also

been ignored in this intuitive approach to the tunnel

integral. The major source of discrepancy between the

observed value of $i'_{ss}(2\Delta^-)$ and the above expression

however will be due to the factor $\left(\frac{\Delta}{2x}\right)^{1/2}$. This factor

departs seriously from the BCS function G for values of

$x \doteq \Delta$ as may be seen from Table A 3.1, so that it

does not represent the distribution ρ_s well in this region.

Table A 3.1

Comparison of the BCS function with $\left(\frac{\Delta}{2x}\right)^{1/2}$

| $\frac{\omega}{\Delta}$	G	$\left(\frac{\Delta}{2x}\right)^{1/2}$
1.05	3.29	3.16
1.10	2.39	2.24
1.15	2.02	1.82
1.20	1.81	1.58
1.25	1.67	1.41
1.30	1.56	1.29
2.00	1.15	0.71
3.00	1.06	0.50

It does not represent the actual ρ_s very well near the

gap edge either because of the broadening effects. However,

the above expression has the advantage that it may be readily

evaluated since the integral reduces to a gamma function.

One obtains

$$I(2\Delta^-) \equiv \frac{i_{ss}(2\Delta^-)}{i_{nn}(2\Delta)} \doteq 1.06 \left(\frac{\pi T}{2\Delta}\right)^{1/2} e^{-\frac{\Delta}{T}}$$

$$= 1.33 \left(\frac{T}{\Delta}\right)^{1/2} e^{-\frac{\Delta}{T}} \quad . \qquad (A\ 3.1)$$

In this approximation then, one has a simple

connection between the temperature T and the observables

$I(2\Delta^-)$ and Δ . The observed values of $I(2\Delta^-)$ as a

function of the observed temperature T_R are plotted in

Figure A 3.2 for two specimens along with equation A 3.1

as a function of temperature T . One would expect the

observed points to at least lie parallel to equation A 3.1,

since the exponential term due to the energy gap should be

dominant in any reasonable expression for $I(2\Delta^-)$. Some

experimental results published by Giaever are shown in

Figure A 3.2 and they confirm this argument. One is forced

to conclude than that the tunnel junction temperature for

specimen Al-34 was not the same as the temperature of the

resistance thermometer with which T_R was observed. Better

agreement was obtained for specimen Al-42, probably as a

result of better evacuation of the vacuum chamber of the

cryostat and a more liberal use of solder at the connection

Figure A 3.2

Graphical presentation of equation A 3.1 along
with some experimental results. The experimental
results of Giaever have been obtained from one of
his publications (Giaever et al, 1962). The
temperature scale shown has been calculated on
the basis of $\Delta(o) = 0.20$ mv .
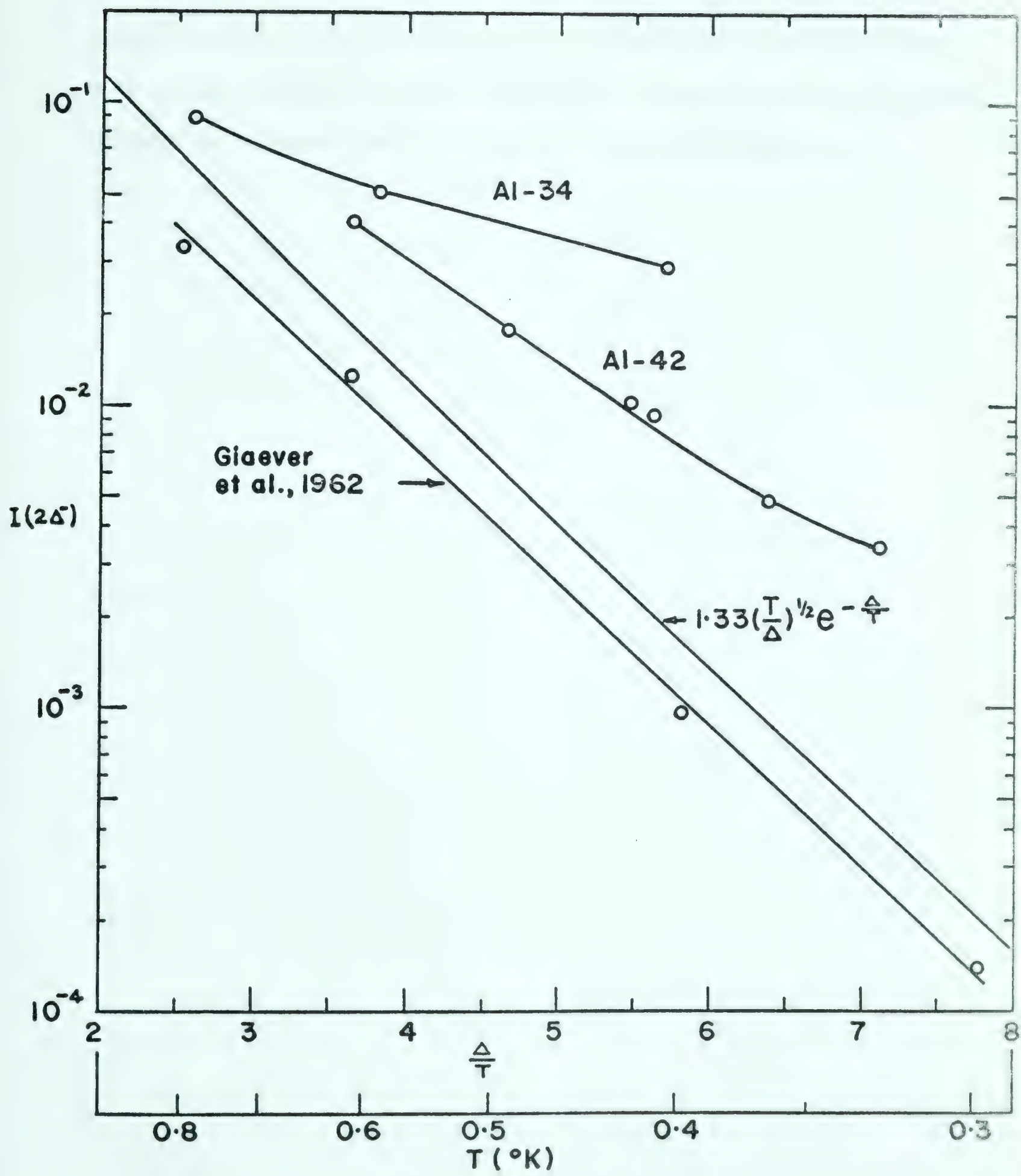
between the He^3 chamber on which the resistance thermometer was mounted and the specimen chamber, but it may be seen that further improvement will be necessary if experiments are to be conducted which require a knowledge of the tunnel junction temperature to within a few millidegrees.

APPENDIX IV

DISTORTIONS INTRODUCED BY THE PROBE DISTRIBUTION

It was stated in Chapter III that the normalized dynamic conductance σ should be quite similar to the normalized density of states in one of the superconductors, ρ_{sa}, for certain probe distributions ρ_{sb}. The correspondence is not complete however, so that σ must be viewed as a distorted form of ρ_{sa}. The size and shape of these distortions will be derived here for some simple forms of ρ_{sa}.

It has been shown that the variation of the tunnelling probablility with applied voltage has a neglibible influence on our results, so we will assume a constant transition probability here in order to **simplify** calculations. We will also assume that there is a negligible number of thermally excited electrons and holes in the distributions for the superconductors. The expressions for the tunnel current between the superconductors may then be written

$$i_s(v) = c \int_0^{\check{v}} \rho_{sa}(\omega) \rho_{sb}(\omega-v) \, d\omega \, ,$$

$$= c \int_0^{\check{v}} \rho_{sa}(x-v) \, \rho_{sb}(x) \, dx \, .$$

The last expression is obtained by setting $x = v - \omega$ and noting that the distributions are symmetric in their arguments. The current between these metals when they are normal is $i_n(v) = cv$. The normalized dynamic

conductance is therefore

$$\sigma = \frac{d}{dv} \int_0^v \rho_{Sa}(x-v) \, \rho_{Sb}(x) \, dx \quad .$$

(4.1)

For cases where M_b is normal, we will use the Fermi function $f(\omega,T)$ for ρ_{nb} in order to take into account the effect of a non-zero temperature on the probe distribution.

We now take the point of view generally used by electrical engineers and consider equation A 4.1 as a mathematical system with one input quantity ρ_{Sa} and one output quantity σ . The two quantities are not identical due to the distortion introduced by the system parameter ρ_b . We then calculate the distortion introduced into some simple forms for ρ_{Sa} . For these simple forms we choose a step function, a ramp function, and a parabola, as indicated in Figure A 4.1. The voltage origin for ρ_{Sa} is chosen at the discontinuity in the step function, and the ρ_{Sa} functions are taken to be zero for $V < 0$, so that higher derivatives of all of them are discontinuous at $V = 0$. The output results σ can then be calculated for a given ρ_{Sa} . The results of some calculations of this nature are shown in Figure A 4.1. Allowance has been made for the energy gap in choosing the origin for the σ results. The energy scale is given

Figure A4.1

Distortions introduced by the probe distributions.
Parts (a) to (c) are for a superconducting probe
distribution, while parts (d) and (e) are for a
normal probe distribution. The distribution $\rho_{S\alpha}$
for parts (a) and (d) is a unit step function;
for parts (b) and (e) it is a ramp function, and
for part (c) it is a parabola.

(a)

(b)

(c)

(d)

(e)
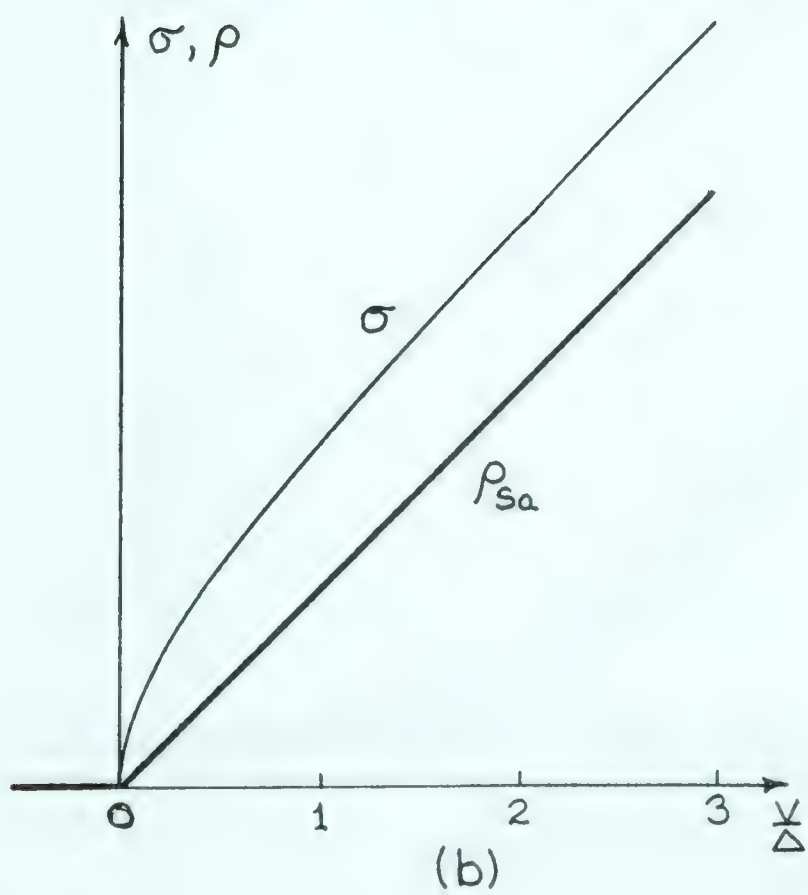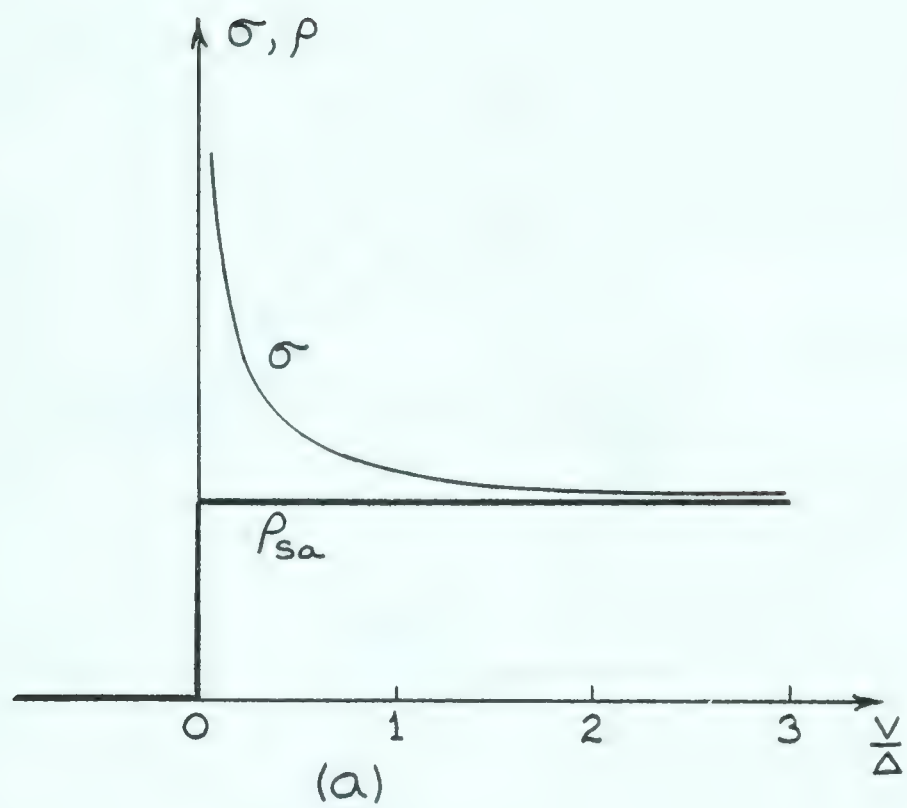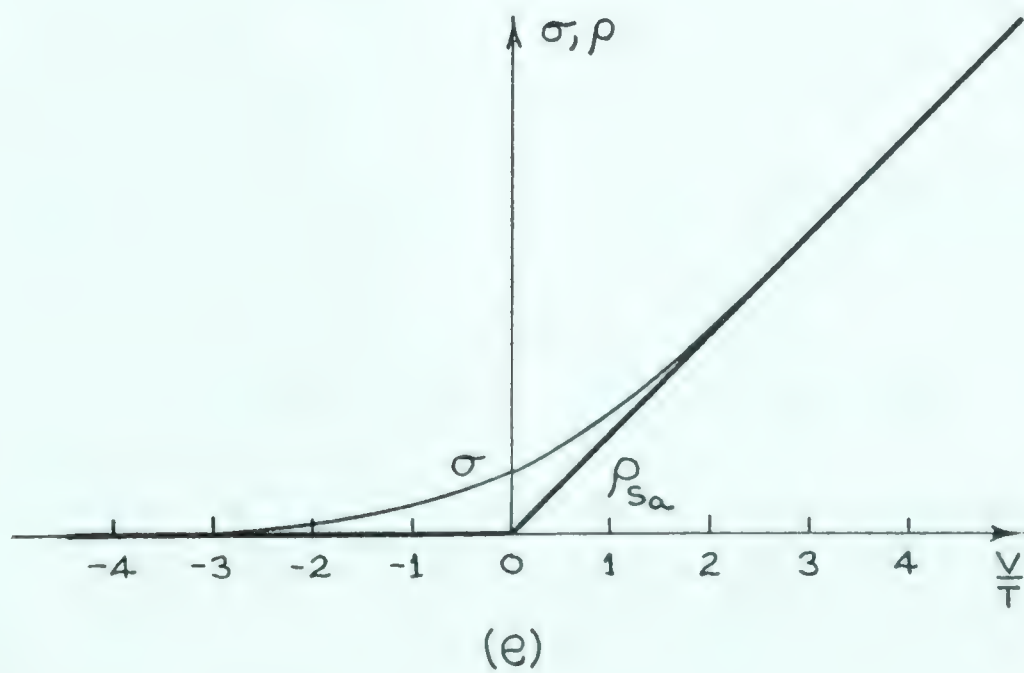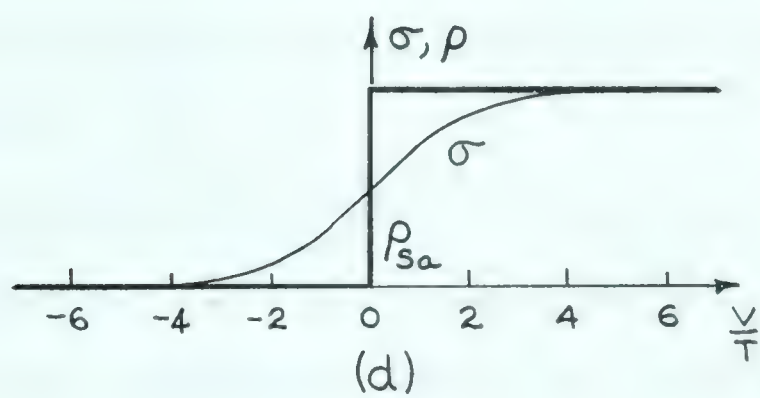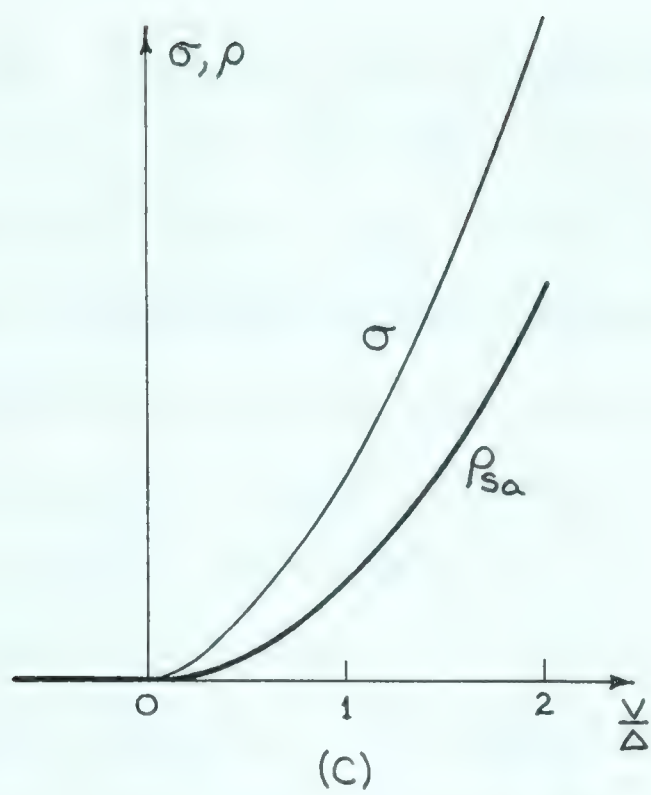
in units of Δ for the superconducting probe distribution

and in units of $\top$ for the normal probe distribution. The

unit step function form for ρ_{sa} causes σ to be identical

with the probe distribution, apart from a reversal of

coordinate direction, so that the shape of the probe

distribution used for the calculations has not been repeated

in a separate part of the figure.

A study of Figure A 4.1 will reveal some of the

higher derivative results. For example, the derivative

of the result for the ramp form of ρ_{sa} is identical with

the probe distribution, as is the second derivative of the

parabolic form of ρ_{sa} .

The conclusion which we have drawn from the results

shown in Figure A 4.1 is that the critical point fits shown

in Chapter V are reasonably valid for energies removed from

the critical point energy by an amount $|x| \geqslant \Delta_{Al}$.

BIBLIOGRAPHY

Adkins, C. J., 1963. Phil. Mag. 8, 1051.

Adler, J. G., and Rogers, J.S., 1963. Phys. Rev. Letters 10, 217.

Adler, J. G., 1963. Electron Tunnelling Into Superconductors. Doctoral Thesis, University of Alberta.

Bardeen, J., 1961. Phys. Rev. Letters 6, 57.

Bardeen, J., Cooper, L. N., and Schrieffer, J. R., 1957 a. Phys. Rev. 106, 162.

Bardeen, J., Cooper, L. N., and Schrieffer, J. R., 1957 b. Phys. Rev. 108, 1175.

Bermon, S., and Ginsberg, D. M., 1963. Bull. Am. Phys. Soc. II, 8, 232.

Bhatia, A. B., 1955. Phys. Rev. 97, 363.

Blatt, J. M., and Thompson, C. J., 1963. Phys. Rev. Letters 10, 332.

Bogoliubov, N. N., Tolmachev, V. V., and Shirkov, D. V., 1959. A New Method in the Theory of Superconductivity, Consultants Bureau, New York.

Brockhouse, B. N., Arase, T., Caglioti, G., Rao, K. R., and Woods, A. D. B., 1962. Phys. Rev. 128, 1099.

Clement, J.R., and Quinnell, E. H., 1952. Rev. Sci. Instrum. 23, 213.

Cooper, L. N., 1956. Phys. Rev. 104, 1189.

Dicke, R. H., and Wittke, J. P., 1960. Introduction to Quantum Mechanics, Addison-Wesely Publishing Co., Reading Mass.

Douglass, D. N., Jr., and Meservey, R., 1962. Proc. 8th Int. Conf. on Low Temp. Phys. (to be published).

Eliashberg, G. M., 1960. Soviet Phys. - JETP II, 696.

Fisher J. C., and Giaever, I., 1961 Jour. Appl. Phys. 32, 172.

Handy, R.M., 1962. Phys. Rev. 126, 1962

Harrison, W.A., 1961. Phys. Rev. 123, 85.

Holland, L., 1961. Vacuum Deposition of Thin Films, Aberdeen University Press Ltd., Aberdeen, Scotland.

Josephson, B. D., 1962. Physics Letters 1, 251.

Kittel, C., 1960. Introduction to Solid State Physics, John Wiley and Sons Ltd., New York.

Krumhansel, J. A., 1962. Journ. Appl. Phy. supp. 33, 307.

Muhlschlegel, B., 1959. Z. Phys. 155, 313.

Musgrave, M J. P., 1963. Proc. Roy. Soc., (London) A272, 503.

Phillips, J. C., 1959. Phys. Rev. 113, 147.

Rowell, J. M., Anderson, P. W., and Thomas, D. E., 1963. Phys. Rev. Letters 10, 334.

Scalapino, D. J., and Anderson, P. W., 1964. Phys. Rev. 133, A921.

Schrieffer, J. R., Scalapino, D. J., and Wilkins, J. W., 1963. Phys. Rev. Letters 10, 336.

Schrieffer, J. R., and Wilkins, J. W., 1963. Phys. Rev. Letters 10, 17.

Shapiro, S., Smith, P. H., Nicol, J., Miles, J. L., and Strong, P. F., 1962. I.B.M. Jour. Research and Developement 6, 34.

Taylor, B.N., and Burstein, E., 1963. Phys. Rev. Letters 10, 14.

Thomas, D. E., and Klein, J. M., 1963. Rev. Sci. Instr. 34, 920.

Van Hove, L., 1953. Phys. Rev. 89, 1189.

Walker, C.B., 1956. Phys. Rev. 103, 547.

Woods, A. D. B., Brockhouse, B. N., March, R. H., and Stewart, A. P., 1962. Phys. Rev. 128, 1112.

Zavaritskii, N. V., 1961. Sov. Phys. JETP 14, 470.